

中英文摘要：

本研究報告提出一頻域光波導模態的高階精確計算方法和其應用。我們以擬譜法為基礎將麥克士威方程式進行離散，邊界條件的配置是以補償法嵌入格式中，所得的方程為線性系統方程組。我們對格式進行了詳細的穩定性分析，接著進程式編寫和測試。計算結果與理論分析是一致的。最後，我們以演算法對各類光波導進行傳播特性分析，並討論計算的物理現象。

In this report, we propose a high-order accurate scheme for computing optical waveguide modes. We employ the Legendre pseudospectral method to discretize the Maxwell's equations. Boundary conditions are imposed to the scheme through the penalty methodology. This approach leads to a system of linear equations. We pay special attention to analysis the stability of the schemes, and we obtain suitable penalty parameters for stable computations. The numerical method is validated through direct computations, and the results are consistent with the theoretical analysis. In addition, we conduct optical wave analysis for various kinds of waveguides to study wave propagations in these devices.

關鍵字：擬譜法，邊界補償法，頻域麥克士威方程式，光波導

Keywords: pseudospectral methods, penalty boundary conditions, frequency-domain Maxwell's equations, optical waveguides

Summary of the Report

Frequency-domain (FD) and Time-domain (TD) computational electromagnetic (EM) methods are playing important roles in optic wave analysis. To investigate the transition of EM waves, TD methods (see [10, 11, 14, 15] for example) are suitable. On the other hand, FD algorithms [4, 7, 8, 12, 13] are commonly used for studying the time-harmonic electromagnetic wave properties, since the methods solve EM wave problems based on a single frequency. In this report we describe a novel method for computing accurate propagation characteristics of optical waveguide of complex geometries.

The traditional methods for analyzing optical waves in guiding devices are based on solving the Helmholtz equations which involves second derivatives in space. The numerical formulations results into linear systems of equations having large condition numbers, due to the numerical second differential operators. Hence, the numerical solutions require many iterations to converge within the desired accuracy. To overcome this issue we propose a formulation based on the Maxwell's equations which involves first derivatives in space only. Thus, the condition numbers of the Maxwell-based formulation are smaller than those of the Helmholtz-based formulation. This leads to less iteration steps toward to the convergence of solutions. Moreover, another potential advantage of using the Maxwell equations based formulation is that one can directly borrow important numerical theories developed from the TD Maxwell equations based computational framework [10, 11], for instance, the penalty methodology for imposing boundary conditions [5, 6, 9] and perfectly matched layer type absorbing boundary conditions [1, 2, 3] which have been used in real applications.

In addition, inspired by the constructed pseudospectral FD method for optic waveguide analysis, we construct an error minimized pseudospectral penalty direct Poission solver. It is found the that imposition of boundary conditions has great effects on the solution accuracy and the penalty parameters can be obtained analytically to yield numerical solutions with error being minimized. Numerical experiments are conducted and the results are consistent with the theoretical analysis. The method is very easy to implement and it can help improve the accuracy of pseudospectral Poission solver used in the scientific community.

The details and applications of these methods are summarized in the following journal papers included in this report.

1. C. Y. Wang, S. Y. Chung, C. H. Teng, J. K. Wang, C. P. Chen, H. C. Chang, A high-accuracy multidomain Legendre pseudospectral frequency-domain method with penalty scheme for solving scattering and coupling problems of nano-cylinders, *IEEE/OSA J. Lightw. Technol.*, 31, pp. 768-778, (2013).
(SCI), IF=2.782, RANKING 5/79 \approx 6.3% IN TELECOMMUNICATION.
2. S. F. Chiang, B. Y. Lin, H. C. Chang, C. H. Teng, C. Y. Wang, S. Y. Chung, A multidomain pseudospectral mode solver for optical waveguide analysis, *J. Lightw. Technol.*, 30, pp. 2077-2087, (2012).
(SCI), IF=2.782, RANKING 5/79 \approx 6.3% IN TELECOMMUNICATION.
3. T. L. Horng, C. H. Teng, An error minimized pseudospectral penalty direct Poisson solver, *J. Comput. Phys.*, 231, pp. 2498-2509, (2012)
(SCI) IF: 2.310, RANKING 5/55 \approx 9.1% IN PHYSICS, MATHEMATICS.

References

- [1] Abarbenel S., Gottlieb D. (1998). On the construction and analysis of absorbing layer in CEM. *Appl. Numer. Math.*, 27, 331-340.
- [2] Abarbenel S., Gottlieb D., Hesthaven J. (1999). Well-posed Perfectly Matched Layers for Advective Acoustics. *J. Comput. Phys.*, 154, 266-283.
- [3] Berenger J. P. (1994). A perfectly matched layer for the absorption of electromagnetic wave. *J. Comput. Phys.*, 114, 185-200.
- [4] Chiang Y. C., Chiou Y. P., Chang H. C. (2002). Improved full-vectorial finite-difference mode solver for optical waveguides with step-index profiles. *J. Lightw. Technol.*, vol. 20, no. 8, pp. 1609-1618.
- [5] Funaro D., Gottlieb D. (1988). A new method of imposing boundary conditions in pseudospectral approximations of hyperbolic equations. *Math. Comp.* 51, 599-613.
- [6] Funaro D., Gottlieb D. (1991). Convergence results for pseudospectral approximations of hyperbolic systems by a penalty-type boundary treatment. *Math. Comp.* 57, 585-596.

- [7] Hadley G. H. (2002). High-accuracy finite-difference equations for dielectric waveguide analysis I: Uniform regions and dielectric interfaces. *J. Lightw. Technol.*, vol. 20, no. 7, pp. 1210-1218.
- [8] Hadley G. H. (2002). High-accuracy finite-difference equations for dielectric waveguide analysis II: Dielectric corners. *J. Lightw. Technol.*, vol. 20, no. 7, pp. 1219-1232.
- [9] Hesthaven J. S. (2000). Spectral penalty methods. *Appl. Numer. Math.*, 33, 23-41.
- [10] Hesthaven J. S., Gottlieb D. (1999). Spectral collocation time-domain modeling of diffractive optical elements. *J. Comput. Phys.*, 155, 287-306.
- [11] Hesthaven J. S., Warburton T. (2002). Nodal high-order methods on unstructured grids. I. Time-domain solution of Maxwell's equations. *J. Comput. Phys.*, 181, 186-221.
- [12] Jiang P. J., Wu C. L., Teng C. H., Yang C. S., Chang H. C. (2008). Full-Vectorial Optical Waveguide Mode Solvers Using Multidomain Pseudospectral Frequency-Domain (PSFD) Formulations. *IEEE Journal of Quantum Electronics*, 44, 56-66.
- [13] M.Koshiha M., Tsuji Y. (2000). Curvilinear hybrid edge/nodal elements with triangular shape for guided-wave problems. *J. Lightw. Technol.*, vol. 18, no. 5, pp. 737-743.
- [14] Taflove A., Hagness S. C. (2000). *Computational Electrodynamics: The Finite-Difference Time-Domain Method* (2nd ed). Artech House, Boston, London.
- [15] Yee, K. S. (1966). Numerical solution of initial boundary value problems involving Maxwell's equations in isotropic media. *IEEE Trans. Antennas Propagat.*, 14, 302-307.

A High-Accuracy Multidomain Legendre Pseudospectral Frequency-Domain Method With Penalty Scheme for Solving Scattering and Coupling Problems of Nano-Cylinders

Chih-Yu Wang, Shih-Yung Chung, Chun-Hao Teng, Juen-Kai Wang, Chung-Ping Chen, *Member, IEEE*, and Hung-chun Chang, *Senior Member, IEEE, Fellow, OSA*

Abstract—A new multidomain pseudospectral frequency-domain (PSFD) method based on the Legendre polynomials with penalty scheme is developed for numerically modeling electromagnetic wave scattering problems. The primary aim of the proposed method is to more accurately analyzing scattering and coupling problems in plasmonics, in which optical waves interact with nanometer-sized metallic structures. Using light scattering by a silver circular cylinder as a first example, the formulated method is demonstrated to achieve numerical accuracy in near-field calculations on the order of 10^{-9} with respect to a unity field strength of the incident wave with excellent exponentially convergent behavior in numerical accuracy. Then, scattering by a dielectric square cylinder and that by several coupled metallic structures involving circular cylinders, square cylinders, or dielectric coated cylinders are examined to provide high-accuracy coupled near-field results.

Index Terms—Electromagnetic near fields, electromagnetic wave scattering, plasmonics, pseudospectral frequency-domain (PSFD) method.

I. INTRODUCTION

PLASMONICS is a relatively new field concerning the collective electromagnetic resonances of free electrons inside nanometer-scaled metallic structures [1], which has been

Manuscript received February 04, 2012; revised November 11, 2012, November 23, 2012; accepted November 26, 2012. Date of publication December 12, 2012; date of current version January 23, 2013. This work was supported in part by the National Science Council of the Republic of China under Grant NSC99-2628-M-002-008, Grant NSC99-2221-E-002-107-MY2, Grant NSC99-2115-M-009-012-MY3, and Grant NSC 101-2811-M-009-040, in part by the Excellent Research Projects of National Taiwan University under Grant 10R80919-1, and in part by the Ministry of Education of the Republic of China under “The Aim of Top University Plan” Grant.

C.-Y. Wang, S.-Y. Chung, and C.-P. Chen are with the Graduate Institute of Electronics Engineering and the Department of Electrical Engineering, National Taiwan University, Taipei 10617, Taiwan.

C.-H. Teng is with the Department of Applied Mathematics and Center of Mathematical Modeling and Scientific Computing, National Chiao Tung University, Hsinchu 30010, Taiwan.

J.-K. Wang is with the Institute of Atomic and Molecular Sciences, Academia Sinica, and the Center for Condensed Matter Sciences, National Taiwan University, Taipei 10617, Taiwan.

H. Chang is with the Department of Electrical Engineering, the Graduate Institute of Photonics and Optoelectronics, and the Graduate Institute of Communication Engineering, National Taiwan University, Taipei 10617, Taiwan (e-mail: hcchang@cc.ee.ntu.edu.tw).

Digital Object Identifier 10.1109/JLT.2012.2233714

widely studied and applied in many areas, like surface enhanced Raman scattering (SERS) [2], nanoantennas [3], waveguides [4], etc. Strong electromagnetic fields can be locally enhanced and radiated by this collective oscillation of electric charges. The field coupling between metallic nanoparticles under different incident polarizations thus plays an important role in such plasmonics research. Accurate electromagnetic near-field calculation is essential and significant for understanding the underlying optical behaviors [5]. However, due to the nanometer-sized dimension and spacing of metallic particles as well as strongly enhanced near fields, there exist challenges to achieve relevant numerical simulations with good accuracy. The Mie theory [6] and the multiple scattering methods [7], [8] for analytically calculating light wave scattering by spheres or circular cylinders have been proposed. But for more general geometries of the plasmonic objects, numerical methods, like the finite-difference time-domain (FDTD) method [9], [10] and the finite element method (FEM) [11], [12], could provide more flexibilities. Plasmon resonance and field enhancement in complicated structures have also been analyzed using the surface integral method [13] and the volume integral method [14] and discussed by the surface-charge hybridization picture [15].

To more accurately model the interaction of electromagnetic waves with metallic structures, we present here a new Legendre pseudospectral frequency-domain (PSFD) method to solve Maxwell’s equations for relevant two-dimensional (2-D) scattering problems. Although not so popularly used, the pseudospectral methods have been demonstrated their high-order accuracy and fast convergence behavior in applications to computational electromagnetics in time domain [16]–[19]. The idea of the pseudospectral method in frequency domain was initially proposed by Liu [20] based on Chebyshev polynomials and the second-order Helmholtz equation to solve a scattering problem. Later, based on Helmholtz equations, pseudospectral eigenmode solvers have been established for analyzing 2-D photonic crystals [21] and obtaining full-vector optical waveguide modes [22]. In this paper, we formulate our new PSFD method, instead, from the first-order differential equations using the similar scheme of a related Legendre pseudospectral time-domain (PSTD) method recently established [23] and utilizing the Legendre polynomials as the interpolation basis. Besides, the penalty scheme as developed in [23] is used to better handle boundary conditions for well-posedness consideration, and the perfectly matched layers (PMLs) [24]–[26]

are incorporated into the PSFD formulation to absorb outward propagating waves and effectively reduce reflection of out-going waves. The multidomain approach is employed, as in [23], with which the computational domain with the PMLs is divided into suitable number of subdomains, with the material interfaces fitting the sides of some subdomains, so that the field continuity conditions can be accurately fulfilled. The equations approximating the physical processes of the corresponding subdomains are finally packed into a linear matrix equation which can be easily solved by iterative algorithms. Using the PSFD method, we will show that numerical accuracy on the order of 10^{-9} can be achieved in the scattered-field calculation of a circular metallic cylinder, as compared with known analytical results provided in [27], [28]. More importantly, this PSFD method provides exponentially convergent rate in numerical accuracy with respect to grid resolution, which implies its efficiency in that few grid points added can exponentially increase computation accuracy. We believe this method can provide high-accuracy results in the analysis of electromagnetic field characteristics of plasmonic problems including the important ones of coupled cylinder structures.

The finite-difference time-domain (FDTD) method [9] has been a popular numerical analysis and simulation method in computational electromagnetics, including plasmonics. For curved material interfaces, the simple stair-casing approximation of such interfaces as often utilized in the FDTD calculation of the electromagnetic field may result in numerical-accuracy reduction in field values along the curved interface [29]. However, obtaining high-accuracy near fields for such situations can be important for understanding the plasmonic phenomenon and proposing relevant applications. More efforts must be paid for overcoming such stair-casing problem in the FDTD method, e.g., using the conformal scheme [30], the triangular mesh [31], the effective permittivity [32], etc. The PSFD method, however, can avoid such stair-casing problem since its subdomain partitioning with curvilinear geometries can match exactly to the shape of the structure interface [33], thus can provide accurate computation.

Furthermore, in numerically modeling the plasmonic structures, material dispersive properties of metals need to be carefully considered. In time-domain computation methods, the auxiliary differential equation (ADE) technique [9] can be employed to take into account the Drude-Lorentz material model for a metal in the simulation. But the parameters in the material dispersion model need to be carefully assigned through curve fitting the measured dielectric function of the metal [34], [35]. As a frequency-domain method, however, the PSFD method can directly adopt the measured or given complex dielectric constant of the metal at the considered frequency without needing the ADE approach and the associated curve-fitting procedure for treating material dispersion in the electromagnetic calculations.

The remainder of this paper is outlined as follows. Maxwell's equations with the penalty scheme for the 2-D scattering problem are described in Section II. The Legendre pseudospectral method is introduced in Section III. Scattering calculation results for a silver circular cylinder, a dielectric square cylinder, and several coupled metallic structures involving circular cylinders, square cylinders, or dielectric coated cylinders are presented and discussed in Section IV. Some remarks on the

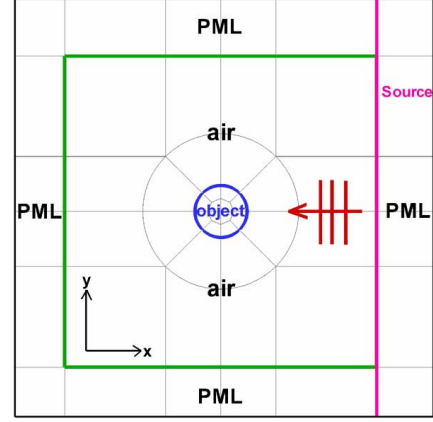


Fig. 1. Computational domain with pseudospectral subdomain division for the scenario in which a plane wave is scattered by a 2-D object.

proposed formulation and scheme are given in Section V. The conclusion is drawn in Section VI.

II. MAXWELL'S EQUATIONS WITH THE PENALTY SCHEME

For time-harmonic electromagnetic fields, \mathbf{E} and \mathbf{H} , in a linear isotropic medium region with permittivity ϵ and permeability μ , Maxwell's curl equations can be written in the complex form as

$$-j\omega\mu\mathbf{H} - \nabla \times \mathbf{E} = \mathbf{M} \quad (1a)$$

$$-j\omega\epsilon\mathbf{E} + \nabla \times \mathbf{H} = \mathbf{J} \quad (1b)$$

where \mathbf{J} and \mathbf{M} represent the source electric and magnetic current densities, respectively, and ω is the angular frequency. Here, we consider the 2-D problem with no field variation along the z direction. Fig. 1 shows one example scenario in which a plane wave is scattered by a 2-D circular cylinder. We particularly study the transverse-magnetic (TM) waves with E_x , E_y , and H_z field components because of plasmonics applications. Therefore, Maxwell's curl equations become three first-order equations as

$$-\frac{\partial H_z}{\partial y} - j\omega\epsilon E_x = J_x \quad (2a)$$

$$-\frac{\partial H_z}{\partial x} - j\omega\epsilon E_y = J_y \quad (2b)$$

$$\frac{\partial E_x}{\partial y} - \frac{\partial E_y}{\partial x} - j\omega\mu H_z = M_z. \quad (2c)$$

In the multidomain PSFD method, the computational domain is partitioned into suitable non-overlapping subdomains of curvilinear quadrilateral shape. Using the scattering by a circular cylinder as depicted in Fig. 1 as an example, if boundary conditions are rigorously considered at the interface between adjacent subdomains I and II with the unit normal vector perpendicular to the interface expressed as $\hat{n} = n_x\hat{x} + n_y\hat{y}$, the continuity of tangential fields across the interface for source-free dielectrics requires that

$$H_z^I = H_z^{II} \quad (3a)$$

$$E_t^I = E_t^{II} \quad (3b)$$

for the TM waves, where the superscripts, I and II , denote the subdomains and E_t denotes the tangential electric field, i.e., $E_t = n_y E_x - n_x E_y$.

In our formulation, an incident TM plane wave is generated by assigning a uniform y -directed source surface current density \mathbf{J}_s with unit A/m on the PML/air interface, as shown in Fig. 1, using the required boundary condition, $\hat{n} \times (\mathbf{H}^I - \mathbf{H}^{II}) = \mathbf{J}_s$, where I and II refer to the corresponding PML subdomain and air subdomain, respectively, and M_z is taken to be zero in (2c). This y -directed \mathbf{J}_s would generate both y -polarized rightward (to the PML) and leftward propagating plane waves [36], with the rightward wave absorbed by the PML. Note that the relation between \mathbf{J}_s and \mathbf{J} , the latter being the volume current density with unit A/m², is $\mathbf{J}_s = \int \mathbf{J} dx$ if \mathbf{J}_s flows in the y direction, and we would have $\mathbf{J} = \mathbf{J}_s/\omega_0$, where ω_0 is the quadrature weight on the interface which will be defined in the next section.

In [23], the Legendre PSTD formulation with the penalty scheme based on well-posed boundary impositions of physical boundary conditions in terms of characteristic variables has been discussed in detail. The same penalty scheme is employed here to impose weakly characteristic boundary conditions. Briefly speaking, (2) can be first written as

$$j\omega Mq + A_x \frac{\partial q}{\partial x} + A_y \frac{\partial q}{\partial y} = J_{\text{current}} \quad (4)$$

where $q = [E_x, E_y, H_z]^T$, $M = -\text{diag}[\epsilon, \epsilon, \mu]$, and the matrices A_x and A_y are simply constructed with 0, 1, and -1 corresponding to the presence of fields in (2). Next, the penalty term $P = (\delta/\omega_0)S(n)\Lambda[R(n) - R^{BC}(n)]$ will be added. The matrices, Λ and $S(n)$, are constructed respectively from the eigenvalues and eigenvectors of the matrix $A(n)$, which is defined as $A(n) = n_x A_x + n_y A_y$, and the characteristic state vectors $R(n)$ are defined as $R(n) = S^T(n)q$ as in [23]. Then, after matrix multiplications of $S(n)$, Λ , and $[R(n) - R^{BC}(n)]$ in the penalty term P , Maxwell's equations in (2) with penalty $(\tau/2)P$ added become

$$-j\omega\epsilon E_x^I + \frac{\partial H_z^I}{\partial y} - \frac{\tau}{2} \frac{\delta}{\omega_0} n_y^I (H_z^I - H_z^{II}) = J_x \quad (5a)$$

$$-j\omega\epsilon E_y^I - \frac{\partial H_z^I}{\partial x} + \frac{\tau}{2} \frac{\delta}{\omega_0} n_x^I (H_z^I - H_z^{II}) = J_y \quad (5b)$$

$$\begin{aligned} -j\omega\mu H_z^I + \frac{\partial E_x^I}{\partial y} - \frac{\partial E_y^I}{\partial x} - \frac{\tau}{2} \frac{\delta}{\omega_0} n_y^I (E_x^I - E_x^{II}) \\ + \frac{\tau}{2} \frac{\delta}{\omega_0} n_x^I (E_y^I - E_y^{II}) = M_z \end{aligned} \quad (5c)$$

where δ is unity when the grid point is on the boundary edge, and is zero otherwise [23]. The variable τ is a free parameter defined by Theorem 3.1 in [23] with value $\tau \geq 1$ for supporting (5) to be a convergent system during iteration processes. In the PML subdomains, (5) are rewritten, following the derivations in [23] and [26], as

$$\begin{aligned} -j\omega\epsilon E_x^I + (2\sigma_y - j\sigma_y^2)\omega\epsilon E_x^I + \frac{\partial H_z^I}{\partial y} \\ - \frac{\tau}{2} \frac{\delta}{\omega_0} n_y^I (H_z^I - H_z^{II}) = J_x \end{aligned} \quad (6a)$$

$$\begin{aligned} -j\omega\epsilon E_y^I - (2\sigma_x - j\sigma_x^2)\omega\epsilon E_y^I - \frac{\partial H_z^I}{\partial x} \\ + \frac{\tau}{2} \frac{\delta}{\omega_0} n_x^I (H_z^I - H_z^{II}) = J_y \end{aligned} \quad (6b)$$

$$\begin{aligned} -j\omega\mu H_z^I + \frac{\sigma'_y}{j\omega + \sigma_y} E_x^I \\ - \frac{\sigma'_x}{j\omega + \sigma_x} E_y^I + \frac{\partial E_x^I}{\partial y} - \frac{\partial E_y^I}{\partial x} \\ - \frac{\tau}{2} \frac{\delta}{\omega_0} n_y^I (E_x^I - E_x^{II}) + \frac{\tau}{2} \frac{\delta}{\omega_0} n_x^I (E_y^I - E_y^{II}) = M_z \end{aligned} \quad (6c)$$

where σ_x and σ_y are absorbing profiles along the x and y axes, respectively, and σ'_i denotes the derivative of σ_i with respect to i ($i = x, y$). Taking σ_x as an example, we choose $\sigma_x = \kappa(|x - x_0|/L_{\text{PML}})^m$, where $|x - x_0|$ is the distance of the point, x , from the initial point, x_0 , L_{PML} is the total length of PML, and the parameters κ and m are free variables for tuning the PML performance. After employing the Legendre pseudospectral scheme and packing all subdomains, (5) and (6) would lead to a linear matrix equation, $AX = B$, with the unknown vector X consisting of \mathbf{E} and \mathbf{H} fields, the vector B corresponding to the known sources, and the A matrix consisting of spatial differential operators and penalty terms. The unknown electric and magnetic fields can be solved from $X = A^{-1}B$ using efficient iterative algorithms such as the bi-conjugate gradient (BiCG) method.

III. LEGENDRE PSEUDOSPECTRAL METHOD

Now, we discuss the Legendre pseudospectral method for numerically treating the spatial derivatives in the above governing equations. Under the multidomain scheme, each curvilinear quadrilateral subdomain region in Cartesian coordinates (x, y) can be mapped onto a square region $[-1, 1] \times [-1, 1]$ in curvilinear coordinates (ξ, η) by using the transfinite blending function described in [29] to construct $\xi = \xi(x, y)$ and $\eta = \eta(x, y)$. Applying the chain rule, derivatives of a 2-D function $f(x, y)$ will then become

$$\frac{\partial f(x, y)}{\partial x} = \frac{\partial \xi}{\partial x} \frac{\partial f(x, y)}{\partial \xi} + \frac{\partial \eta}{\partial x} \frac{\partial f(x, y)}{\partial \eta} \quad (7a)$$

$$\frac{\partial f(x, y)}{\partial y} = \frac{\partial \xi}{\partial y} \frac{\partial f(x, y)}{\partial \xi} + \frac{\partial \eta}{\partial y} \frac{\partial f(x, y)}{\partial \eta}. \quad (7b)$$

Some properties of Legendre polynomials, which we use as the basis for the interpolation of a function, will be given below.

In the Legendre pseudospectral method, spatial arrangement of grid points is defined by the Legendre–Gauss–Lobatto (LGL) quadrature points ξ_i arranged in the interval $[-1, 1]$, which are the roots of the polynomial $(1 - \xi^2)P'_N(\xi)$ [23] with the prime denoting derivative and P_N being the Legendre polynomial of degree N defined by

$$P_N(\xi) = \frac{1}{2^N N!} \frac{d^N}{d\xi^N} (\xi^2 - 1)^N. \quad (8)$$

Associated with these LGL quadrature points are a set of quadrature weights ω_i for $i = 0, 1, 2, \dots, N$. If $f(\xi)$ is a

polynomial of degree at most $2N + 1$, we have the quadrature rule [23]

$$\sum_{i=0}^N f(\xi_i) \omega_i = \int_{-1}^1 f(\xi) d\xi \quad (9)$$

where the quadrature weights are defined by

$$\omega_i = \begin{cases} \frac{2}{N(N+1)}, & i = 0, N \\ -\frac{2}{(N+1)} \frac{1}{P_N(\xi_i) P'_{N-1}(\xi_i)}, & \text{otherwise.} \end{cases} \quad (10)$$

Based on these LGL collocation points, one can use the degree- N Lagrange interpolation polynomials $l_j(\xi)$ as the bases to approximate an arbitrary function $f(\xi)$ such that

$$f(\xi) \approx \sum_{j=0}^N f(\xi_j) l_j(\xi) \quad (11)$$

where

$$l_j(\xi) = -\frac{(1 - \xi^2) P'_N(\xi)}{N(N+1)(\xi - \xi_j) P_N(\xi_j)}. \quad (12)$$

Then, the derivative of the function $f(\xi)$ at the LGL quadrature point ξ_i can also be approximated as

$$\frac{df(\xi_i)}{d\xi} \approx \sum_{j=0}^N \frac{dl_j(\xi_i)}{d\xi} f(\xi_j) = \sum_{j=0}^N D_{ij} f(\xi_j). \quad (13)$$

The differential coefficient D_{ij} is defined in [23] by

$$D_{ij} = \begin{cases} -\frac{N(N+1)}{4}, & i = 0 \\ \frac{N(N+1)}{4}, & i = N \\ 0, & \text{otherwise} \end{cases} \quad (14)$$

if $i = j$; and

$$D_{ij} = \frac{P_N(\xi_i)}{P_N(\xi_j)} \frac{1}{\xi_i - \xi_j} \quad (15)$$

if $i \neq j$. The so-called differential matrix operator with D_{ij} elements can thus be substituted into the spatial derivative in (13) as

$$\frac{\partial}{\partial \xi} = \begin{bmatrix} D_{00} & D_{01} & \cdots & D_{0N} \\ D_{10} & D_{11} & \cdots & D_{1N} \\ \vdots & \vdots & \ddots & \vdots \\ D_{N0} & D_{N1} & \cdots & D_{NN} \end{bmatrix}. \quad (16)$$

This is the key feature of the Legendre PSFD method, i.e., for the 1-D example, the derivative of $f(\xi)$ at an LGL point ξ_i in the region $[-1, 1]$ can be approximated in terms of $f(\xi)$ values at the $N + 1$ LGL points in the same region. Spatial derivatives of fields in (5)–(7) can be simply replaced by these differential matrix operators D_{ij} in the linear matrix system. The matrix A thus becomes a sparse matrix containing penalty, PML, and D_{ij} terms. Note that those D_{ij} terms for spatial derivatives repeatedly appear in A and are located with regularity, thus only this small D matrix in (16) is needed to be stored and our PSFD implementation will be memory-saving, which can then be applied to solve large problems or those requiring dense grid points. In

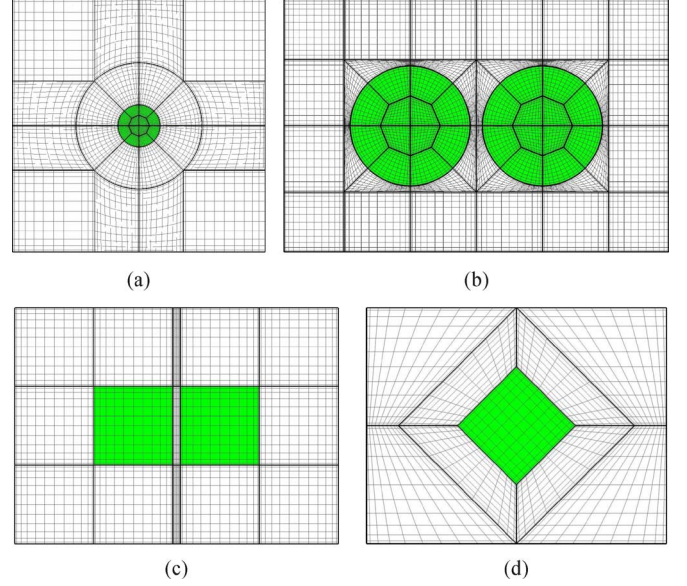


Fig. 2. Portion of the subdomain division profile in the computational domain near the cylinder scatterers (the colored region) for $N = 12$. (a) A single circular cylinder. (b) Two coupled circular cylinders. (c) Two coupled rectangular cylinders. (d) 45° -tilted square cylinder.

Fig. 2, the grid meshes based on the LGL points in each subdomain, except the PML ones, are plotted for $N = 12$. As shown in the figure, the curved structure and the whole computational region are partitioned into curvilinear subdomains, and $(N + 1) \times (N + 1)$ LGL grid points are not uniformly distributed but somewhat following the outline of the domain edges. Please note that the LGL grid points at each edge side of a subdomain are collocated with the LGL grid points at one edge side of its adjacent subdomain. These collocated grid points are counted as distinct sets of points, and the penalty scheme is applied on the two sets for exchanging information of boundary conditions.

IV. NUMERICAL RESULTS

Here, the PSFD method is applied to analyze some basic scattering problems. Accuracy will be first verified by examining a circular-metallic-cylinder problem and comparing the results with those obtained from the analytical approach. With the high accuracy provided, the PSFD method is then applied to simulate several coupled structures between closely placed, in nanometer scale, metallic cylinders and investigate their optical behaviors.

A. Single Circular Metallic Cylinder

First, we examine the accuracy of the formulated Legendre PSFD method by solving a simple problem of TM scattering of a plane wave by a silver circular cylinder in free space at an optical wavelength. Such problem is known to have an analytical solution [27], [28]. Nevertheless, it is a good example to test how accurate a numerical analysis method can perform when dealing with plasmonic structures. The computational-domain setup with PMLs and the subdomain division is as shown in Fig. 1, and the grid mesh is as depicted in Fig. 2(a). The radius of the cylinder is $R = 0.25 \mu\text{m}$ and the wavelength of the incident plane wave is $\lambda = 1 \mu\text{m}$. At this wavelength, the

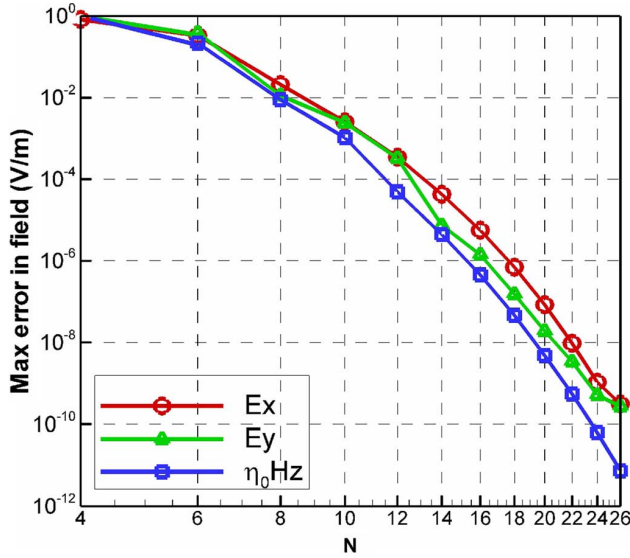


Fig. 3. Maximum absolute difference between the PSFD calculated field value and its corresponding analytical one scanned over the computational domain versus the degree N of the Legendre polynomial used for the E_x , E_y , and H_z components, respectively, for TM scattering of a plane light wave at $\lambda = 1 \mu\text{m}$ by a silver circular cylinder of radius $0.25 \mu\text{m}$ in free space.

measured complex dielectric constant of silver is about $\varepsilon_r = -50.981 + i0.562$ [34]. Fig. 3 shows the maximum absolute difference, $|\Delta q|$, between the PSFD calculated field value and its corresponding analytical one scanned over the computational domain versus the degree N of the Legendre polynomial used for the E_x , E_y , and H_z components, respectively, when the incident electric field intensity is 1 V/m, where q refers to the field component. For H_z , the difference in $\eta_0 H_z$ is considered, where η_0 is the free-space impedance. It is seen that the errors are on the order of 10^{-2} when $N = 8$ and on the order of 10^{-4} when $N = 12$ and can get down to 10^{-9} when $N > 22$. These results demonstrate that our PSFD algorithm can provide high accuracy for solving light scattering by plasmonic structures. Also, the convergent plots show that the error exponentially, rather than linearly, decreases with respect to N . This is the inherent characteristic of the spectral method having the convergent ratio proportional to $(\Delta x)^N \sim (1/N)^N$. Fig. 4(a)–(c) plots the field profiles for $|E_x|$, $|E_y|$, and $\eta_0 |H_z|$, respectively, when the incident TM wave comes from right with $|E_y|$ polarization. The computing resources used are described as follows. For $N = 6, 8, 10$, and 12 , the required matrix sizes are 31 164, 51 516, 76 956, and 107 484, respectively, the computer running times are 175, 429, 958, and 1970 s, respectively, and the memory usages are 9, 14, 20, and 27 Mb, respectively, executed by a single processing core on a personal computer with quad-core i7 3.42-GHz CPU in Linux environment. The computation time approximately doubles as N is increased by two, and the memory usages are not much. Note that the accuracy with $N = 12$ can be more than what is required in practice since the error in the calculated field is on the order of 10^{-4} as mentioned above.

In this verifying example of the PSFD method achieving such high accuracy, PML tuning is also an important process. From the given absorbing profile σ of PML, free parameters κ and m can be varied to optimize the accuracy. According to our

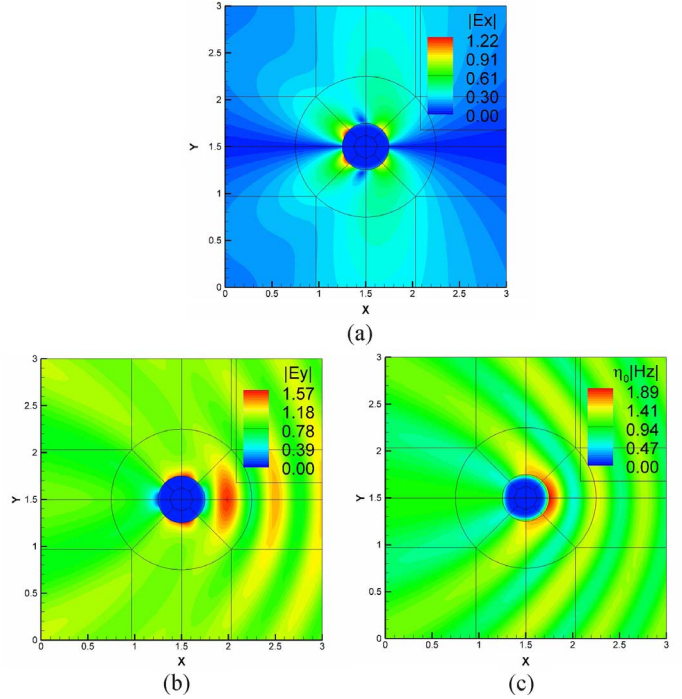


Fig. 4. Field profiles for (a) $|E_x|$, (b) $|E_y|$, and (c) $|H_z|$, respectively, for the case of Fig. 3, with the incident wave propagating from right to left.

experiences and in this case, the choices of $20 \leq \kappa \leq 30$ and $m = 2$ or 3 can provide better results as shown. This gives a gradually growing profile, and we adopt a wide PML with $3\text{-}\mu\text{m}$ thickness for reducing reflection of waves.

B. The Single Dielectric Square Cylinder

Scattering of a 45° -tilted dielectric square cylinder investigated in [37] is considered next. The side length of the square is $d = 3.5/k$, where $k = 2\pi/\lambda_0$ is the free-space wavenumber, and the plane wave incidence is as indicated in the inset of Fig. 5 with wavelength λ_0 . Here, the dimensions are all normalized to k according to [37], so the size of the dielectric cylinder is measured in terms of $\lambda_0/(2\pi)$. Note that the square was assumed in [37] to have rounded corners with a radius of curvature $\rho = 0.01/k$ but it is assumed to have sharp corners in our calculations. Thus, there would be four singular points expected at these sharp corners in our results. The tangential electric field of the TM case versus kS , where S is the distance along the upper square surface from the left apex to the right apex, is shown in Fig. 5(a) and (b) for cylinders of dielectric constants $\varepsilon_r = 2.5$ and $\varepsilon_r = 10$, respectively. The calculations were done for N from 12 up to 28. The results are seen to well agree with those of [37], even for smaller N s. Notice that the fields at the singular points, $kS = 3.5$ for example, grow up as the grid resolution (or N) increases. Here, we used only one subdomain for this square structure, and there are $2 \times (N + 1)$ points along $kS = 0$ to $kS = 7$. The field distributions with $\varepsilon_r = 10$ are depicted in Fig. 6. Because the incident wave comes from the left, the fields are seen to be longitudinally symmetric. The singular points can be observed at the upper and bottom apices in Fig. 6(b). To observe more clearly the singular-point characteristics, the expanded view of those results in Fig. 5(a) near $kS = 3.5$ is shown in Fig. 5(c). Note that, at $kS = 3.5$, there

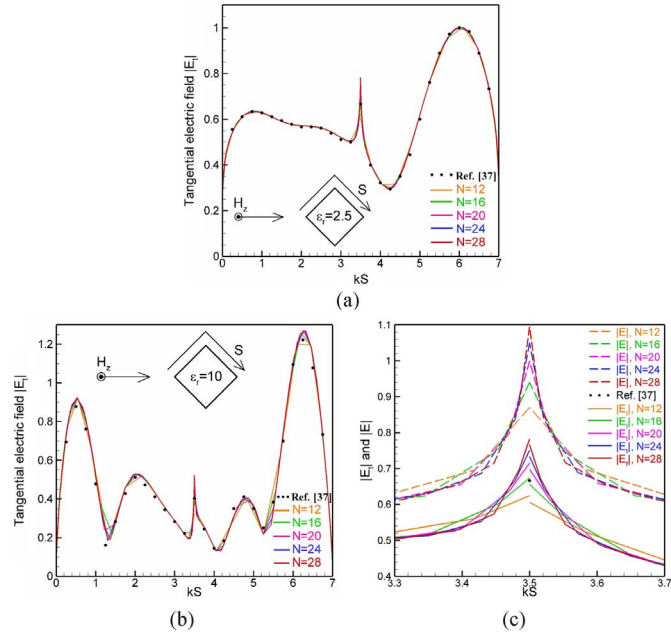


Fig. 5. Tangential electric field ($|E_t|$) versus kS ($k = 2\pi/\lambda_0$) for (a) $\epsilon_r = 2.5$ and (b) $\epsilon_r = 10$ for the scattering of a 45° -tilted dielectric square cylinder with side length $d = 3.5/k$. The dots are adopted from [37] and other lines stand for PSFD calculated results of different degrees (N). (c) The expanded view of those results in (a) near $kS = 3.5$ together with the corresponding PSFD calculated total electric field ($|E|$) results for showing the singular electric-field characteristic at the dielectric corners.

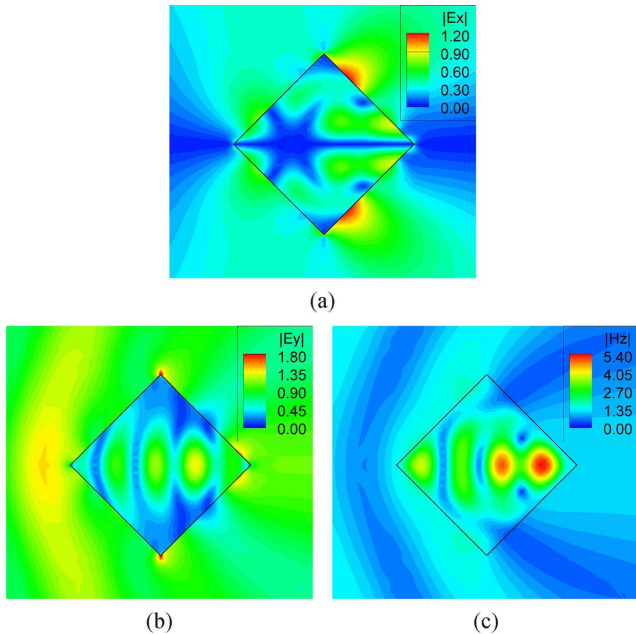


Fig. 6. Field profiles for (a) $|E_x|$, (b) $|E_y|$, and (c) $|H_z|$, respectively, for the case of Fig. 5(b).

are two $|E_t|$ values for each N since the tangential component value referring to the left side and that referring to the right side are different. Also displayed in Fig. 5(c) are the corresponding profiles for the magnitudes of the total electric field, $|E|$, which show sharper singular behavior. The subdomain division profile near the square cylinder is plotted in Fig. 2(d).

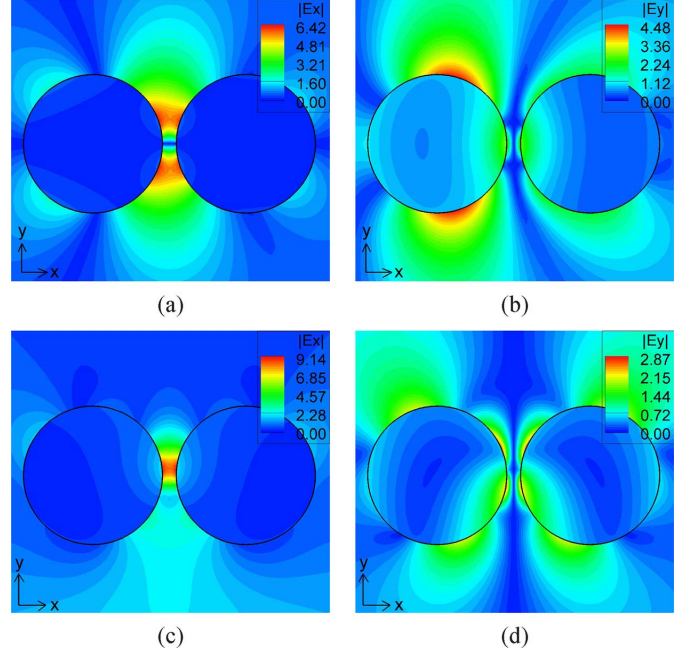


Fig. 7. $|E_x|$ and $|E_y|$ field distributions for plane-wave scattering by two coupled silver circular cylinders. The plane wave is incident from left in (a) and (b), and from bottom in (c) and (d). The radii are 50 nm and the side spacing between the two cylinders is 10 nm.

C. Two Coupled Circular Metallic Cylinders

The field coupling between metallic nanoparticles plays an important role in plasmonic research, which in particular may result in strong local-field enhancement that can provide many useful applications. We apply the PSFD method to study the phenomenon of field coupling between two silver nano-cylinders, with focus on two closely placed cylinders interacting with incident light waves of different directions and polarizations.

The first case is a system of two 50-nm-radius circular cylinders with 10-nm spacing allocated along the x -axis. For the $|E_x|$ and $|E_y|$ distribution results shown in Fig. 7(a) and (b), the wave is incident from left at $\lambda = 0.421 \mu\text{m}$ and with E_y polarization. The measured complex dielectric constant of silver at this wavelength is $-5.598 + i0.213$. The two cylinders are coupled such that strong electric field enhancement occurs within the gap between them, with the maximum $|E_x|$ being about 6.42 times the incident electric field intensity, as indicated in the color bar in Fig. 7(a). Due to the direction of the incident wave, the electric field profile is longitudinally symmetric with respect to the arrangement of cylinders. There is a null at the center, and the fields below and above it are oppositely signed in phase. Also, the incident E_y polarization causes the first cylinder to oscillate with strong E_y fields on both y -ended surfaces, as depicted in Fig. 7(b), and less influence is on the second cylinder due to the shielding from the first cylinder.

If the propagation direction of the incident wave is changed to be bottom-up with E_x polarization, strong field enhancement occurs at $\lambda = 0.4 \mu\text{m}$ with the $|E_x|$ and $|E_y|$ field distributions shown in Fig. 7(c) and (d), respectively. At this wavelength, the measured complex dielectric constant of silver is about $-4.435 + i0.211$. In this case, obviously, the incident E_x field leads the free electrons in both cylinders to oscillate horizontally and induces a strongly coupled E_x field within the gap,

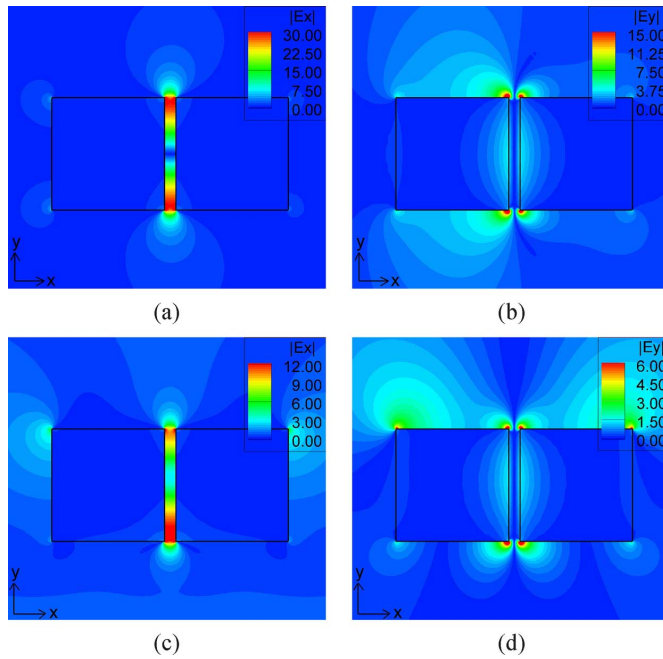


Fig. 8. $|E_x|$ and $|E_y|$ field distributions for plane-wave scattering by two coupled silver rectangular cylinders. The plane wave is incident from left in (a) and (b), and from bottom in (c) and (d). The edge length are 100 nm and the side spacing between the two cylinders is 10 nm.

which is about 9.14 times enhancement. Note that the maximum induced E_x field is not exactly located right at the center, but about 5 nm upper. The induced E_y field is transversely symmetric and not strongly enhanced, and the E_y phases of the two cylinders are reversed such that there also exists a null in between. It is seen in the above two situations that the plane wave incident from the bottom provides higher field enhancement than that from the left.

D. Two Coupled Square Metallic Cylinders

Next, we study the field coupling between two square metallic cylinders. Different from the circular ones, the square cylinders have four sharp corners, which would cause singular points and thus induce extremely, infinity theoretically, strong fields would exist around these apexes, causing challenges in numerical computations.

The simulated case is a system of two square cylinders, each having 100-nm edge width, again with 10-nm spacing. This structure is to be compared with the above one of circular cylinders. Fig. 8(a) and (b) shows the $|E_x|$ and $|E_y|$ distributions when the wave is incident from left at $\lambda = 0.627 \mu\text{m}$. The complex dielectric constant of silver at this wavelength is about $-17.98 + i0.485$. From the $|E_x|$ field shown in Fig. 8(a), it reveals two spots of field enhancement at the upper and lower corners in the gap, with the field enhancement being as high as up to 30 times. The calculated fields at the apexes would be even higher as N is increased. As in the case of coupled circular cylinders, the $|E_y|$ profile is distributed mainly at both y -ended edges of the first cylinder. The appearance of symmetric upper and lower field-enhancement regions is quite similar to those in Fig. 7(a) and (b).

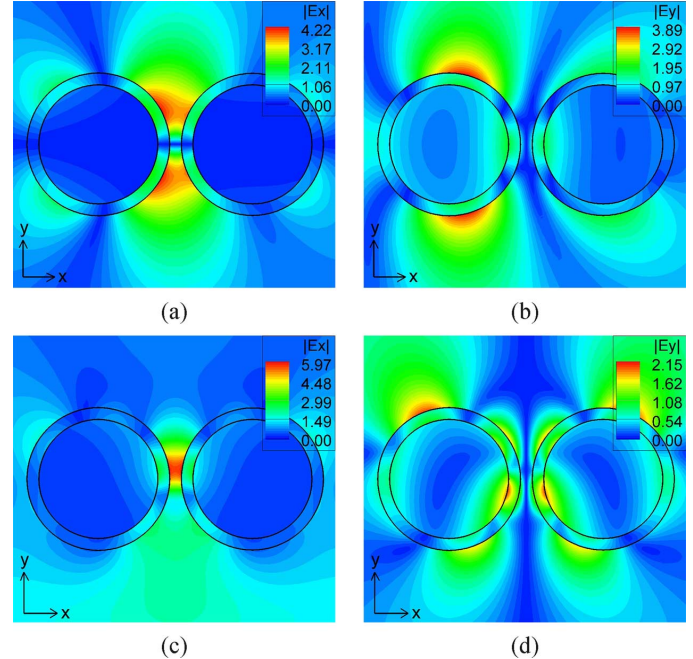


Fig. 9. $|E_x|$ and $|E_y|$ field distributions for plane-wave scattering by two coupled silver circular cylinders having a dielectric coating of 10-nm thickness. The plane wave is incident from left in (a) and (b), and from bottom in (c) and (d).

Likewise, if we change the incident wave direction to bottom-up at $\lambda = 0.613 \mu\text{m}$, the strong $|E_x|$ enhancement appears in the gap near the bottom corner, as shown in Fig. 8(c), due to the x -polarized incident field, with the enhancement being up to 12 times, which is smaller than that in Fig. 8(a). The complex dielectric constant of silver at this wavelength is $-16.96 + i0.485$. Note that the field is now not enhanced at the center but near the bottom of the gap. Opposite field phases in Fig. 8(a) with respect to horizontal symmetric plane and in Fig. 8(d) with respect to the vertical symmetric plane in Fig. 8(d) cause obvious null-field appearances within the gap region.

E. Two Coupled Metallic Cylinders With Dielectric Coating

We further study the situations with each of the cylinders in Figs. 7 and 8 coated with a 10-nm-thickness dielectric layer of dielectric constant $\epsilon_r = 3$. We maintain the diameter or edge width of each silver cylinder, and the gap size is still kept as 10 nm. It is known that this outer dielectric material can make the plasmonic resonant frequency shifted, but the optical field characteristics are rarely seen, especially for coupled cylinders. The results corresponding to Fig. 7 are shown in Fig. 9 and those corresponding to Fig. 8 are shown in Fig. 10. The incident wavelengths in Fig. 9(a)–(b), Fig. 9(c)–(d), and Fig. 10(a)–(b), and Fig. 10(c)–(d) are 0.467, 0.417, 0.649, and 0.616 μm , respectively, with the corresponding complex dielectric constants of $-7.97 + i0.270$, $-5.42 + i0.219$, $-19.42 + i0.46$, and $-17.193 + i0.496$, respectively. The characteristics of $|E_x|$ and $|E_y|$ profiles are seen to be quite similar with those in Figs. 7 and 8, but the localized fields now appear mainly at the dielectric-dielectric interfaces and in the gaps, which could reduce the ohmic losses in the metals. The field enhancement is found to be lower compared with uncoated cases, which can be explained by the

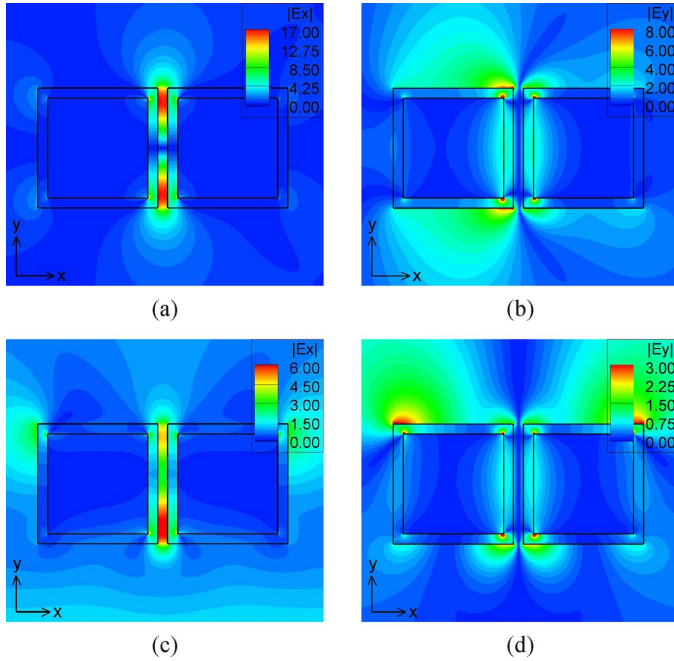


Fig. 10. $|E_x|$ and $|E_y|$ field distributions for plane-wave scattering by two coupled silver rectangular cylinders having a dielectric coating of 10-nm thickness. The plane wave is incident from left to right in (a) and (b) and from bottom in (c) and (d).

fact that the actual distance between the metallic cylinders is 30 nm rather than 10 nm.

F. Three Pairs of Circular Metallic Cylinders

We finally investigate two-by-three arranged six-silver-cylinder arrays studied in [10], where the FDTD method was used for simulations. This cylinder arrangement is shown to give not only particle-particle but pair-pair interactions, thus strong localized field enhancement could be generated in the gap of the middle pair [10]. In [10], measured material characteristics for silver given in [35] instead of [34] were used. We also adopt the data in [35] in our calculations for comparison. Our PSFD results given in Fig. 11 are for the incident wave from left to right and the spacing between adjacent cylinders being 20 nm. In [10], it was found that with gap size of 20 nm and at $\lambda = 460$ nm, the maximum field enhancement of about 8.89 occurs when the cylinder radius is 36 nm. Our PSFD simulated $|E|$ profile for this case is shown in Fig. 11(a), where the maximum $|E|$ field value is 11.11 V/m, referring to the incident field of 1 V/m, and the field value at the center of the gap of the middle pair is about 9.33 V/m, which is larger than that value of [10] by 4.72%. The $|E|$ value is defined here by $|E| = (|E_x|^2 + |E_y|^2)^{1/2}$. The measured complex dielectric constant of silver given in [35] is about $\epsilon_r = -6.53 + i0.737$ at this wavelength. If the value given in [34], $\epsilon_r = -7.585 + i0.245$, is used, the PSFD calculated maximum $|E|$ field value and the field value at the center of the gap of the middle pair would be about 13.78 and 11.65 V/m, respectively.

When the wavelength is changed to 650 nm, the cylinder radius was found in [10] to be 58 nm for generating largest field enhancement of 13.04. Our results for this case are presented

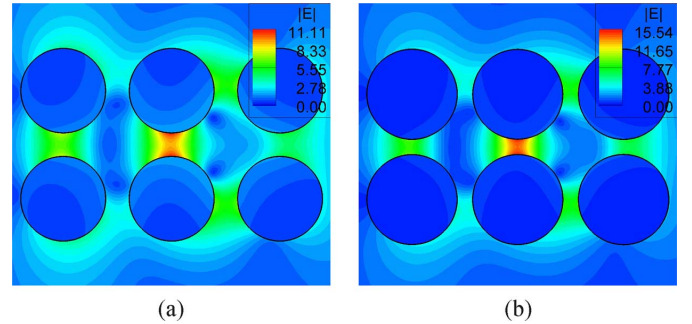


Fig. 11. $|E|$ field distributions for plane-wave scattering by six silver circular cylinders with incident wave from left. (a) Cylinder radius $R = 36$ nm at $\lambda = 460$ nm. (b) Cylinder radius $R = 58$ nm at $\lambda = 650$ nm. All gap widths are 20 nm.

in Fig. 11(b), where the maximum $|E|$ field is 15.54 V/m and the field value at the same gap center is about 14.09 V/m, again larger than those values of [10] by 8.05%. The complex dielectric constant of silver cylinder is about $\epsilon_r = -17.2 + i1.16$ from [35] for this incident wavelength. Again, if we choose to adopt the measured parameter from [34], which is $\epsilon_r = -19.493 + i0.462$, the PSFD calculated maximum $|E|$ field value and the field value at the center of the gap of the middle pair would be about 17.07 V/m and 15.51 V/m, respectively.

V. SOME REMARKS ON THE PROPOSED FORMULATION AND SCHEME

The proposed pseudospectral formulation and scheme in this paper have been based on the Legendre collocation points, the first-order Maxwell's equations, and the penalty scheme for interface conditions, which are in contrast to some existing ones based on the Chebyshev collocation points, the second-order Helmholtz equations, and/or directly matching interface conditions. The advantages of our ones are discussed in the following.

A. Legendre Collocation Points Versus Chebyshev Collocation Points

A major factor, which makes the Chebyshev pseudospectral approximations based on the Chebyshev–Gauss–Lobatto points more popular than the Legendre pseudospectral approximations based on the Legendre–Gauss–Lobatto points, is the fast Fourier transform (FFT). This technique allows the numerical derivatives to be computed in $N \log(N)$ operations. Indeed, Chebyshev pseudospectral method is very attractive for problems defined on regular domains, based on single domain computational framework. For these problems, either time-dependent or time-independent, if the required number of grid points is beyond 100, then the FFT technique does improve the computational efficiency. However, in a multidomain computational framework which can be used to solve problems defined on complicated domains, the number of grid points in each subdomain is generally much less than 100 and thus, we do not gain efficiency on using Chebyshev pseudospectral method [38]. Of course this does not mean we need to use Legendre pseudospectral method instead. The reason of using Legendre pseudospectral approximation will be discussed after addressing issues related to the penalty methodology of imposing boundary conditions.

B. Penalty Method for Interface Conditions and Directly Matching Interface Conditions

We now address issues related to the approaches of imposing boundary conditions. Generally speaking, an interface boundary condition is a constraint relating field values on both sides of the interface in a specific way, possibly involving differentiations and geometrical parameters. In the present study, the geometrical parameter is the unit vector normal to the interface. In a multidomain computational framework, a problem domain is decomposed into a union of subdomains. Thus, at the subdomain interfaces we need to enforce interface boundary conditions. As a consequence, it is necessary to specify a unique normal vector at every boundary grid point, and this becomes a problem at a vertex point of a 2-D subdomain. Is it possible to assign a unique normal vector at a vertex point? Or does it exist a unique normal vector at a vertex point? Frankly speaking, we have no answer to the problem and we doubt that there is an answer to the problem. Thus, this becomes a problem when we want to impose boundary condition through a directly matching approach at a location shared by vertex points of different subdomains, and great care must be exercised to resolve this issue. In contrast, the penalty methodology offers an edge-by-edge approach to impose boundary conditions [23], [39], [40]. It is not necessary to specify a unique normal vector at a vertex point, because a vertex point is an intersection of two boundary edges of a subdomain. Since we can specify normal vector functions along the edges of a subdomain, we define two normal vectors at a vertex point based on the normal vectors on the edges that intersect at the vertex. As a result, every vertex point is enforced with two penalty boundary conditions with field values from two attached edges belonging to different subdomains. This does not ruin the consistency (accuracy) of the scheme at all. As we have shown in our numerical experiments, the results are exponentially convergent. This explains why we adopt the penalty methodology for imposing boundary conditions.

C. Why the Legendre Pseudospectral Method?

The penalty method incorporates numerical partial differential equations and boundary conditions through a linear combination parameterized by a penalty parameter [23], [39]–[41]. The value of this parameter is commonly determined such that the scheme is stable in an energy sense. To conduct such an analysis, one needs to establish a discrete energy norm measurement. This issue makes Legendre pseudospectral method very attractive, because Legendre pseudospectral method is equipped with a quadrature integration rule (Legendre–Gauss–Lobatto quadrature rule) which can be used to construct a discrete L_2 norm measurement for grid-functions [42]. The Chebyshev pseudospectral method also has a quadrature integration rule [42]. However, the rule does not coincide with the usual L_2 energy norm measurements for functions. Using the Legendre–Gauss–Lobatto quadrature rule to conduct an energy estimate, one can determine the value of the penalty parameter to ensure the stability of a scheme in a theoretical basis, instead of a trial-and-error basis. This procedure is useful and important, because high-order accurate numerical methods, compared to the low-order accurate ones, are very sensitive to the impositions of boundary conditions [42], [43]. For time-dependent problems, if boundary conditions are not imposed

properly, it often causes numerical blow-up solutions because of numerical instability inducing from subdomain boundaries. For time-independent or time-harmonic problems, improper impositions of boundary conditions may cause non-convergent solutions during iteration processes. Roughly speaking, these instabilities and nonconvergence problems are often resulting from numerical solution operators being unstable, in the sense that some eigenvalues of the solution operators have positive real part, commonly due to the impositions of boundary conditions. To avoid these unwanted situations, constructing a L_2 energy stable scheme in the theoretical stage becomes important in building a multidomain computational framework for simulations. Thus, based on the above arguments we adopt the Legendre pseudospectral method instead of the Chebyshev pseudospectral methods.

D. Why First-Order Maxwell's Equations Instead of Second-Order Helmholtz Equations?

In the present study, we solve first-order system Maxwell's equations instead of the equivalent second-order Helmholtz equations. This approach, indeed, is a drawback of the present formulation because it requires to solve more equations. In 2-D space, three coupled first-order partial differential equations need to be solved but only one equation to be solved if the problem is described by the second-order Helmholtz equation. However, the present first-order system formulation can be directly extended for waves in anisotropic media, even possibly with permittivity or permeability of media being a tensor. It is because the material parameters are not associated with the curl operator parts [23], [40]. Thus, we do not need to reformulate the penalty boundary condition formulations. As mentioned earlier, the penalty type boundary formulations avoid the ambiguity of specifying normal vectors at subdomain vertex points and this simplifies the imposing of interface boundary conditions. Of course, it would be even more attractive to construct pseudospectral penalty schemes for Helmholtz equations directly. A possible way is first identifying well-posed boundary operators for vectorial second-order wave equations which are the time-domain representation of Helmholtz equations. Once the well-posed operators for the second-order wave equations are identified, a pseudospectral penalty scheme may be formulated for the second-order wave equations. We can then easily convert the time-domain scheme to frequency-domain equations, which becomes a pseudospectral penalty scheme for the equivalent Helmholtz equations. We are putting our effort on this subject and hope to report the results in the future.

VI. CONCLUSION

A multidomain PSFD method has been developed based on the Legendre polynomials and a penalty scheme for solving Maxwell's equations. The application is particularly aimed at electromagnetic wave scattering problems in plasmonics with the goal of obtaining high-accuracy near fields. Calculation of light scattering by a silver circular cylinder has demonstrated that this PSFD method indeed provides high-order accuracy with the obtained field error down to 10^{-9} referring to 1-V/m incident electric field strength, thanks to the spectral convergence property of the spectral method and the accurate fulfillment of the field continuity conditions across the material interfaces provided by the multidomain approach as well as global

interpolation by Legendre polynomials. In the multidomain approach, the whole computational domain is properly partitioned into curvilinear subdomains fitting the generally curved material-interface shapes. With this demonstrated extremely high numerical accuracy, the formulated method should be useful for plasmonics research and can provide reliable results for the calculation of field enhancement near metal surface, as shown in the numerical examples including coupled plasmonic cylinders of either circular or square shape. Our analysis results also provide a good reference for other numerical methods to compare with. Moreover, the frequency-domain approach has the advantage of directly using a given complex dielectric constant of the material in the calculation with no need of implementing a dispersive material model like in the time-domain approach.

A final remark goes to the possible singular-field behavior when the material interface is non-smooth such as in the square-shaped-cylinder cases, as was discussed in connection with Fig. 5. Although the spectral convergence property of the PSFD method has been demonstrated when simulating round cylinders, when interface corners appear, numerical convergence would unavoidably be degraded. In Fig. 5(c), it was demonstrated that, although only one subdomain is employed for the square-cylinder cross-section, the singular-field characteristic evolves as the degree N in the PSFD calculation is increased so that the grid size near the dielectric corner shrinks. Related treatment of such singularities based on the finite element method has been reported through using algebraically graded grids near the corner where a singularity exists [38]–[40]. Further treatment and more detailed study about the corner singularities using the PSFD method, such as with refined arrangement of subdomains, would worth being pursued as a more basic topic.

ACKNOWLEDGMENT

The authors would like to thank the National Center for High-Performance Computing, Hsinchu, Taiwan, the Academia Sinica Computing Center, Taipei, Taiwan, and the Computer and Information Networking Center, National Taiwan University, Taipei, for providing useful computing resources.

REFERENCES

- [1] S. A. Maier and H. A. Atwater, "Plasmonics: Localization and guiding of electromagnetic energy in metal/dielectric structures," *J. Appl. Phys.*, vol. 98, no. 1, Jul. 2005, Art. ID 011101.
- [2] M. Moskovits, "Surface-enhanced spectroscopy," *Rev. Mod. Phys.*, vol. 57, no. 3, pp. 783–826, July 1985.
- [3] P. Mülschlegel, H. J. Eisler, O. J. F. Martin, B. Hecht, and D. W. Pohl, "Resonant optical antennas," *Science*, vol. 308, pp. 1607–1609, 2005.
- [4] S. A. Maier, P. G. Kik, and H. A. Atwater, "Optical pulse propagation in metal nanoparticle chain waveguides," *Phys. Rev. B*, vol. 67, p. 205402, 2003.
- [5] J. P. Kottmann and O. J. F. Martin, "Retardation-induced plasmon resonances in coupled nanoparticles," *Opt. Lett.*, vol. 26, no. 14, pp. 1096–1098, July 2001.
- [6] C. F. Bohren and D. R. Huffman, *Absorption and Scattering of Light by Small Particles*. New York: Wiley, 1983.
- [7] R. L. Chern, X. X. Liu, and C. C. Chang, "Particle plasmons of metal nanospheres: Application of multiple scattering approach," *Phys. Rev. E*, vol. 76, 2007, Art. ID 016609.
- [8] R. Gomez-Medina, M. Laroche, and J. J. Saenz, "Extraordinary optical reflection from sub-wavelength cylinder arrays," *Opt. Exp.*, vol. 14, no. 9, pp. 3730–3737, May 2006.
- [9] A. Taflov and S. C. Hagness, *Computational Electrodynamics: The Finite-Difference Time-Domain Method*, 3rd ed. Norwood, MA: Artech House, 2005.
- [10] M. Y. Ng and W. C. Liu, "Local-field confinement in three-pair arrays of metallic nanocylinders," *Opt. Exp.*, vol. 14, no. 10, pp. 4504–4513, May 2006.
- [11] J. P. Kottmann and O. J. F. Martin, "Plasmon resonant coupling in metallic nanowires," *Opt. Exp.*, vol. 8, no. 12, pp. 655–663, Jun. 2001.
- [12] M. W. Chen, Y. F. Chau, and D. P. Tsai, "Three-dimensional analysis of scattering field interactions and surface plasmon resonance in coupled silver nanospheres," *Plasmonics*, vol. 3, pp. 157–164, Oct. 2008.
- [13] R. Rodriguez-Oliveros and J. A. Sanchez-Gil, "Localized surface-plasmon resonances on single and coupled nanoparticles through surface integral equations for flexible surfaces," *Opt. Exp.*, vol. 19, no. 13, pp. 12208–12219, Jun. 2011.
- [14] J. P. Kottmann, O. J. F. Martin, D. R. Smith, and S. Schultz, "Plasmon resonances of silver nanowires with a nonregular cross section," *Phys. Rev. B*, vol. 64, 2001, Art. ID 235402.
- [15] E. Prodan, C. Radloff, N. J. Halas, and P. Nordlander, "A hybridization model for the plasmon response of complex nanostructures," *Science*, vol. 302, no. 5644, pp. 419–422, Oct. 2003.
- [16] B. Yang, D. Gottlieb, and J. S. Hesthaven, "Spectral simulations of electromagnetic wave scattering," *J. Comput. Phys.*, vol. 134, pp. 216–230, 1997.
- [17] B. Yang and J. S. Hesthaven, "A pseudospectral method for time-domain computation of electromagnetic scattering by bodies of revolution," *IEEE Trans. Antennas Propagat.*, vol. 47, no. 1, pp. 132–141, Jan. 1999.
- [18] J. S. Hesthaven, P. G. Dinesen, and J. P. Lynov, "Spectral collocation time-domain modeling of diffractive optical elements," *J. Comput. Phys.*, vol. 155, pp. 287–306, Nov. 1999.
- [19] G. Zhao and Q. H. Liu, "The 3-D multidomain pseudospectral time-domain algorithm for inhomogeneous conductive media," *IEEE Trans. Antennas Propagat.*, vol. 52, no. 3, pp. 742–749, Mar. 2004.
- [20] Q. H. Liu, "A pseudospectral frequency-domain (PSFD) method for computational electromagnetics," *IEEE Antennas Wireless Propagat. Lett.*, vol. 1, pp. 131–134, 2002.
- [21] P. J. Chiang, C. P. Yu, and H. C. Chang, "Analysis of two-dimensional photonic crystals using a multidomain pseudospectral method," *Phys. Rev. E*, vol. 75, Feb. 2007, Art. ID 026703.
- [22] P. J. Chiang, C. L. Wu, C. H. Teng, C. S. Yang, and H. C. Chang, "Full-vectorial optical waveguide mode solvers using multidomain pseudospectral frequency-domain (PSFD) formulations," *IEEE J. Quantum Electron.*, vol. 44, no. 1, pp. 56–66, Jan. 2008.
- [23] C. H. Teng, B. Y. Lin, H. C. Chang, H. C. Hsu, C. N. Lin, and K. A. Feng, "A Legendre pseudospectral penalty scheme for solving time-domain Maxwell's equations," *J. Sci. Comput.*, vol. 36, pp. 351–390, 2008.
- [24] J. P. Berenger, "A perfectly matched layer for the absorption of electromagnetic waves," *J. Comput. Phys.*, vol. 114, no. 2, pp. 185–200, Oct. 1994.
- [25] S. Abarbanel and D. Gottlieb, "A mathematical analysis of the PML method," *J. Comput. Phys.*, vol. 134, pp. 357–363, 1997.
- [26] S. Abarbanel and D. Gottlieb, "On the construction and analysis of absorbing layers in CEM," *Appl. Numer. Math.*, vol. 27, pp. 331–340, 1998.
- [27] L. Rayleigh, "The dispersal of light by a dielectric cylinder," *Philos. Mag.*, vol. 36, pp. 365–376, 1918.
- [28] J. R. Wait, "Scattering of plane wave from a circular dielectric cylinder at oblique incidence," *Can. J. Phys.*, vol. 33, no. 5, pp. 189–195, 1955.
- [29] W. J. Gordon and C. A. Hall, "Transfinite element methods: Blending function interpolation over arbitrary curved element domains," *Numer. Math.*, vol. 21, pp. 109–129, 1973.
- [30] S. Dey and R. Mittra, "A locally conformal finite-difference time-domain (FDTD) algorithm for modeling three-dimensional perfectly conducting objects," *IEEE Microw. Guided Wave Lett.*, vol. 7, pp. 273–275, Sept. 1997.
- [31] Y. Liu, C. D. Sarris, and G. V. Eleftheriades, "Triangular-mesh-based FDTD analysis of two-dimensional plasmonic structures supporting backward waves at optical frequencies," *J. Lightw. Technol.*, vol. 25, no. 3, pp. 938–946, Mar. 2007.
- [32] Y. Zhao and Y. Hao, "Finite-difference time-domain study of guided modes in nano-plasmonic waveguides," *IEEE Trans. Antennas Propagat.*, vol. 55, no. 11, pp. 3070–3077, Nov. 2007.
- [33] W. J. Gordon and C. A. Hall, "Transfinite element methods: Blending-function interpolation over arbitrary curved element domains," *Numer. Math.*, vol. 21, pp. 109–129, 1973.

- [34] P. B. Johnson and R. W. Christy, "Optical constants of the noble metals," *Phys. Rev. B*, vol. 6, no. 12, pp. 4370–4379, Dec. 15, 1972.
- [35] E. D. Palik, *Handbook of Optical Constants of Solids*. New York: Academic, 1985.
- [36] N. N. Rao, *Elements of Engineering Electromagnetics*, 6th ed. Upper Saddle River, NJ: Prentice-Hall, 2004.
- [37] J. B. Andersen and V. V. Solodukhov, "Field behavior near a dielectric wedge," *IEEE Trans. Antennas Propagat.*, vol. 26, no. 4, pp. 598–602, Jul. 1978.
- [38] W. S. Don and A. Solomonoff, "Accuracy and speed in computing the Chebyshev collocation derivative," *SIAM J. Sci. Comput.*, vol. 16, no. 6, pp. 1253–1268, 1995.
- [39] J. S. Hesthaven, "A stable penalty method for the compressible Navier-Stokes equations: III. Multidimensional domain decomposition schemes," *SIAM J. Sci. Comput.*, vol. 20, no. 1, pp. 62–93, 1998.
- [40] J. S. Hesthaven and T. Warburton, "Nodal high-order methods on unstructured grids: I. Time-domain solution of Maxwell's equations," *J. Comput. Phys.*, vol. 181, pp. 186–221, 2002.
- [41] D. Funaro and D. Gottlieb, "A new method of imposing boundary-conditions in pseudospectral approximations of hyperbolic-equations," *Math. Computation*, vol. 51, pp. 599–613, 1988.
- [42] J. S. Hesthaven, S. Gottlieb, and D. Gottlieb, *Spectral Methods for Time-Dependent Problems*. Cambridge, U.K.: Cambridge Univ., 2007.
- [43] D. Gottlieb, M. Gunzburger, and E. Turkel, "On numerical boundary treatment of hyperbolic systems for finite difference and finite element methods," *SIAM J. Numer. Anal.*, vol. 19, no. 4, pp. 671–681, 1982.
- [44] T. Apel and S. Nicaise, "The finite element method with anisotropic mesh grading for elliptic problems in domains with corners and edges," *Math. Methods Appl. Sci.*, vol. 21, pp. 519–549, 1998.
- [45] T. Apel, A.-M. Sandig, and J. R. Whiteman, "Graded mesh refinement and error estimates for finite element solutions of elliptic boundary value problems in non-smooth domains," *Math. Methods Appl. Sci.*, vol. 19, pp. 63–85, 1996.
- [46] K. Schmidt and P. Kauf, "Computation of the band structure of two-dimensional photonic crystals with HP finite elements," *Comput. Methods Appl. Mech. Eng.*, vol. 198, pp. 1249–1259, 2009.

Chih-Yu Wang received the B.S. degree from the Department of Engineering Science, National Cheng Kung University, Taiwan, in 2004, and the M.S. and Ph.D. degrees from the Graduate Institute of Electronics Engineering, National Taiwan University, Taiwan, in 2006 and 2012, respectively.

Her current research interests include the pseudospectral electromagnetics modeling in frequency domain.

Shih-Yung Chung received the B.S. degree from the Department of Electrical Engineering, National Cheng Kung University, Tainan, Taiwan, in 2004, and the M.S. and Ph.D. degrees from the Graduate Institute of Electronics Engineering, National Taiwan University, Taipei, Taiwan, in 2006 and 2012, respectively.

His current research interests include the electromagnetic simulations using the pseudospectral time-domain method.

Chun-Hao Teng was born in Tainan, Taiwan, on February 14, 1970. He received the diploma in mechanical engineering from National Taipei Institute of Technology, Taipei, Taiwan, in 1990, the M.S. degree in mechanical engineering from Clarkson University, Potsdam, NY, in 1996, and the M.S. and Ph.D. degrees in applied mathematics from Brown University, Providence, RI, in 2001.

From 2003 to 2009, he was an Assistant Professor with the Department of Mathematics, National Cheng Kung University, Tainan, Taiwan. He is currently an Assistant Research Fellow with the Center of Mathematical Modeling and Scientific Computing, National Chiao Tung University, Hsinchu, Taiwan. His research interests are the developments and applications of high-order numerical methods for partial differential equations.

Juen-Kai Wang was born in Tainan, Taiwan, on July 9, 1961. He received the B.S. degree in electrical engineering from National Taiwan University, Taipei, Taiwan, in 1983, and the M.S. and Ph.D. degrees in applied physics from Harvard University, Cambridge, MA, in 1986 and 1992, respectively.

From 1992 to 1994, he was with Arthur Amos Noyes Laboratory of Chemical Physics, California Institute of Technology, Pasadena. In December 1994, he joined the faculty of the Center for Condensed Matter Sciences, National Taiwan University, Taipei, Taiwan, where he is currently a Research Fellow. He is also jointly appointed with the Institute of Atomic and Molecular Sciences (IAMS) of Academia Sinica. He has acted as a consultant to Industrial Technology Research Institute since 2002. His current research interests include nanometer-scaled optical spectroscopy, ultrafast laser spectroscopy, surface-enhanced Raman spectroscopy, plasmonics, surface vibrational spectroscopy, biomedical vibrational spectroscopy, physical studies of organic semiconductors and their photovoltaic applications, and intense laser interaction with matters.

Dr. Wang was the recipient of the Executive Yuan Award for Outstanding Contributions in Science and Technology in 2009 and the Nano-Tech Award in 2010 that he shared with Dr. Yuh-Lin Wang of IAMS and Prof. Chi-Hung Lin of National Yang-Ming University for their contribution in developing high-speed detection technology for microbiology.

Chung-Ping Chen (M'96) received the B.S. degree in computer science and information engineering from National Chiao-Tung University, Hsinchu, Taiwan, in 1990, and the M.S. and Ph.D. degrees in computer science from the University of Texas, Austin, in 1996 and 1998, respectively.

From 1996 to 1999, he was with Strategic Computer-Aided Design (CAD) Labs, Intel Corporation, Hillsboro, OR, as a Senior CAD Engineer. Since 1999, he has been an Assistant Professor with the Department of Electrical and Computer Engineering, University of Wisconsin, Madison. Since 2003, he has been an Associate Professor with the Electrical Engineering Department, National Taiwan University, Taipei, Taiwan. Currently, he is a Professor with the Graduate Institute of Electronics Engineering, Biomedical Electronics and Bioinformatics and Electrical Engineering Departments, National Taiwan University. His research interests include the areas of electronic design automation and BIO topics, including computer-aided design and microprocessor circuit design with an emphasis on interconnect and circuit optimization, circuit simulation, statistical design, and signal/power/thermal integrity analysis and optimization.

Dr. Chen was the recipient of the D2000 Award from Intel Corporation and the National Sciences Foundation Faculty Early Career Development awards (CAREER) from 1999 to 2001, respectively. He also received the 2002 Special Interest Group on Design Automation/ACM Outstanding Young Faculty Award and the 2002 IBM Peter Schneider Faculty Development Award. He served the program committee and is an organizer of the Design Automation Conference, the International Conference on Computer-Aided Design, Design, Automation, and the Test in Europe Conference, the International Symposium on Physical Design, the Asia and South Pacific Design Automation Conference, the International Symposium on Quality Electronic Design, Synthesis and System Integration of Mixed Information, the VLSI/CAD Symposium, and the International Technology Roadmap for Semiconductors Conference.

Hung-Chun Chang (S'78–M'83–SM'00) was born in Taipei, Taiwan, on February 8, 1954. He received the B.S. degree from National Taiwan University, Taipei, Taiwan, in 1976, and the M.S. and Ph.D. degrees from Stanford University, Stanford, CA, in 1980 and 1983, respectively, all in electrical engineering.

From 1978 to 1984, he was with the Space, Telecommunications, and Radioscience Laboratory of Stanford University. In August 1984, he joined the faculty of the Electrical Engineering Department, National Taiwan University, Taipei, Taiwan, where he is currently a Distinguished Professor. He was the NTU Himax Chair Professor during 2011. He served as Vice-chairman of the EE Department from 1989 to 1991, and Chairman of the newly established Graduate Institute of Electro-Optical Engineering at the same university from 1992 to 1998. His current research interests include the electromagnetic theory, design, and application of photonic structures and devices for fiber optics, integrated optics, optoelectronics, nanophotonics, and plasmonics.

Dr. Chang is a Fellow of the Optical Society of America and the Electromagnetics Academy. He served as the IEICE (Japan) Overseas Area Representative in Taipei from 2002 to 2007.

A Multidomain Pseudospectral Mode Solver for Optical Waveguide Analysis

Shun-Fan Chiang, Bang-Yan Lin, Hung-Chun Chang, *Senior Member, IEEE, Fellow, OSA*, Chun-Hao Teng, Chih-Yu Wang, and Shih-Yung Chung

Abstract—We propose a pseudospectral mode solver for optical waveguide mode analysis formulated by the frequency-domain Maxwell equations. Special attention is paid upon identifying the required boundary operator for the formulation and the relationships between the derived operator and the physical boundary conditions. These theoretical results are adopted into a Legendre pseudospectral multidomain computational framework to compute the propagation characteristics of optical waveguides. Numerical experiments are conducted, and the expected spectral convergence of the scheme is observed for smooth problems and for problems having field jumps at material interfaces. For dielectric waveguides with sharp corners, the spectral convergence is lost due to the singular nature of fields at the corner. Nevertheless, compared with other methods, the present formulation remains as an efficient approach to obtain waveguide modes.

Index Terms—Frequency-domain Maxwell's equations, optical waveguides, penalty boundary conditions, pseudospectral methods, waveguide analysis.

I. INTRODUCTION

IN modal analysis for optical waveguides, the propagation constants and the associated field distributions of guided modes provide useful information in designing and operating optical guiding devices such as filters, switches, modulators, and fibers. To obtain these guiding characteristics, one needs to solve either Maxwell's equations or the vectorial Helmholtz

equations, subject to boundary conditions. However, due to the involved mathematical difficulties raised from either the geometry configurations of devices or the heterogeneous distributions of material properties, waveguide problems are in general very hard to solve analytically. For realistic cases, numerical methods are employed to obtain the guiding characteristics.

Among numerical methods, Cartesian finite difference methods [1]–[6] are popular for waveguide problems if the geometry of the guiding structure is confined to the grid lines. However, for problems involving curved interfaces, special difference stencils are required to treat field values in the vicinity of curved interfaces to maintain accurate computations [7]–[9]. Also commonly used in modal analysis, body-fitted finite element methods [10]–[13] adopt unstructured and structural meshes to fit the geometries and employ edge elements and tangential elements to discretize the equations and boundary conditions. Most of the aforementioned methods are low-order accurate methods, typically first or second order. As the complexity of waveguide problems increases, these finite difference and finite element schemes require using dense meshes to perform accurate computations. Hence, these approaches lead to large systems of equations to be solved, which may consume lots of computational resources and time. An approach for overcoming this issue is designing high-order accurate schemes based on spectral/pseudospectral methods [14]–[17]. Generally, these schemes can compute accurate results by using a coarse mesh, compared to low-order methods. However, this advantage does not come along freely, and great care must be exercised to ensure the high-order convergence rate, because these methods are very sensitive to the smoothness of the solutions and the imposition of boundary conditions [18].

In this study, we present a high-order accurate and geometrically flexible computational approach for waveguide mode analysis. Unlike the mentioned pseudospectral approaches that adopt the vectorial Helmholtz equations as the main equations, we consider the frequency-domain Maxwell's equations as the governing equations. Special attention is paid upon analyzing the required boundary operator for the frequency-domain Maxwell's equations and its relationships with the common physical boundary conditions. These analytic results are then adopted into a multidomain pseudospectral computational framework through the penalty methodology [19]–[22]. The proposed formulation is validated through computing the propagation characteristics of fundamental modes of a number of waveguide structures. We observe the expected spectral convergence results for smooth waveguide problems and for problems having finite jumps of fields at material interfaces. However, for dielectric waveguides having sharp corners, it is found that the spectral convergence is lost, due to the singular

Manuscript received January 19, 2012; revised March 13, 2012; accepted March 17, 2012. Date of publication March 23, 2012; date of current version April 27, 2012. This work was supported in part by the National Science Council of Taiwan under Grant NSC99-2115-M-009-012-MY3, Grant NSC97-2221-E-002-043-MY2, and Grant NSC99-2221-E-002-107-MY2, the Excellent Research Projects of National Taiwan University under Grant 10R80919-1, and the Ministry of Education of Taiwan under The Aim of Top University Plan Grant. The work of C.-H. Teng was supported by the National Science Council of Taiwan under Research Fellow Program NSC099-2811-M-009-047 and NSC100-2811-M-009-055.

S.-F. Chiang was with the Graduate Institute of Photonics and Optoelectronics Engineering, National Taiwan University, Taipei 10617, Taiwan. He is now with Hon Hai Precision Industry Company Ltd., Taipei 20306, Taiwan (e-mail: r95941007@ntu.edu.tw).

B.-Y. Lin was with the Graduate Institute of Communication Engineering, National Taiwan University, Taipei 10617, Taiwan. He is now with Taiwan Semiconductor Manufacturing Company, Hsinchu 30077, Taiwan (e-mail: bangyan.lin@gmail.com).

H.-C. Chang is with the Department of Electric Engineering, National Taiwan University, Taipei 10617, Taiwan (e-mail: hcchang@cc.ee.ntu.edu.tw).

C.-H. Teng is with the Department of Applied Mathematics and the Center of Mathematical Modeling, National Chiao Tung University, Hsinchu 30010, Taiwan (e-mail: tengch@math.nctu.edu.tw).

C.-Y. Wang and S.-Y. Chung are with the Graduate Institute of Electronics Engineering, National Taiwan University, Taipei 10617, Taiwan (e-mail: d95943034@ntu.edu.tw; d95943006@ntu.edu.tw).

Digital Object Identifier 10.1109/JLT.2012.2191937

nature of optical fields at the corner. Nevertheless, the results show that the present scheme remains competitive compared to other finite difference approaches on solving the same problem. Preliminary results of this study were reported in [23]. In this paper, we give the detailed formulation with numerous numerical examples.

The rest of this paper is organized as follows. In Section II, we present the mathematical formulation of the concerned problems and seek the required boundary operator as well as its relationships with common physical boundary conditions to complete the formulation. Section III is devoted to the construction of the discrete scheme of the formulation based on the multidomain pseudospectral penalty approach. The validation of the proposed formulation is presented in Section IV. Concluding remarks are given in Section V.

II. MATHEMATICAL FORMULATION

A. Maxwell's Equations

The Maxwell equations for optical fields in linear, lossless, source-free, and nonmagnetic medium are

$$\varepsilon_r c^{-1} \partial_t \hat{E} = Z_0 \nabla \times \hat{H} \quad (1a)$$

$$-Z_0 c^{-1} \partial_t \hat{H} = \nabla \times \hat{E} \quad (1b)$$

$$\nabla \cdot \hat{H} = 0 \quad (1c)$$

$$\nabla \cdot \hat{E} = 0 \quad (1d)$$

where ε_0 , μ_0 , $Z_0 = (\mu_0/\varepsilon_0)^{1/2}$, and $c = 1/(\varepsilon_0\mu_0)^{1/2}$ are the permittivity, permeability, impedance, and speed of light in free space, respectively, ε_r assumed real constant is the relative permittivity of medium, \hat{E} and \hat{H} are the electric and magnetic fields, respectively, and ∂_t denotes the partial differential operator with respect to t .

Let the z axis be the propagation direction. To solve the transverse wave fields in waveguides, we assume the fields having the space-time dependence of the form

$$(\hat{E}, Z_0 \hat{H})(x, y, z, t) = (E, H)(x, y) \exp(i\beta z - i\omega t) \quad (2)$$

where $i = \sqrt{-1}$, E and H are the normalized complex-valued phasors of \hat{E} and $Z_0 \hat{H}$, respectively, β is the propagation constant, and ω is the angular frequency. Substitution of (2) into (1) leads to the phasor component equations

$$i\beta E_x = ik_0 H_y + \partial_x E_z \quad (3a)$$

$$i\beta E_y = -ik_0 H_x + \partial_y E_z \quad (3b)$$

$$i\beta E_z = -\partial_x E_x - \partial_y E_y \quad (3c)$$

$$i\beta H_x = -ik_0 \varepsilon_r E_y + \partial_x H_z \quad (3d)$$

$$i\beta H_y = ik_0 \varepsilon_r E_x + \partial_y H_z \quad (3e)$$

$$i\beta H_z = -\partial_x H_x - \partial_y H_y \quad (3f)$$

$$\partial_x E_y = ik_0 H_z + \partial_y E_x \quad (3g)$$

$$\partial_x H_y = -ik_0 \varepsilon_r E_z + \partial_y H_x \quad (3h)$$

where $k_0 = \omega/c$ is the space wavenumber in vacuum. Notice that (3g)–(3h) can be derived from (3a)–(3e). We have six independent equations governing the six field variables formulated as an eigensystem, with β and the phasor fields being the eigenvalue and eigenvectors, respectively.

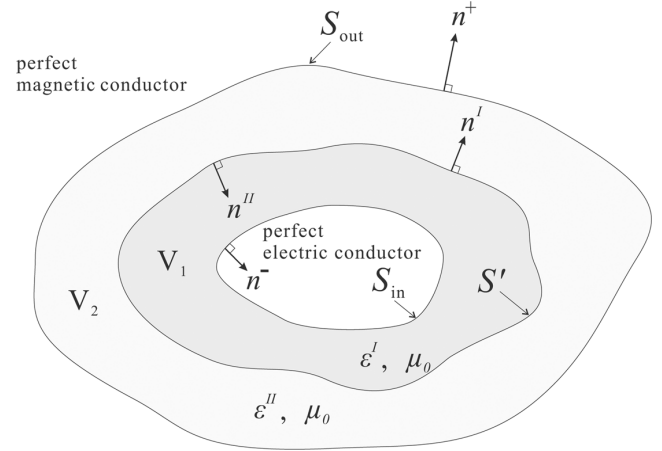


Fig. 1. Schematic view of the cross section of a waveguide.

B. Boundary Operators

Consider the waveguide having a cross section as depicted in Fig. 1. The structure is closed by perfect magnetic conductor (PMC) and perfect electric conductor (PEC) at the outer and inner surfaces, S_{out} and S_{in} , respectively. Within the structure, the surface S' divides the guiding area into two regions V_1 and V_2 , characterized by the permittivity and permeability of the material, (ε^I, μ_0) and $(\varepsilon^{II}, \mu_0)$, respectively. n^- and n^+ denote the outward pointing unit vectors normal to the surfaces S_{in} and S_{out} , respectively, and n^I and n^{II} are unit vectors normal to the surface S' pointing from region V_1 to region V_2 and from region V_2 to region V_1 , respectively.

To seek the boundary operator required by (3a)–(3e), we rewrite these equations in the matrix form

$$i\beta A_3 q = -ik_0 A_0 q + A_1 \partial_x q + A_2 \partial_y q \quad (4)$$

where $q = [\varepsilon_r E_x, \varepsilon_r E_y, E_z, H_x, H_y, H_z]^T$ is the state vector with T denoting the vector transpose, and for $i = 0, 1, 2, 3$

$$A_i = \begin{bmatrix} \delta_{3i} \varepsilon_r^{-1} & 0 & \delta_{1i} & 0 & -\delta_{0i} & 0 \\ 0 & \delta_{3i} \varepsilon_r^{-1} & \delta_{2i} & \delta_{0i} & 0 & 0 \\ \delta_{1i} & \delta_{2i} & -\delta_{3i} \varepsilon_r & 0 & 0 & 0 \\ 0 & \delta_{0i} & 0 & \delta_{3i} & 0 & \delta_{1i} \\ -\delta_{0i} & 0 & 0 & 0 & \delta_{3i} & \delta_{2i} \\ 0 & 0 & 0 & \delta_{1i} & \delta_{2i} & -\delta_{3i} \end{bmatrix}$$

with δ_{ij} being the Kronecker delta function. Multiplying (4) by q^* from the left, where $(\cdot)^*$ denotes the Hermitian of the variable (\cdot) , and multiplying the Hermitian of (4) by q from the right, integrating the entire domain $V_1 \cup V_2$, summing the resultants, and invoking the divergence theorem to change the volume integrals to surface integrals, we obtain

$$0 = \int_{S_{in}} q^* A(n^-) q dx + \int_{S'_I} q^* A(n^I) q dx + \int_{S'_{II}} q^* A(n^{II}) q dx + \int_{S_{out}} q^* A(n^+) q dx \quad (5)$$

where $A(n) = n_x A_1 + n_y A_2$ with $n = (n_x, n_y)$ being the outward pointing unit vector normal to a domain boundary, and $\int_S (\cdot) dx$ denotes the integration along the path S . Note that the second and the third integrations on the right-hand side (RHS)

of (5) are evaluated with variables defined on the interface S' but in regions V_1 and V_2 , respectively.

To proceed further, we introduce the characteristic variables at the boundaries. Since $A(n) = A^T(n)$, there exists a unitary matrix $S(n)$ such that

$$S^* A(n) S = \Lambda = \text{diag}(\lambda_1, \lambda_2, \lambda_3, \lambda_4, \lambda_5, \lambda_6)$$

with $\lambda_1 = \lambda_6 = -1$, $\lambda_2 = \lambda_5 = 1$, and $\lambda_3 = \lambda_4 = 0$. Notice that $S^* = S^T = S^{-1}$ because $A(n)$ is real. Employing S , we define the characteristic state vector

$$R = [R_1, R_2, R_3, R_4, R_5, R_6]^T = S^* q.$$

The explicit expressions of S and R are

$$S(n) = \frac{1}{\sqrt{2}} \begin{bmatrix} n_x & n_x & \sqrt{2}n_y & 0 & 0 & 0 \\ n_y & n_y & -\sqrt{2}n_x & 0 & 0 & 0 \\ -1 & 1 & 0 & 0 & 0 & 0 \\ 0 & 0 & 0 & \sqrt{2}n_y & n_x & n_x \\ 0 & 0 & 0 & -\sqrt{2}n_x & n_y & n_y \\ 0 & 0 & 0 & 0 & 1 & -1 \end{bmatrix} \quad (6)$$

$$R(n) = \frac{1}{\sqrt{2}} \begin{bmatrix} \varepsilon_r(n \cdot E_{\parallel}) - e_z \cdot E_{\perp} \\ \varepsilon_r(n \cdot E_{\parallel}) + e_z \cdot E_{\perp} \\ -\sqrt{2}\varepsilon_r e_z \cdot (n \times E_{\parallel}) \\ -\sqrt{2}e_z \cdot (n \times H_{\parallel}) \\ (n \cdot H_{\parallel}) + e_z \cdot H_{\perp} \\ (n \cdot H_{\parallel}) - e_z \cdot H_{\perp} \end{bmatrix} \quad (7)$$

where e_z is the unit vector in the z -direction, E_{\parallel} (H_{\parallel}) is the transverse electric (magnetic) field, and E_{\perp} (H_{\perp}) is the electric (magnetic) field perpendicular to the xy plane.

Equation (5) implies that the required boundary conditions must lead to the vanishing of the RHS of the equation. We now examine whether the specified boundary conditions satisfy this constrain.

a) *PMC Condition at S_{out}* : The conditions are

$$n^+ \cdot E_{\parallel} = 0, \quad n^+ \times H_{\parallel} = 0, \quad e_z \cdot H_{\perp} = 0.$$

It follows from (7), $n^+ \cdot E_{\parallel} = 0$ and $e_z \cdot H_{\perp} = 0$, that

$$R_1(n^+) + R_2(n^+) = \sqrt{2}n^+ \cdot \varepsilon_r E_{\parallel} = 0 \quad (8a)$$

$$R_5(n^+) - R_6(n^+) = \sqrt{2}e_z \cdot H_{\perp} = 0. \quad (8b)$$

Thus, $|R_1(n^+)|^2 = |R_2(n^+)|^2$ and $|R_5(n^+)|^2 = |R_6(n^+)|^2$. Furthermore, since $\lambda_3 = \lambda_4 = 0$, we obtain

$$q^* A(n^+) q = R^*(n^+) \Lambda R(n^+) = 0$$

indicating that $\int_{S_{\text{out}}} q^* A(n^+) q dx = 0$ in (5).

b) *PEC at S_{in}* : The conditions are

$$n^- \times E_{\parallel} = 0, \quad e_z \cdot E_{\perp} = 0, \quad n^- \cdot H_{\parallel} = 0.$$

It follows from (7), $e_z \cdot E_{\perp} = 0$ and $n^- \cdot H_{\parallel} = 0$, that

$$R_1(n^-) - R_2(n^-) = -\sqrt{2} e_z \cdot E_{\perp} = 0 \quad (9a)$$

$$R_5(n^-) + R_6(n^-) = \sqrt{2} n^- \cdot H = 0. \quad (9b)$$

Thus, $|R_1(n^-)| = |R_2(n^-)|^2$ and $|R_5(n^-)|^2 = |R_6(n^-)|^2$. Since $\lambda_3 = \lambda_4 = 0$, we obtain

$$q^* A(n^-) q = R^*(n^-) \Lambda R(n^-) = 0$$

indicating that $\int_{S_{\text{in}}} q^* A(n^-) q dx = 0$ in (5).

c) *Material Interface Condition at S'* : The interface boundary conditions relating fields on both sides of the interface S' are

$$n^I \times E_{\parallel}^I = n^I \times E_{\parallel}^{II} \quad (10a)$$

$$e_z \cdot E_{\perp}^I = e_z \cdot E_{\perp}^{II} \quad (10b)$$

$$n^I \cdot \varepsilon^I E_{\parallel}^I = n^I \cdot \varepsilon^{II} E_{\parallel}^{II} \quad (10c)$$

$$n^I \times H_{\parallel}^I = n^I \times H_{\parallel}^{II} \quad (10d)$$

$$e_z \cdot H_{\perp}^I = e_z \cdot H_{\perp}^{II} \quad (10e)$$

$$n^I \cdot H_{\parallel}^I = n^I \cdot H_{\parallel}^{II} \quad (10f)$$

where n^I is the unit vector normal to S' pointing from region V_1 to region V_2 , and the superscripts I and II denote the regions where the field variables are defined on the S' interface, respectively. From (7), we have

$$\begin{aligned} \sqrt{2}R_1^I(n^I) &= \varepsilon_r^I n^I \cdot E_{\parallel}^I - e_z \cdot E_{\perp}^I \\ \sqrt{2}R_2^{II}(n^{II}) &= \varepsilon_r^{II} n^{II} \cdot E_{\parallel}^{II} + e_z \cdot E_{\perp}^{II}. \end{aligned}$$

Invoking (10b) and (10c) as well as $n^I = -n^{II}$, we yield

$$R_1^I(n^I) = -R_2^{II}(n^{II}). \quad (11)$$

Following similar procedures, we obtain the conditions

$$R_2^I(n^I) = -R_1^{II}(n^{II}) \quad (12)$$

$$R_5^I(n^I) = -R_6^{II}(n^{II}) \quad (13)$$

$$R_6^I(n^I) = -R_5^{II}(n^{II}). \quad (14)$$

It follows from these expressions and $\lambda_3 = \lambda_4 = 0$ that

$$\begin{aligned} q^* A(n^I) q &= R^*(n^I) \Lambda R(n^I) \\ &= -R^*(n^{II}) \Lambda R(n^{II}) \\ &= -q^* A(n^{II}) q. \end{aligned}$$

Therefore, $\int_{S'_I} q^* A(n^-) q dx + \int_{S'_{II}} q^* A(n^+) q dx = 0$.

The analysis shows that to satisfy (5), we need to specify R_1 , R_2 , R_5 , and R_6 on the boundary to complete the system. The explicit expressions of these characteristic components and their relationships with the common physical boundary conditions are established. In the next section, we shall apply these result and construct a pseudospectral penalty scheme for solving wave fields in waveguides.

III. NUMERICAL FORMULATION

A. Legendre Pseudospectral Method

Let $\mathbf{I} = [-1, 1]$ and N be a positive integer. Introduce the Legendre–Gauss–Lobatto (LGL) points ξ_i for $0 \leq i \leq N$. These points are roots of the polynomial $(1 - \xi^2)P'_N(\xi)$ where $P_N(\xi)$ is the N th degree Legendre polynomial and $'$ denotes

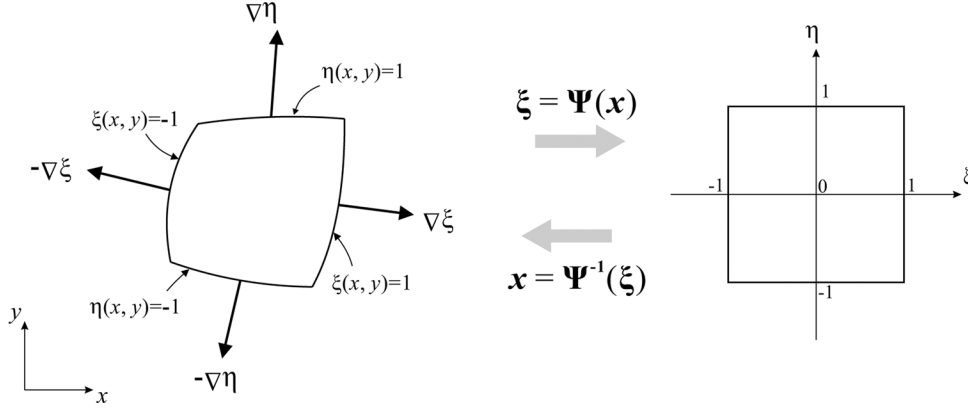


Fig. 2. Coordinate mapping of a square in $\xi = (\xi, \eta)$ coordinate and a general curvilinear quadrilateral in $\mathbf{x} = (x, y)$ coordinate.

the differentiation. To approximate a function f defined on \mathbf{I} , we seek a polynomial f_N of the form

$$f_N(\xi) = \sum_{j=0}^N l_j(\xi) f_j$$

$$l_j(\xi) = -\frac{(1 - \xi^2) P'_N(\xi)}{N(N+1)(\xi - \xi_j) P_N(\xi_j)}$$

where $f_j = f(\xi_j)$ and $l_j(\xi)$ are the Lagrange interpolating functions. The 1-D pseudospectral method can be extended to a 2-D framework through the tensor product formulation. Let N_ξ and N_η be positive integers. Denote $\mathbf{I}^2 = [-1, 1]^2$ and term the coordinates (ξ, η) . Consider the grid points ξ_i for $0 \leq i \leq N_\xi$ and η_j for $0 \leq j \leq N_\eta$, where ξ_i and η_j are the LGL grid points along the ξ - and η -axis, respectively. Then, the grid points are defined as (ξ_i, η_j) . To approximate $f(\xi, \eta)$ defined on \mathbf{I}^2 , we construct a polynomial $f_N(\xi, \eta)$ of the form

$$f_N(\xi, \eta) = \sum_{j=0}^{N_\eta} \sum_{i=0}^{N_\xi} l_i^\xi(\xi) l_j^\eta(\eta) f_{ij}, \quad f_{ij} = f(\xi_i, \eta_j)$$

where $l_i^\xi(\xi)$ and $l_j^\eta(\eta)$ are the 1-D Lagrange interpolating functions based on the grid points ξ_i and η_j , respectively. The partial derivatives of f are approximated as

$$\partial_\xi f(\xi_p, \eta_q) \approx \partial_\xi f_N(\xi_p, \eta_q) = \sum_{j=0}^{N_\eta} \sum_{i=0}^{N_\xi} \frac{dl_i^\xi(\xi_p)}{d\xi} l_j^\eta(\eta_q) f_{ij}$$

$$\partial_\eta f(\xi_p, \eta_q) \approx \partial_\eta f_N(\xi_p, \eta_q) = \sum_{j=0}^{N_\eta} \sum_{i=0}^{N_\xi} l_i^\xi(\xi_p) \frac{dl_j^\eta(\eta_q)}{d\eta} f_{ij}.$$

We have reviewed some basic concepts related to the Legendre pseudospectral method. For further details on the method, we refer the reader to [18].

B. Equations in Curvilinear Coordinates

The tensor-product-based pseudospectral formulation is for problems defined on standard domain $[-1, 1]^2$. To apply the

formulation for problems defined on general complex domains, an approach is decomposing the global domains into unions of smooth quadrilateral subdomains which can be mapped onto a standard domain. We understand that establishing a general coordinate transformation for mapping an arbitrary quadrilateral domain onto a square domain may not be always possible. Hence, we describe the methodology for problems defined on a curvilinear quadrilateral element that can be mapped onto a square.

Consider a general curvilinear quadrilateral Ω and a square \mathbf{I}^2 defined in coordinate systems termed (x, y) and (ξ, η) , respectively (see Fig. 2). We apply the transfinite blending interpolation method [24] and construct a coordinate mapping $(\xi, \eta) = \Psi(x, y)$ and its inverse $(x, y) = \Psi^{-1}(\xi, \eta)$ to establish a one-to-one correspondence between Ω and \mathbf{I}^2 . The transformation metric functions are then computed as

$$\frac{\partial(\xi, \eta)}{\partial(x, y)} = \begin{bmatrix} \partial_x \xi & \partial_y \xi \\ \partial_x \eta & \partial_y \eta \end{bmatrix}, \quad \frac{\partial(x, y)}{\partial(\xi, \eta)} = \begin{bmatrix} \partial_\xi x & \partial_\eta x \\ \partial_\xi y & \partial_\eta y \end{bmatrix}$$

and they are related as $(\partial(\xi, \eta))/(\partial(x, y))(\partial(x, y))/(\partial(\xi, \eta)) = I$ where I is the identity matrix. Using the coordinate transformation and the chain rule of differentiation, we rewrite (4) as

$$i\beta A_z q = -i\omega A_t q + A_\xi \partial_\xi q + A_\eta \partial_\eta q \quad (15)$$

where $q(\xi, \eta) = q(\Psi^{-1}(\xi, \eta))$, $A_3 = A_3$, $A_0 = A_0$, $A_\xi = A_1 \partial_x \xi + A_2 \partial_y \xi$, and $A_\eta = A_1 \partial_x \eta + A_2 \partial_y \eta$.

Denote $\mathbf{n} = (n_\xi, n_\eta)$ as the unit vector normal to the boundary of \mathbf{I}^2 in the (ξ, η) coordinate system. On the boundary of \mathbf{I}^2 , we define the variables $A(\mathbf{n})$, $S(\mathbf{n})$, $\Gamma(\mathbf{n})$ and $R(\mathbf{n})$, related by $A(\mathbf{n}) = n_\xi A_\xi + n_\eta A_\eta$, $S^*(\mathbf{n})A(\mathbf{n})S(\mathbf{n}) = \Gamma(\mathbf{n})$, and $R = S^*(\mathbf{n})q$. The variables S , Γ , and R and their transformed correspondences S , Λ , and R defined on the boundary of Ω are related as follows. Denote the unit vectors along the ξ - and η -axes by $\hat{\xi} = (1, 0)$ and $\hat{\eta} = (0, 1)$, respectively. On the edges $\xi(x, y) = \pm 1$, we have $\Gamma(\pm \hat{\xi}) = |\nabla \xi| \Lambda$, $S(\pm \hat{\xi}) = S(\pm \nabla \xi / |\nabla \xi|)$, and $R(\pm \hat{\xi}) = R(\pm \nabla \xi / |\nabla \xi|)$. Replacing the symbol ξ by η in the aforementioned expressions, we obtain the corresponding relationships for the variables defined on $\eta(x, y) = \pm 1$.

C. Numerical Scheme

We now present the numerical scheme for solving (15). Let q_{ij} denote the numerical state vectors at the grid points (ξ_i, η_j) satisfying the collocation schemes

$$i\beta A_3 q_{ij} = -ik_0 A_0 q_{ij} + A_\xi \partial_\xi q_{ij} + A_\eta \partial_\eta q_{ij} - \frac{1}{2} \sum_{\nu=1}^4 P_{ij}^{(\nu)} \quad (16)$$

where

$$P_{ij}^{(1)} = \delta_{i0} |\nabla \xi|_{ij} \left(\omega_i^\xi \right)^{-1} S_{ij}(-\hat{\xi}) \Lambda \left(R_{ij}(-\hat{\xi}) - R_{ij}^{BC} \right) \quad (17a)$$

$$P_{ij}^{(2)} = \delta_{iN_\xi} |\nabla \xi|_{ij} \left(\omega_i^\xi \right)^{-1} S_{ij}(\hat{\xi}) \Lambda \left(R_{ij}(\hat{\xi}) - R_{ij}^{BC} \right) \quad (17b)$$

$$P_{ij}^{(3)} = \delta_{j0} |\nabla \eta|_{ij} \left(\omega_j^\eta \right)^{-1} S_{ij}(-\hat{\eta}) \Lambda \left(R_{ij}(-\hat{\eta}) - R_{ij}^{BC} \right) \quad (17c)$$

$$P_{ij}^{(4)} = \delta_{jN_\eta} |\nabla \eta|_{ij} \left(\omega_j^\eta \right)^{-1} S_{ij}(\hat{\eta}) \Lambda \left(R_{ij}(\hat{\eta}) - R_{ij}^{BC} \right) \quad (17d)$$

with ω_i^ξ and ω_j^η being the quadrature weights [18] associated with the grid points ξ_i and η_j , respectively. It is shown in (16) that the boundary conditions are enforced into the scheme weakly through the characteristic variables.

To complete the construction of the scheme, we need to provide the explicit expression of R_{ij}^{BC} . For simplicity, we consider the imposition of boundary conditions on the $\xi = 1$ edge as an example. To impose PMC condition, it is suggested from (8a) and (8b) to construct $R^{BC} = [-R_2, -R_1, R_3, R_4, R_6, R_5]^T$, leading to

$$|\nabla \xi| \mathcal{S} \Lambda (R - R^{BC}) = 2[0, 0, \varepsilon_r \nabla \xi \cdot E_{\parallel}, (\partial_x \xi) H_z, (\partial_y \xi) H_z, 0]^T$$

where $E_{\parallel} = (E_x, E_y)$. Likewise, to enforce PEC condition, it is suggested from (9a) and (9b) to construct $R^{BC} = [R_2, R_1, R_3, R_4, -R_6, -R_5]^T$. Thus,

$$|\nabla \xi| \mathcal{S} \Lambda (R - R^{BC}) = 2[(\partial_x \xi) E_z, (\partial_y \xi) E_z, 0, 0, 0, \nabla \xi \cdot H_{\parallel}]^T$$

where $H_{\parallel} = (H_x, H_y)$. We now discuss the imposition of interface boundary condition. From (11)–(14), it is suggested to take $R^{I,BC} = [-R_2^{II}, -R_1^{II}, R_3^I, R_4^I, -R_6^{II}, -R_5^{II}]^T$. Hence,

$$\begin{aligned} |\nabla \xi| \mathcal{S} \Lambda (R^I - R^{I,BC}) \\ = \sqrt{2} [(\partial_x \xi) [E_z]_{II}^I, (\partial_y \xi) [E_z]_{II}^I, \nabla \xi \cdot [\varepsilon_r E_{\parallel}]_{II}^I, \\ (\partial_x \xi) [H_z]_{II}^I, (\partial_y \xi) [H_z]_{II}^I, \nabla \xi \cdot [H_{\parallel}]_{II}^I]^T \end{aligned}$$

where $[E_z]_{II}^I = E_z^I - E_z^{II}$ and similarly for the other parallel notations.

By employing (16) and the aforementioned boundary relationship, the wave fields on the transverse plane of a waveguide can be formulated as an eigenvalue problem of the form $\mathcal{A} \mathcal{Q} = i\beta \mathcal{Q}$, where the propagation constant β is the eigenvalue, \mathcal{Q} is the eigenvector composed of the collocated state vectors, and \mathcal{A} is a matrix. Solving the eigensystem, we obtain β and the transverse wave fields.

IV. NUMERICAL VALIDATIONS AND DISCUSSION

A. Errors of Effective Index and Residual Functions

We examine the performance of the method by measuring the error of the computed effective index $|\delta n_{\text{eff}}|$ defined as

$$|\delta n_{\text{eff}}| = |n_{\text{eff}} - n'_{\text{eff}}|, \quad n_{\text{eff}} = \beta k_0^{-1} = (2\pi)^{-1} \beta \lambda_0$$

where n'_{eff} and n_{eff} are the exact and the computed effective indexes and λ_0 is the operating wavelength. To measure how well the computed eigenmode solutions are, we employ the expressions in (3g) and (3h), which are omitted in computations, and define the residual functions r_1 and r_2 as

$$r_1^2 = \int_{\Omega} |ik_0 H_z + \partial_y E_x - \partial_x E_y|^2 dx$$

$$r_2^2 = \int_{\Omega} |-ik_0 \varepsilon_r E_z + \partial_y H_x - \partial_x H_y|^2 dx$$

where the integrals are evaluated numerically by the LGL integration quadrature rule [18]. The residual functions can be served as accuracy indicators of the numerical eigenmode solution because if the computed fields are obtained by the scheme convergence to the exact fields of (3a)–(3h), then the residual functions shall decay as the mesh is refined.

The convergence rate of the computed effective index is calculated as

$$\zeta = \frac{\log(|\delta n_{\text{eff}}(N_1)|/|\delta n_{\text{eff}}(N_2)|)}{\log(N_2/N_1)}$$

where N_1 and N_2 are the characterized degrees of the approximation polynomials during mesh refinement. Replacing δn_{eff} in the aforementioned expression by r_1 and r_2 , we compute the convergence rates of the residual functions r_1 and r_2 , respectively.

B. Partially Filled Metallic Waveguide

Consider a half-filled metallic waveguide structure with the geometry and the refractive indexes shown in Fig. 3. The effective index of the fundamental longitudinal-section electric (LSE₁₀) mode at the operating wavelength $\lambda_0 = 2\pi \mu\text{m}$ is solved by the present method with a computational mesh shown in Fig. 3.

A grid convergence study is given in Table I. We see that the error of the effective index decays exponentially as the mesh is refined. The convergence study illustrates the efficiency of the proposed formulation in computing accurate solutions. It is observed that the computed effective index has reached machine accuracy level even using coarse grid meshes. In addition, it is also shown that the residual r_1 vanishes as the polynomial degree N increases. The values of r_2 are at machine accuracy level for different values of N , because the E_z , H_x , and H_y fields are zero for this particular mode.

C. Circular Metallic Waveguide

Consider an air-filled circular metallic waveguide with the geometry and the refractive indexes shown in Fig. 4. The effective index for the fundamental transverse electric (TE₁₁) mode at the operating wavelength $\lambda_0 = 0.2 \mu\text{m}$ is solved by the

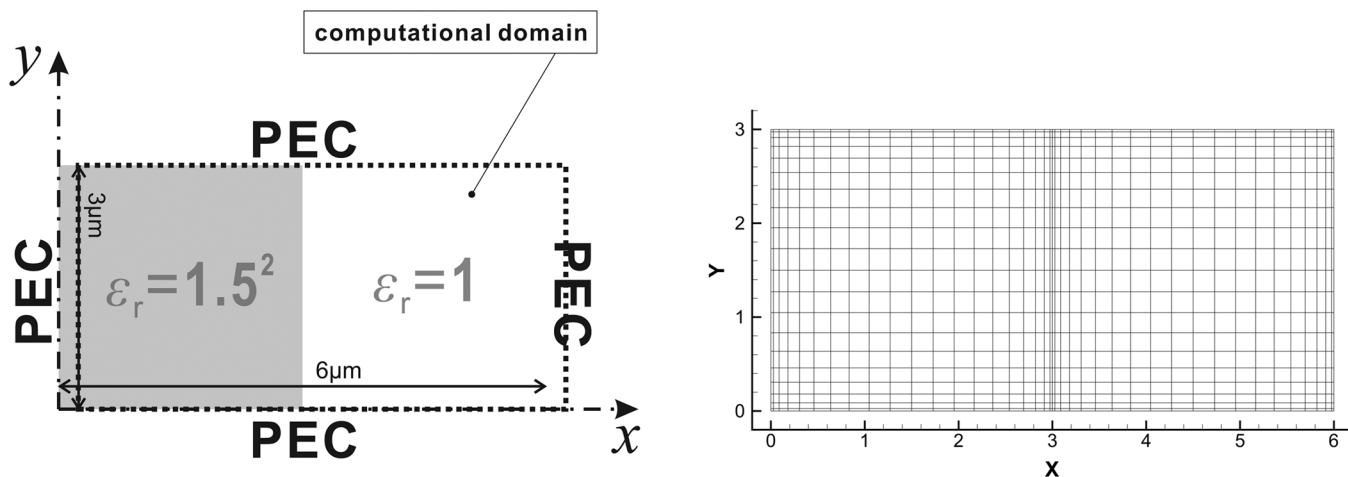


Fig. 3. Schematic view of (left) a partially filled metallic waveguide and (right) a multidomain computational mesh composed of two subdomains. Each subdomain contains $(N + 1) \times (N + 1)$ grid points, where N is the degree of the approximation polynomial.

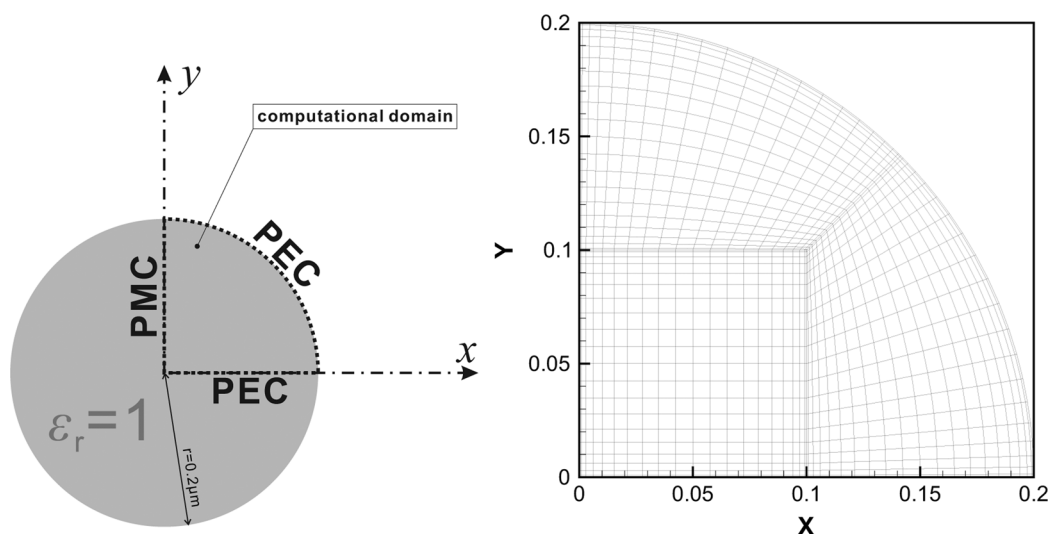


Fig. 4. (Left) Schematic diagram of a circular metallic waveguide. (Right) Multidomain mesh composed of three subdomains.

TABLE I

CONVERGENCE STUDY OF THE PARTIALLY FILLED METALLIC WAVEGUIDE. $n'_{\text{eff}} = 1.27575556678727$, REFERENCED EFFECTIVE INDEX FOR THE LSE₁₀ MODE AT THE OPERATING WAVELENGTH $2\pi \mu\text{M}$ OBTAINED BY SOLVING TRANSCENDENTAL EQUATIONS [25]

N	$ \delta n_{\text{eff}} $	ζ	N	r_1	ζ	r_2	ζ
4	1.78E-04	-	8	5.06E-05	-	2.84E-15	-
6	1.74E-08	22.7	10	2.24E-07	24.2	4.96E-15	-2.4
8	3.76E-12	29.3	12	1.70E-09	26.7	3.53E-15	1.9
10	7.10E-15	28.1	14	4.56E-12	38.4	3.74E-15	-0.4

TABLE II

CONVERGENCE STUDY OF THE CIRCULAR METALLIC WAVEGUIDE. $n'_{\text{eff}} = 0.9561021744104193$, REFERENCED EFFECTIVE INDEX FOR THE TE₁₁ MODE AT THE OPERATING WAVELENGTH $\lambda_0 = 0.2 \mu\text{M}$

N	$ \delta n_{\text{eff}} $	ζ	N	r_1	ζ	r_2	ζ
3	1.49E-06	-	6	2.24E-06	-	1.20E-06	-
4	4.30E-08	12.3	8	2.68E-08	15.3	1.60E-08	15.0
5	1.47E-10	25.4	10	4.95E-11	28.2	2.53E-11	28.9
6	2.42E-12	22.5	12	1.91E-12	17.8	1.25E-12	16.5
7	1.02E-14	35.4	14	1.02E-12	4.06	7.81E-13	3.04

present method. Due to the geometrical symmetry, we only need to solve the problem on the upper right quarter fan region supported by the PEC and PMC conditions at the two straight edges.

A grid convergence study is given in Table II. We observe that the error of the computed effective index and the residuals r_1 and r_2 vanish rapidly to machine accuracy level, as N increases. The results indicate that the present formulations incorporated with the transfinite blending mapping also perform very well for solving problems involving curved boundary.

D. Fiber Waveguide

Consider a fiber waveguide with the geometry and the refractive indices as shown in Fig. 5. We use the present method to solve the effective index for the fundamental HE₁₁ mode of the fiber waveguide at the operating wavelength $\lambda_0 = 1.5 \mu\text{m}$. Notice that this problem has a high index difference between the core and the surrounding areas, which causes fields having jumps at the dielectric interface. Thus, this problem is suitable

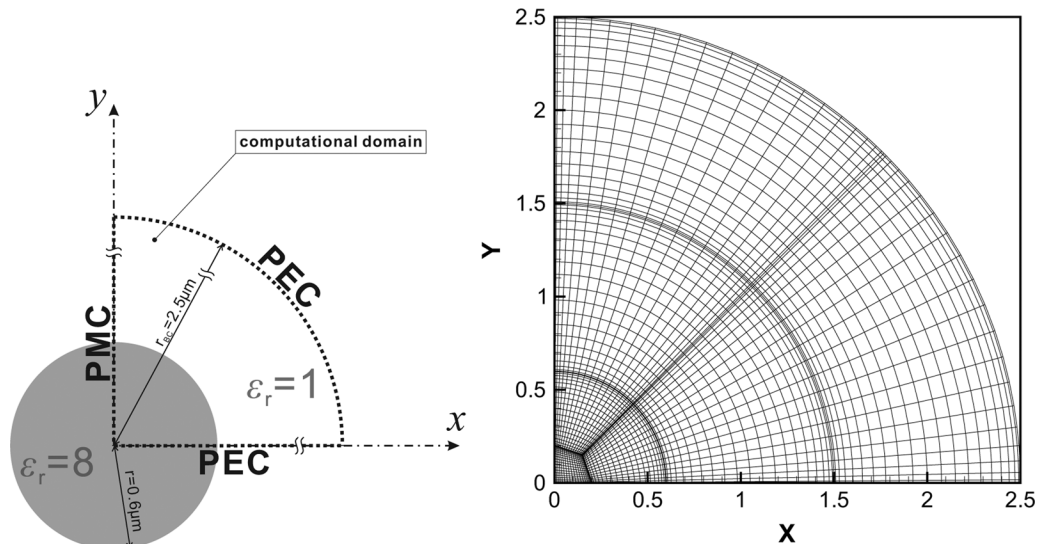


Fig. 5. Schematic view of (left) a fiber waveguide and (right) a multidomain mesh.

for validating the numerical boundary impositions of the present formulation.

Notice that the problem domain radially extends to infinity, which cannot be directly solved by the present formulation for problems defined on finite regions. However, since the fields in the air region are of evanescent type, the amplitude of each field vanishes in the far zone. Employing this property, we terminate the domain by a virtual boundary and enforce PEC or PMC condition at the artificial closure. As will be shown soon, such an arrangement does not harm the computation accuracy provided that the artificial boundary is far away from the fiber core. Furthermore, since the problem domain possesses circular symmetry, it is sufficient enough to consider the problem defined on the upper right quarter of the waveguide cross section. We use a mesh composed of seven subdomains as shown in Fig. 5.

A grid convergence study is provided in Table III. It is shown that the errors of the computed effective index and the residual functions r_1 and r_2 all vanish exponentially as the mesh is refined. We also obtain $n_{\text{eff}} = 2.6840193216091506$ when using $N = 15$, which gives a $|\delta n_{\text{eff}}|$ less than 10^{-14} . The computed fields of the fundamental HE_{11} mode with $N = 20$ are shown in Fig. 6. We observe that the field components are mostly confined in the guiding core area and in the vicinity of the dielectric interface, and the amplitude of each field component decays to zero away from the core area. We observe the field jumps at the circular dielectric interface, indicating that the proposed boundary formulation does well capture the essential character of fields at the material interface.

E. Channel Waveguide With Sharp Corners

We now examine the performance of the formulation on solving propagation characteristics of a square channel waveguide with the geometry and the refractive indexes shown in Fig. 7. A special feature of the considered dielectric channel waveguide is that the electric fields at the dielectric sharp corners are singular (see [5] and the references therein). There, an analysis was conducted to compute the propagation characteristics involving the singular behavior of fields at sharp

corners and the result obtained by the difference method is adopted here as a reference.

A grid convergence study is provided in Table IV. We observe that the residual functions r_1 and r_2 only decay in three-quarter rate at most and a second-order rate, respectively, as the computational mesh is refined. The spectral convergence rate is ruined due to the weakly divergent behavior of the E_x and E_y field components at the sharp corner [5], [13], which indeed has a great impact on the convergence of the scheme. In our computation, it is found that the local residual $|ik_0 H_z + \partial E_x / \partial y - \partial E_y / \partial x|^2$ at the corner does not decay. This ill behavior, thus, leads to a very poor convergence of the residual r_1 . On the other hand, it is found that the local residual $|-ik_0 \varepsilon_r E_z + \partial H_x / \partial y - \partial H_y / \partial x|$ at the corner decays in the first-order rate. As a consequence, the residual function r_2 vanishes in a second-order rate.

Although the spectral convergence of the scheme is lost for this problem, it is shown that the effective index obtained by the present method still agrees well with the referenced one. In fact, from the computed results, we observe that by employing a coarse grid mesh (four subdomains with 7×7 grid points in each subdomain), it is sufficient enough to compute the effective index having a similar accuracy as the referenced one obtained by a 150×150 finite difference grid mesh. This advantage allows one to compute more accurate results by increasing the resolution of the grid mesh. We close this section by providing more accurate results of the effective index of the channel waveguide for $\varepsilon_r = 2.25$ in Table V and for $\varepsilon_r = 8$ in Table VI. It is shown that the effective indexes are approximately 1.276274037 for $\varepsilon_r = 2.25$ and approximately 2.656796923 for $\varepsilon_r = 8$. These values are consistent with those obtained by a recently developed waveguide mode solver based on Neumann-to-Dirichlet operators and boundary integral equations [26], in which an accuracy comparison has been made with the result in [23].

V. CONCLUDING REMARKS

We have presented a pseudospectral computational framework for computing the propagation characteristics of optical

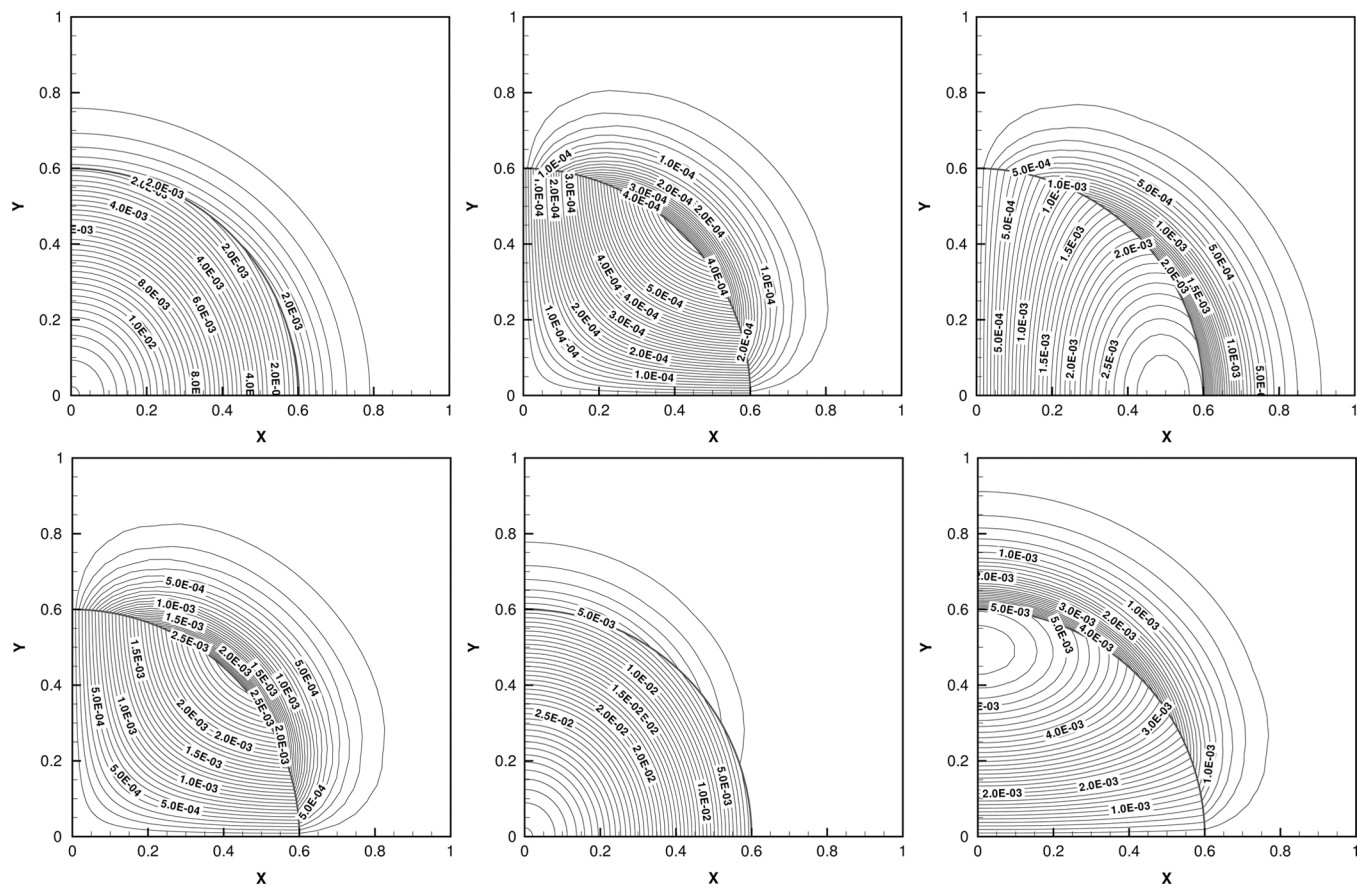


Fig. 6. Field amplitude contour line plots of the fiber waveguide problem. $|E_x|$, $|E_y|$, and $|E_z|$ are placed on the top row from left to right. $|H_x|$, $|H_y|$, and $|H_z|$ are placed on the bottom row from left to right.

TABLE III

CONVERGENCE STUDY OF THE FIBER WAVEGUIDE. $n'_{\text{eff}} = 2.684019321609156$, REFERENCED EFFECTIVE INDEX OF THE HE_{11} FUNDAMENTAL MODE AT THE OPERATING WAVELENGTH $\lambda_0 = 1.5 \mu\text{m}$

N	$ \delta n_{\text{eff}} $	ζ	N	r_1	ζ	r_2	ζ
4	7.98E-04	-	8	3.11E-03	-	8.52E-03	-
6	1.54E-05	9.7	12	1.87E-05	12.6	5.07E-05	12.6
8	1.07E-07	17.2	16	6.71E-08	19.5	1.81E-07	19.5
10	4.25E-10	24.8	20	2.34E-10	25.3	6.28E-10	25.3
12	9.68E-12	20.8	24	1.33E-12	28.3	3.83E-12	27.9

wave fields in waveguides. The mathematical formulation is based on the Maxwell equations in frequency domain, and the required boundary operator to complete the formulation was identified. Relationships between the mathematically derived boundary operator and the common boundary conditions were also established. We constructed a multidomain Legendre pseudospectral scheme with boundary condition weakly imposed through the penalty methodology. Numerical experiments were conducted and we observed the expected spectral convergence of the scheme for both smooth problems and those having finite jump discontinuities at material interfaces. However, for problems involving singular wave fields occurring at sharp dielectric corners, the numerical experiments showed that the spectral convergence of the scheme is ruined and the order of the convergence is at most first-order accurate in the global sense. Nevertheless, the present pseudospectral method remains an efficient

approach to compute the results compared to those obtained by finite difference methods [5].

For waveguide analysis, a common approach is solving full-vectorial wave equations in terms of the two transverse magnetic field components. The total number of discrete equations raised by the transverse field formulations is less than that raised by the present six-component formulation. We admit that the present method requires more computational work. To overcome this issue, we have reformulated our method to reduce the number of equations. The idea is mimicking the procedure of obtaining the full-vectorial wave equations from the Maxwell equations, which involves taking the partial derivatives of the first-order system of equations and then conducting algebraic eliminations to yield decoupled second-order wave equations. For the present method, we can write (16) and (17) into their continuous representations, and then take derivatives and conduct algebraic eliminations to obtain a system of second-order equations composed of the transverse magnetic field components and the nontransverse electric field component. Thus, the total number of discrete equations is reduced and the computational work can be reduced. To completely eliminate the nontransverse electric field requires further investigation. The details of this study will be further conducted and presented elsewhere in the future.

Although the present formulation results into a larger system compared to the transverse magnetic field components ap-

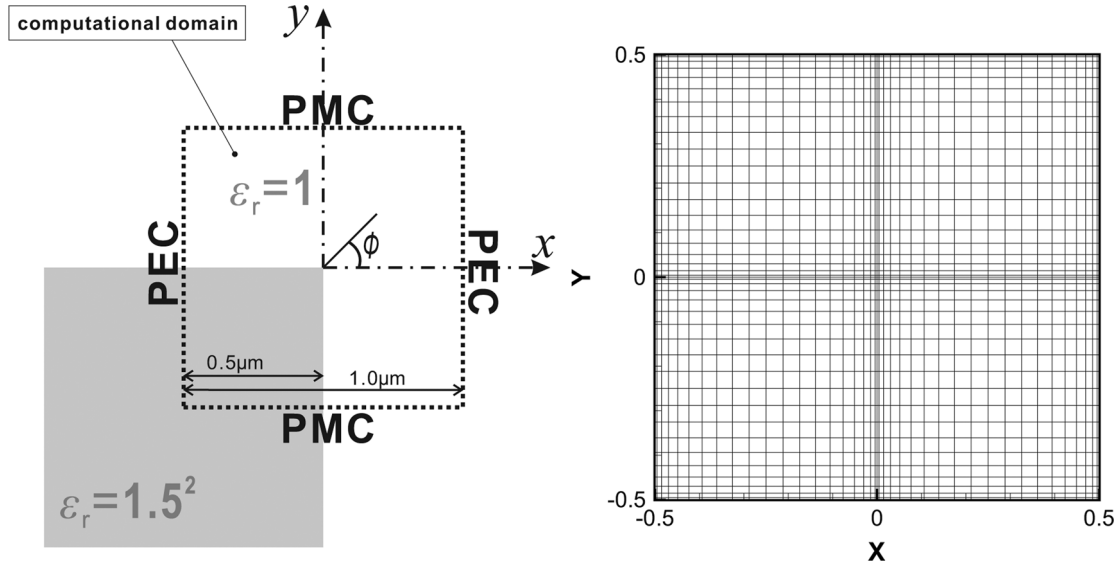


Fig. 7. Cross-sectional view of (left) a dielectric waveguide and (right) a computational mesh composed of four subdomains.

 TABLE IV
 GRID CONVERGENCE STUDY OF THE CHANNEL WAVEGUIDE. $n_{eff}^i = 1.27627404 \pm 10^{-8}$, REFERENCE EFFECTIVE INDEX FOR THE FUNDAMENTAL MODE AT THE OPERATING WAVELENGTH $\lambda_0 = 1.5 \mu\text{m}$ ADOPTED FROM [5]

N	n_{eff}	$ \delta n_{eff} $	N	r_1	ζ_{r_1}	r_2	ζ_{r_2}
4	1.27627574310227	1.70E-06	8	6.91E-03	-	4.77E-04	
6	1.27627406000974	2.00E-08	12	5.22E-03	0.69	2.14E-04	1.97
8	1.27627401416807	2.58E-08	16	4.25E-03	0.71	1.19E-04	2.02
10	1.27627402128922	1.87E-08	20	3.62E-03	0.71	7.58E-05	2.04
12	1.27627402754483	1.24E-08	24	3.17E-03	0.72	5.20E-05	2.06

 TABLE V
 EFFECTIVE INDEX OF THE FUNDAMENTAL MODE OF THE CHANNEL WAVEGUIDE COMPUTED BY THE SCHEME WITH VERY DENSE MESHES WITH $\varepsilon_r = 2.25$. OPERATING WAVELENGTH $\lambda_0 = 1.5 \mu\text{m}$

N	n_{eff}
40	1.276274037658855
44	1.276274037716481
48	1.276274037755042
52	1.276274037781696

 TABLE VI
 EFFECTIVE INDEX OF THE FUNDAMENTAL MODE OF THE CHANNEL WAVEGUIDE COMPUTED BY THE SCHEME WITH VERY DENSE MESHES WITH $\varepsilon_r = 8$. OPERATING WAVELENGTH $\lambda_0 = 1.5 \mu\text{m}$

N	n_{eff}
8	2.656796890564512
16	2.656796916630881
24	2.656796921885117
32	2.656796923270166
40	2.656796923780370

proach, the present method may have a possible advantage on solving problems involving tensor permittivity. For this situation, the full-vectorial formulation may involve cross differentiation terms, which may become complicated for imposing boundary conditions. However, in the present method, tensor permittivity will only affect the matrix A_3 which is a low-order term in (4). Consequently, the present boundary formulation, which is related to the A_1 and A_2 matrices, may

remain valid. Detail investigations will be explored in the future.

Before the end of this paper, we briefly discuss two issues related to the further development of the present method. The first one regards computing waves propagating toward to far fields along the transverse plane. In this study, we only conduct experiments either for wave problems defined on closed domain or for problems where the waves are evanescent in the far field, so the domain can be terminated into a finite region supported by artificial boundary conditions. Because of the lack of methods on absorbing waves propagating toward to far zone for the present formulation, the performance of the scheme on solving leaky mode solutions of certain optical waveguide structures has not yet been examined. Hence, to extend the applicability of the present method for calculating leaky modes of waveguides, it is worth to develop suitable perfectly matched layer methods to absorb outgoing waves and maintain the solution accuracy in the guiding regions. The second issue regards the blow-up behavior of wave fields at dielectric corners. Although the present formulation remains a competitive approach, compared to other finite difference methods, for computing the propagation characteristics of waveguides involving dielectric corners, the singular nature does ruin the exponential convergence order of the scheme. It would be interesting to develop methods to enhance the convergence order, so the computations can be more efficient and accurate to resolve the singular behavior of fields at dielectric corners. We hope to report this development in the future.

ACKNOWLEDGMENT

The authors would like to thank the National Center for High-Performance Computing, Hsinchu, Taiwan, for providing useful computing resources.

REFERENCES

- [1] K. Bierwirth, N. Schulz, and F. Arndt, "Finite-difference analysis of rectangular dielectric waveguide structures," *IEEE Trans. Microw. Theory Tech.*, vol. 34, no. 11, pp. 1104–1113, Jan. 1986.
- [2] M. S. Stern, "Semivectorial polarized finite difference method for optical waveguides with arbitrary index profiles," *IEE Proc. J. Optoelectron.*, vol. 135, no. 1, pp. 56–63, 1988.
- [3] C. Vassallo, "Improvement of finite difference methods for step-index optical waveguides," *IEE Proc. J. Optoelectron.*, vol. 139, no. 2, pp. 137–142, 1992.
- [4] P. Lüsse, P. Stuwe, J. Schüle, and H.-G. Unger, "Analysis of vectorial mode fields in optical waveguides by a new finite difference method," *J. Lightw. Technol.*, vol. 12, no. 3, pp. 487–494, Mar. 1994.
- [5] G. R. Hadley, "High-accuracy finite-difference equations for dielectric waveguide analysis: II. Dielectric corners," *J. Lightw. Technol.*, vol. 20, no. 7, pp. 1219–1231, Jul. 2002.
- [6] N. Thomas, P. Sewell, and T. M. Benson, "A new full-vectorial higher order finite-difference scheme for the modal analysis of rectangular dielectric waveguides," *J. Lightw. Technol.*, vol. 25, no. 9, pp. 2563–2570, Sep. 2007.
- [7] Y. P. Chiou, Y. P. Chiang, and H. C. Chang, "Improved three-point formulas considering the interface conditions in the finite-difference analysis of step-index optical devices," *J. Lightw. Technol.*, vol. 18, no. 2, pp. 243–251, Feb. 2000.
- [8] S. Zhao, "Full-vectorial matched interface and boundary (MIB) method for the modal analysis of dielectric waveguides," *J. Lightw. Technol.*, vol. 26, no. 14, pp. 2251–2259, Jul. 2008.
- [9] S. Zhao, "High-order matched interface and boundary methods for the Helmholtz equation in media with arbitrarily curved interfaces," *J. Comput. Phys.*, vol. 229, pp. 3155–3170, 2010.
- [10] M. Koshiba and K. Inoue, "Simple and efficient finite-element analysis of microwave and optical waveguides," *IEEE Trans. Microw. Theory Tech.*, vol. 40, no. 2, pp. 371–377, Feb. 1992.
- [11] J. F. Lee, D. K. Sun, and Z. J. Cendes, "Tangential vector finite element for electromagnetic field computation," *IEEE Trans. Magn.*, vol. 27, no. 5, pp. 4032–4035, Sep. 1991.
- [12] M. Koshiba, S. Maruyama, and K. Hirayama, "A vector finite element method with the high-order mixed-interpolation-type triangular elements for optical waveguiding problems," *J. Lightw. Technol.*, vol. 12, no. 3, pp. 495–502, Mar. 1994.
- [13] D. U. Li and H. C. Chang, "An efficient full-vectorial finite-element modal analysis of dielectric waveguides incorporating inhomogeneous elements across dielectric discontinuities," *IEEE J. Quantum Electron.*, vol. 36, no. 11, pp. 1251–1261, Nov. 2000.
- [14] P.-J. Chiang, C.-L. Wu, C.-H. Teng, C.-S. Yang, and H.-C. Chang, "Full-vectorial optical waveguide mode solvers using multidomain pseudospectral frequency-domain (PSFD) formulations," *IEEE J. Quantum Electron.*, vol. 44, no. 1, pp. 56–66, Jan. 2008.
- [15] C.-C. Huang, C.-C. Huang, and J.-Y. Yang, "An efficient method for computing optical waveguides with discontinuous refractive index profiles using spectral collocation method with domain decomposition," *J. Lightw. Technol.*, vol. 21, no. 10, pp. 2284–2296, Oct. 2003.
- [16] C.-C. Huang, C.-C. Huang, and J.-Y. Yang, "A full-vectorial pseudospectral modal analysis of dielectric optical waveguides with stepped refractive index profiles," *IEEE J. Quantum Electron.*, vol. 11, no. 2, pp. 457–465, Mar./Apr. 2005.
- [17] J. Xiao and X. Sun, "Full-vectorial mode solver for anisotropic optical waveguides using multidomain spectral collocation method," *Opt. Commun.*, vol. 283, pp. 2835–2840, 2010.
- [18] J. S. Hesthaven, S. Gottlieb, and D. Gottlieb, *Spectral Methods for Time-Dependent Problems*. Cambridge, U.K.: Cambridge Univ. Press, 2007.
- [19] D. Funaro and D. Gottlieb, "A new method of imposing boundary conditions in pseudospectral approximations of hyperbolic equations," *Math. Comput.*, vol. 51, pp. 599–613, 1988.
- [20] C. H. Teng, B. Y. Lin, H. C. Chang, H. C. Hsu, C. N. Lin, and K. A. Feng, "A Legendre pseudospectral penalty scheme for solving time-domain Maxwell's equations," *J. Sci. Comput.*, vol. 36, pp. 351–390, 2008.

- [21] B. Y. Lin, H. C. Hsu, C. H. Teng, H. C. Chang, J. K. Wang, and Y. L. Wang, "Unraveling near-field origin of electromagnetic waves scattered from silver nanorod arrays using pseudo-spectral time-domain calculation," *Opt. Exp.*, vol. 17, pp. 14211–14228, 2009.
- [22] B. Y. Lin, C. H. Teng, H. C. Chang, H. H. Hsiao, J. K. Wang, and Y. L. Wang, "Pseudospectral modeling of nano-optics in Ag sphere arrays," *J. Sci. Comput.*, vol. 45, pp. 429–446, 2010.
- [23] S. F. Chiang, B. Y. Lin, C. H. Teng, and H. C. Chang, "Improved analysis of rectangular dielectric waveguides based on a Legendre pseudospectral penalty scheme," presented at the presented at the Integr. Photon. Res., Silicon and Nano Photon., Washington, DC, 2010, Paper IWH8.
- [24] W. J. Gordon and C. A. Hall, "Transfinite element methods: Blending-function interpolation over arbitrary curved element domains," *Numer. Math.*, vol. 21, pp. 109–129, 1973.
- [25] R. Collin, *Field Theory of Guided Waves*. New York: McGraw-Hill, 1960.
- [26] W. Lu and Y. Y. Lu, "Waveguide mode solver based on Neumann-to-Dirichlet operators and boundary integral equations," *J. Comput. Phys.*, vol. 231, pp. 1360–1371, 2012.

Shun-Fan Chiang received the B.S. degree in mechanical engineering from National Taiwan University, Taipei, Taiwan, in 2006, and the M.S. degree in optoelectronics engineering from National Taiwan University, Taipei, in 2008.

Since 2008, he has been with Hon Hai Precision Industry Ltd., Taipei. His research interests include simulation programming design, control system design, and mechanical design.

Bang-Yan Lin received the B.S. degree in electronic engineering from Chung Yuan Christian University, Chung-Li, Taiwan, in 1997, and the M.S. and Ph.D. degrees in communication engineering from the National Taiwan University, Taipei, Taiwan, in 2002 and 2009, respectively.

He was involved in the development of the pseudospectral method and its applications to optoelectronics, including photonic crystals, nanophotonics, and plasmonics. In 2009, he joined Taiwan Semiconductor Manufacturing Company, Hsinchu, Taiwan, as a Principal Engineer, where he is currently involved in research on MOSFET modeling.

Hung-Chun Chang (S'78–M'83–SM'00) was born in Taipei, Taiwan, on February 8, 1954. He received the B.S. degree from National Taiwan University, Taipei, in 1976, and the M.S. and Ph.D. degrees from Stanford University, Stanford, CA, in 1980 and 1983, respectively, all in electrical engineering.

From 1978 to 1984, he was with the Space, Telecommunications, and Radioscience Laboratory, Stanford University. In August 1984, he joined the Department of Electrical Engineering (EE), National Taiwan University (NTU), where he is currently a Distinguished Professor. He was the NTU Himax Chair Professor in 2011. He served as the Vice Chairman of the EE Department from 1989 to 1991, and the Chairman of the newly established Graduate Institute of Electro-Optical Engineering, NTU, from 1992 to 1998. His current research interests include the electromagnetic theory, design, and application of photonic structures and devices for fiber optics, integrated optics, optoelectronics, nanophotonics, and plasmonics.

Dr. Chang served as the Institute of Electronics, Information and Communication Engineers, Japan, Overseas Area Representative in Taipei from 2002 to 2007. He is a Fellow of the Optical Society of America and the Electromagnetics Academy.

Chun-Hao Teng was born in Tainan, Taiwan, on February 14, 1970. He received the Diploma degree in mechanical engineering from the National Taipei Institute of Technology, Taipei, Taiwan, in 1990, the M.S. degree in mechanical engineering from Clarkson University, Potsdam, NY, in 1996, and the M.S. and Ph.D. degrees in applied mathematics from Brown University, Providence, RI, in 1998 and 2001, respectively.

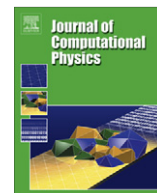
From 2003 to 2009, he was an Assistant Professor in the Department of Mathematics, National Cheng Kung University, Tainan. He is currently an Assistant Research Fellow in the Department of Applied Mathematics and the Center of Mathematical Modeling and Scientific Computing, National Chiao Tung University, Hsinchu, Taiwan. His research interests include the developments and applications of high-order numerical methods for partial differential equations.

Chih-Yu Wang received the B.S. degree from the Department of Engineering Science, National Cheng Kung University, Tainan, Taiwan, in 2004, and the M.S. degree from the Graduate Institute of Electronics Engineering, National Taiwan University, Taipei, Taiwan, in 2006, where she is currently working toward the Ph.D. degree.

Her current research interests include the pseudospectral electromagnetics modeling in frequency domain.

Shih-Yung Chung received the B.S. degree from the Department of Electrical Engineering, National Cheng Kung University, Tainan, Taiwan, in 2004, and the M.S. degree from the Graduate Institute of Electronics Engineering, National Taiwan University, Taipei, Taiwan, in 2006, where he is currently working toward the Ph.D. degree.

His current research interests include the electromagnetic simulations using the pseudospectral time domain method.



An error minimized pseudospectral penalty direct Poisson solver

Tzyy-Leng Horng^a, Chun-Hao Teng^{b,c,*}

^a Department of Applied Mathematics, Feng Chia University, Taichung 40724, Taiwan

^b Department of Applied Mathematics, National Chiao Tung University, 1001 Ta Hsueh Road, Hsinchu 30010, Taiwan

^c Center of Mathematical Modeling and Scientific Computing, National Chiao Tung University, Hsinchu 30010, Taiwan

ARTICLE INFO

Article history:

Received 15 April 2011

Received in revised form 23 November 2011

Accepted 28 November 2011

Available online 13 December 2011

Keywords:

Pseudospectral penalty method

Poisson equations

Diagonalization

ABSTRACT

This paper presents a direct Poisson solver based on an error minimized Chebyshev pseudospectral penalty formulation for problems defined on rectangular domains. In this study the penalty parameters are determined analytically such that the discrete L_2 error is minimized. Numerical experiments are conducted and the results show that the penalty scheme computes numerical solutions with better accuracy, compared to the traditional approach with boundary conditions enforced strongly.

© 2011 Elsevier Inc. All rights reserved.

1. Introduction

Many physics problems require solving Poisson's equation. For problems defined on domains which are confined with the coordinate systems, there are fast and accurate Poisson and Helmholtz direct solvers based on spectral methods. Here, we give a briefly discussion on a number of direct Poisson solvers based on the modal expansion and the pseudospectral approaches.

Haidvogel and Zang [9] developed an efficient and accurate Poisson solver based on the Chebyshev tau formulation [8,18] and the eigenvalue–eigenvector matrix diagonalization method [19]. This approach is, indeed, fast and accurate for solving Poisson equations, and has inspired the development of many other direct Poisson solvers. However, as mentioned in [9] this method suffers from the round off error when the discretized system becomes large. To reduce the ill-condition of the Chebyshev tau method, Dang-Vu and Delcarte [2], employed the three-term-recursion formula of Chebyshev polynomials to simplify the spectral differentiation structure. In addition to the Chebyshev tau expansion, Shen [21] developed a Chebyshev Galerkin Poisson solver based on properly choosing the expansion basis, so the resulting discrete system of equations is less ill-condition and can be solved accurately and efficiently by matrix decomposition methods. Recently, advanced developments of spectral-based Poisson and Helmholtz solvers for problems defined on unbounded domains are discussed in [22] and references therein. Generally speaking, due to recursive mathematical properties inherited in the Chebyshev polynomials these modal expansion approaches are very efficient in solving linear problems with constant coefficients and with variable coefficients of polynomial type. However, for problems involving general variable coefficients the modal expansion methods become less attractive, because the spectral differentiation structure of a differentiation operator involving variable coefficients can become complicated.

In contrast to the modal expansion approaches, pseudospectral methods have also been used to develop direct and iterative Poisson and Helmholtz solvers. For fluid dynamic simulations, Ku et al. [17] presented a Poisson solver, and Ehrenstein and Peyret [4] presented a Helmholtz solver. Both methods utilize the Chebyshev pseudospectral formulation to discretize

* Corresponding author at: Department of Applied Mathematics, National Chiao Tung University, 1001 Ta Hsueh Road, Hsinchu 30010, Taiwan.

E-mail addresses: tlhorng@math.fcu.edu.tw (T.-L. Horng), tengch@math.nctu.edu.tw (C.-H. Teng).

the equations in the cartesian coordinate, and the resulting systems of equations are solved by matrix diagonalization techniques. For problems defined on polar/cylindrical and spherical coordinates, pseudospectral formulations and matrix diagonalization techniques can be easily extended. For instance, Chen et al. [1] proposed direct solvers for problems in polar and cylindrical coordinate systems. Navarro et al. [20] employed Chebyshev collocation method and Newton iterative method to study an optimal control problem in a thermoconvective fluid flow. Huang et al. [16] developed an FFT based fast Poisson solver by using spectral-finite difference method and special mapping for problems defined on spherical shells.

Applying pseudospectral methods for partial differentiation equations involves not only discretizing differential equations but also enforcing boundary conditions. This often leads to a discrete system of equations having more equations than unknowns. To resolve this over determined issue, the traditional approach is enforcing the boundary condition strongly via including the boundary conditions and directly discarding the collocation equations at the boundary points. However, as a global approximation method the way of imposing boundary conditions can greatly affect the behavior of numerical solutions over the entire domain. For example, the aforementioned Chebyshev Galerkin method [21] which utilizes basis functions satisfying boundary conditions yield computation solutions with better accuracy compared to those obtained by the Chebyshev-tau method.

Funaro and Gottlieb [5] proposed a penalty approach for imposing boundary condition in pseudospectral approximations for partial differential equations. The penalty approach links boundary conditions and discretization equations through free parameters whose values are determined analytically by satisfying certain constraints. For time dependent problems the penalty parameter is considered as a stabilizer and, thus, the value of the parameter is determined to make the scheme stable. This stabilizing approach has led to successful constructions of pseudospectral schemes for time dependent problems [5,6,11–15] since then. In [5] it was also demonstrated that the penalty parameter can be considered as an error minimizer on solving model differential equation $u'(x) = f(x)$ subject to a boundary condition. Indeed, the accuracy of the penalty method is better than that of the traditional pseudospectral discretization with strongly enforced boundary conditions. As mentioned in [5] that a penalty scheme leads to a better approximation is because it takes into account the fact that the solution of a partial differential equation satisfies the equation arbitrary close to the domain boundary. Thus, the traditional approach which discards the discretized equations at the boundaries immediately lose certain level of accuracy of the method. This issue has motivated our study for constructing a scheme for Poisson equations, because the traditional approach leads to discarding two discretization schemes. As a consequence certain level of accuracy of the method is lost.

In this study we adopt the concept illustrated in [5] and present an error minimized pseudospectral penalty formulation for the Poisson equation on a rectangle domain, subject to Dirichlet, Neumann and Robin boundary conditions. The values of the penalty parameters are determined analytically such that the L_2 error of the approximation is minimized from a one dimensional analysis. Numerical validations of the constructed pseudospectral penalty formulation are performed. The results, indeed, show that the present penalty scheme computes more accurate solutions than the traditional pseudospectral formulation does. However, due to the involved mathematical difficulties we are unable to directly conduct an analysis to determine values of the penalty parameters for multidimensional problems. Nevertheless, it is found from extensive numerical experiments that the penalty parameters obtained from one dimensional analysis seem to remain applicable for constant coefficient problems in multidimensional spaces. For more complicated problems such as variable coefficient problems, further investigation on the optimal penalty parameters is worthy to be explored. Comparing our results chiefly with Shen [21], Ehrenstein and Peyret [4] and Haidvogel and Zang [9], we observe that the accuracy of the present method can be as good as the Chebyshev Galerkin method [21], considered as the most accurate method for the problem. Considered as an advantage the scheme is very easy to implement. In the traditional method with boundary conditions enforced strongly, one needs to use the boundary conditions to algebraically eliminate collocated field values at boundary points in the discretized Poisson equations. This can be complicated if Neumann and Robin boundary conditions are involved. In the present method, the boundary conditions is directly appended to the discretized Poisson equations and, thus, makes the present method very easy to implement.

This paper is organized as follows. In Section 2 we present a Chebyshev pseudospectral penalty scheme for solving the model Poisson problem, and special attention is paid upon determining the values of the penalty parameters such that the approximation error is minimized. Section 3 is devoted to the generalization and the numerical validations of the pseudospectral penalty scheme for solving two and three dimensional Poisson equations. Concluding remarks are given in Section 4.

2. Model problem and pseudospectral penalty formulation

2.1. Poisson equations and boundary conditions

Consider $u(x)$ satisfying the Poisson equation subject to the boundary conditions of the form,

$$u''(x) = f(x), \quad x \in [-1, 1], \quad (1a)$$

$$\mathcal{B}_\pm u(\pm 1) = g_\pm, \quad \mathcal{B}_\pm = \alpha_\pm \pm \beta_\pm \frac{d}{dx}, \quad (1b)$$

where \mathcal{B}_\pm are the boundary operators, α_\pm and β_\pm are non-negative real numbers, f is a specified function, and g_\pm are given values.

Employing the pseudospectral Chebyshev method [15], we construct the numerical solution $u(x)$ as

$$v(x) = \sum_{j=0}^N l_j(x) v(x_j), \quad l_j(x) = \frac{(-1)^{N+j+1} (1-x^2) T'_N(x)}{c_j N^2 (x-x_j)}, \quad c_j = \begin{cases} 2 & \text{if } j = 0, N, \\ 1 & \text{otherwise,} \end{cases}$$

where N is a positive integer, $x_j = -\cos(j\pi/N)$ for $0 \leq j \leq N$ are the Gauss–Lobatto–Chebyshev points, $u(x_j)$ are the collocated field values approximating $u(x_j)$, and $l_j(x)$ are the Lagrange interpolating functions associated with the grid points. Notice that since $(1-x^2)T'(x) = C \prod_{i=0}^N (x-x_i)$ where C is a constant, the Lagrange interpolating functions satisfy the property $l_j(x_i) = \delta_{ij}$ where δ_{ij} is the usual Kronecker delta function.

To solve Eq. (1) we require $u(x)$ to satisfy the collocation equations

$$v''(x_0) = f(x_0) + \tau_-(\alpha_- v(x_0) - \beta_- v'(x_0) - g_-), \quad (2a)$$

$$v''(x_i) = f(x_i), \quad i = 1, 2, \dots, N-1, \quad (2b)$$

$$v''(x_N) = f(x_N) + \tau_+(\alpha_+ v(x_N) + \beta_+ v'(x_N) - g_+), \quad (2c)$$

where τ_{\pm} are parameters with values depending the type of the imposed boundary conditions. Notice that for a given N if the values of the penalty parameters approach positive and negative infinity, then Eqs. (2a) and (2c) recover the strongly enforced boundary conditions in the following sense:

$$\alpha_- v(x_0) - \beta_- v'(x_0) - g_- = (v''(x_0) - f(x_0))/\tau_- \rightarrow 0,$$

$$\alpha_+ v(x_N) + \beta_+ v'(x_N) - g_+ = (v''(x_N) - f(x_N))/\tau_+ \rightarrow 0.$$

An important issue concerning the use of penalty boundary conditions is how to determine the values of these penalty parameters τ_{\pm} as the degree of the approximation polynomial N increases. This is the main theme of this study and the details are presented next.

2.2. Error minimizer

Consider the model equation

$$u''(x) = -16\pi^2 \sin(4\pi x) \quad (3)$$

subject to following sets of boundary conditions:

Case (A), Dirichlet boundary conditions at $x = \pm 1$,

$$u(\pm 1) = 0. \quad (4)$$

Case (B), Robin boundary conditions at $x = \pm 1$,

$$u(\pm 1) \pm u'(\pm 1) = 4\pi. \quad (5)$$

Case (C), Dirichlet Boundary condition at $x = -1$ and Neumann boundary condition at $x = 1$

$$u(-1) = 0, \quad u'(1) = 4\pi. \quad (6)$$

Case (D), Neumann boundary condition at $x = -1$ and Robin boundary condition at $x = 1$

$$u'(-1) = 4\pi, \quad u(1) + u'(1) = 4\pi. \quad (7)$$

Case (E), Robin boundary condition at $x = -1$ and Dirichlet boundary condition at $x = 1$

$$u(-1) - u'(-1) = -4\pi, \quad u(1) = 0. \quad (8)$$

The exact solutions to all cases are $u = \sin(4\pi x)$.

We first investigate the error behavior of numerical solutions obtained by the present method as the values of the penalty parameters vary. The model equation subject to boundary conditions Case (A) and Case (B) are solved by the scheme Eq. (2). Since for each case the boundary conditions imposed at $x = \pm 1$ are of the same type, we simply take $\tau_+ = \tau_- = \tau \in (-\infty, 0) \cup (0, \infty)$. We define the approximation error as

$$R(\tau_+, \tau_-) = \left(\frac{\pi}{N} \sum_{i=0}^N \frac{(u(x_i) - v(x_i))^2}{c_i} \right)^{1/2}.$$

In Fig. 1 we plot R as a function of τ . It is clearly shown that in each case there exists $\tau = \tau_c$ which minimizes the error. For the Dirichlet case it is found that $\tau_c < 0$ and for the Robin case it is found that $\tau_c > 0$. Depending on the type of the imposed boundary condition, the error behavior is also quite different. For the Dirichlet case the minimum error occurring at τ_c is slightly smaller than the error as $\tau \rightarrow \pm\infty$. However, for the Robin case we observe that the error occurring at $\tau = \tau_c$ is less than the error as $\tau \rightarrow \pm\infty$, at least by two order in magnitude. This indicates that if the value of τ can be properly chosen then the numerical solution computed by the penalty scheme will have better accuracy than the solution obtained by the

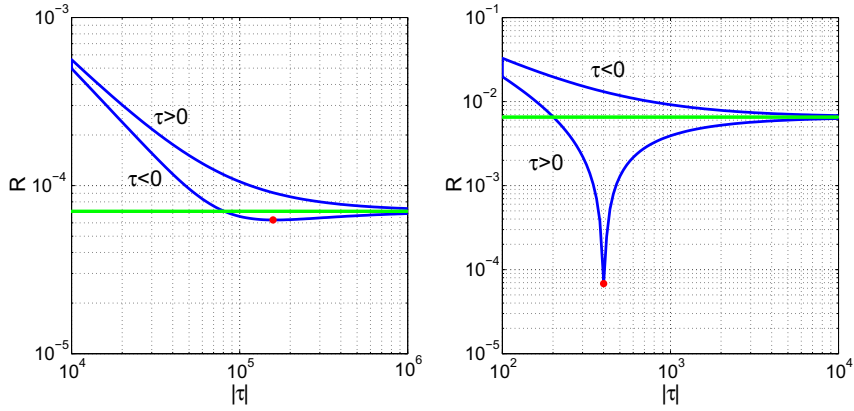


Fig. 1. Error as a function of $\tau_+ = \tau_- = \tau$. Left: Eq. (3) subject to boundary conditions Case (A), Eq. (4). Right: Eq. (3) subject to boundary conditions Case (B), Eq. (5). Red dots: errors corresponding to the penalty parameters determined by Eq. (13). Green line: error corresponding to $|\tau| \rightarrow \infty$ (boundary conditions enforced strongly). $N = 16$. (For interpretation of the references to colour in this figure legend, the reader is referred to the web version of this article.)

traditional pseudospectral scheme with boundary conditions enforced strongly. A question is immediately raised. Can we determined the value of τ in the penalty scheme from the prescribed data stated in a Poisson problem, such that the approximation error is minimized? We answer this question in the following analysis.

Following the error minimizing approach shown in [5] we determine the values of the penalty parameters through minimizing the difference between the numerical solution v satisfying Eq. (2) and the exact solution satisfying the interpolated continuous problem on the grid points, i.e.,

$$u''(x_i) = f(x_i), \tag{9a}$$

$$\mathcal{B}_\pm u(\pm 1) = g_\pm. \tag{9b}$$

Notice that $u(x)$ in Eq. (9), $v(x)$ in Eq. (2), and $f(x)$ in both equations are polynomials of degree at most N . If the degree of $f(x)$ is at most $N - 2$ then $v(x) = u(x)$ though out the whole domain. If the degree of the polynomial f is greater than $N - 2$ then f can be expressed as

$$f(x) = A_- f_-(x) + A_+ f_+(x) + P_{N-2}(x), \quad f_\pm(x) = \frac{(1 \pm x)T'_N(x)}{2N^2},$$

where A_\pm are constants and $P_{N-2}(x)$ is a polynomial of degree $N - 2$. Therefore, we can consider $u = u_1 + u_2$ where u_1 and u_2 satisfy

$$u_1'' = A_- f_-(x) + A_+ f_+(x), \quad \mathcal{B}_\pm u_1(\pm 1) = 0,$$

$$u_2'' = P_{N-2}, \quad \mathcal{B}_\pm u_2(\pm 1) = g_\pm.$$

Because u_2 can be solved exactly by the pseudospectral penalty formulation, the error function R is attributed to numerically solving u_1 . Thus, for error analysis it is sufficient to consider the problem with $f = A_- f_-(x) + A_+ f_+(x)$ in Eq. (9) subject to homogeneous boundary conditions $g_\pm = 0$.

Denote the solutions corresponding to $f = f_+$ and $f = f_-$ by $u = u_+$ and $u = u_-$, respectively. They are

$$u_\pm(x) = \frac{T_{N+1}(x)}{4N^2(N+1)} - \frac{T_{N-1}(x)}{4N^2(N-1)} \pm \frac{T_{N+2}(x)}{8N(N+1)(N+2)} \pm \frac{T_N(x)}{4N^2(N^2-1)} \mp \frac{T_{N-2}(x)}{8N(N-1)(N-2)} + C_\pm T_1(x) + D_\pm T_0(x), \tag{10}$$

where C_+ , C_- , D_+ and D_- are determined by the boundary conditions, given as

$$C_+ = (\alpha_- G_+ - \alpha_+ H_+)/\gamma, \quad D_+ = ((\alpha_- + \beta_-)G_+ + (\alpha_+ + \beta_+)H_+)/\gamma,$$

$$C_- = (\alpha_- G_- - \alpha_+ H_-)/\gamma, \quad D_- = ((\alpha_- + \beta_-)G_- + (\alpha_+ + \beta_+)H_-)/\gamma,$$

with

$$\gamma = (\alpha_+ + \beta_+)\alpha_- + \alpha_+(\alpha_- + \beta_-),$$

$$G_+ = \frac{\alpha_+}{N^2(N^2-4)} - \frac{\beta_+(2N^2-1)}{2N^2(N^2-1)}, \quad G_- = -\frac{3\alpha_+}{N^2(N^2-1)(N^2-4)} + \frac{\beta_+}{2N^2(N^2-1)}, \tag{11a}$$

$$H_+ = -\frac{(-1)^{N-1}3\alpha_-}{N^2(N^2-1)(N^2-4)} + \frac{(-1)^{N-1}\beta_-}{2N^2(N^2-1)}, \quad H_- = \frac{(-1)^{N-1}\alpha_-}{N^2(N^2-4)} - \frac{(-1)^{N-1}\beta_-(2N^2-1)}{2N^2(N^2-1)}. \tag{11b}$$

For $f=f_{\pm}$ the corresponding numerical solutions $v=v_{\pm}(x)$ satisfying Eqs. (2a)–(2c) are linear functions as

$$v_{\pm}(x; \tau_{\pm}) = [-\alpha_{\mp} T_1(x) \mp (\alpha_{\mp} + \beta_{\mp}) T_0(x)] \frac{(\pm 1)^N}{\gamma \tau_{\pm}}. \quad (12)$$

For $f=f_+$ and $f=f_-$ we define the error functions R_+ and R_- , respectively, as

$$R_{\pm}(\tau_{\pm}) = \left(\frac{\pi}{N} \sum_{i=0}^N \frac{A_{\pm}^2}{c_i} [u_{\pm}(x_i) - v_{\pm}(x_i; \tau_{\pm})]^2 \right)^{1/2}.$$

The necessary condition for τ_{\pm} to minimize R_{\pm} is the vanishing of $\partial R_{\pm} / \partial \tau_{\pm}$, leading to following equations

$$\sum_{i=0}^N \frac{1}{c_i} u_{\pm}(x_i) v_{\pm}(x_i; \tau_{\pm}) = \sum_{i=0}^N \frac{1}{c_i} v_{\pm}^2(x_i; \tau_{\pm}).$$

Substituting the expressions of u_{\pm} and v_{\pm} , and employing the discrete orthogonal relationship of Chebyshev polynomials,

$$\sum_{l=0}^N \frac{1}{c_l} T_j(x_l) T_k(x_l) = \frac{\delta_{jk} c_j N}{2},$$

we calculate the summations and obtain the parameters τ_{\pm} as

$$\tau_+ = \frac{-[\alpha_-^2 + 2(\alpha_- + \beta_-)^2]}{[\alpha_-^2 + 2(\alpha_- + \beta_-)^2] G_+ + [2(\alpha_- + \beta_-)(\alpha_+ + \beta_+) - \alpha_- \alpha_+] H_+}, \quad (13a)$$

$$\tau_- = \frac{(-1)^N [\alpha_+^2 + 2(\alpha_+ + \beta_+)^2]}{[2(\alpha_+ + \beta_+)(\alpha_- + \beta_-) - \alpha_+ \alpha_-] G_- + [\alpha_+^2 + 2(\alpha_+ + \beta_+)^2] H_-}, \quad (13b)$$

where G_{\pm} and H_{\pm} are provided in Eqs. (11). For the Dirichlet and the Neumann boundary conditions, the penalty parameters can be deduced from Eq. (13) as follows:

Dirichlet boundary condition: $\alpha_{\pm} = 1$, $\beta_{\pm} = 0$,

$$\tau_+ = \tau_- = \begin{cases} -(N^2 - 1)(N^2 - 4) & \text{for } N \text{ even,} \\ -(N^2 - 1)(N^2 - 4)(1 - 2/N^2)^{-1} & \text{for } N \text{ odd.} \end{cases}$$

Neumann boundary condition: $\alpha_{\pm} = 0$, $\beta_{\pm} = 1$,

$$\tau_+ = \tau_- = \begin{cases} N^2 - 1 & \text{for } N \text{ even,} \\ N^2 & \text{for } N \text{ odd.} \end{cases}$$

Notice that in the above analysis the penalty parameters are derived based on minimizing the error functions R_+ and R_- rather than R . This does not cause any problem, because they are related by

$$R^2(\tau_+, \tau_-) \leq 2(R_+^2(\tau_+) + R_-^2(\tau_-)).$$

This argument is verified by numerical computations. In Fig. 1 the errors corresponding the error minimized penalty parameters are plotted as red dots. It is clearly shown that the penalty parameters provided by Eq. (13), indeed, leads to very accurate computational results.

Tables 1 and 2 show the convergence results of the present method on solving Eq. (1) subject to Dirichlet boundary conditions imposed at both end points (Case (A)) and subject to Robin boundary conditions imposed at both end points (Case (B)). The L_2 and L_{∞} errors are measured for computations with error minimized τ . For comparison, we also measure the L_2 and L_{∞} errors of the solution obtained by the pseudospectral method with strongly enforced boundary conditions. It is shown that the present method is, indeed, better in accuracy. Moreover, we observe that for Robin boundary conditions enforced at the boundaries, the numerical solutions computed by the scheme with error minimized τ are much more accurate than those obtained by the scheme with boundary conditions enforced strongly.

As the penalty parameters vary, the error behavior of numerical solutions obtained by the present method on solving Eq. (1) subject to different types of boundary conditions (Case (C) and (D)) are also conducted. In Figs. 2 and 3 the L_2 errors are plotted as functions of the parameter τ_+ and τ_- for a fixed N . The L_2 errors corresponding to the error minimized penalty parameters τ_+ and τ_- are marked as red dots. It is shown that these red dots are located at the minimum of the error surfaces.

The convergence studies of the present method on solving Poisson equations involving different types of boundary conditions at boundaries (Case (C) and (D)), are presented in Tables 3–5. The results show that for each N the error of the numerical solutions computed by the present error minimized scheme is at least one order of magnitude less than that of the solutions obtained by the scheme with strongly enforced boundary conditions.

Table 1
Convergent tests of the problem, Eq. (3) subject to boundary conditions Case (A), Eq. (6).

N	Present method		Strongly enforced BC	
	L_2 error	L_∞ error	L_2 error	L_∞ error
16	5.8633e-03	4.8134e-03	6.1393e-03	5.6150e-03
20	6.2430e-05	4.6928e-05	7.0416e-05	6.2465e-05
24	3.2081e-07	2.2365e-07	3.8433e-07	3.4827e-07
28	8.7487e-10	5.9210e-10	1.0927e-09	1.0446e-09
32	1.3760e-12	9.6856e-13	1.7426e-12	1.7695e-12

Table 2
Convergent tests of the problem, Eq. (3) subject to boundary conditions Case (B), Eq. (7).

N	Present method		Strongly enforced BC	
	L_2 error	L_∞ error	L_2 error	L_∞ error
16	6.1901e-03	5.6880e-03	2.3737e-01	1.9079e-01
20	6.8103e-05	5.9442e-05	6.5479e-03	5.2502e-03
24	3.5437e-07	3.0959e-07	6.1006e-05	4.8855e-05
28	9.6978e-10	8.6371e-10	2.5653e-07	2.0521e-07
32	1.4800e-12	1.3511e-12	5.6771e-10	4.5389e-10

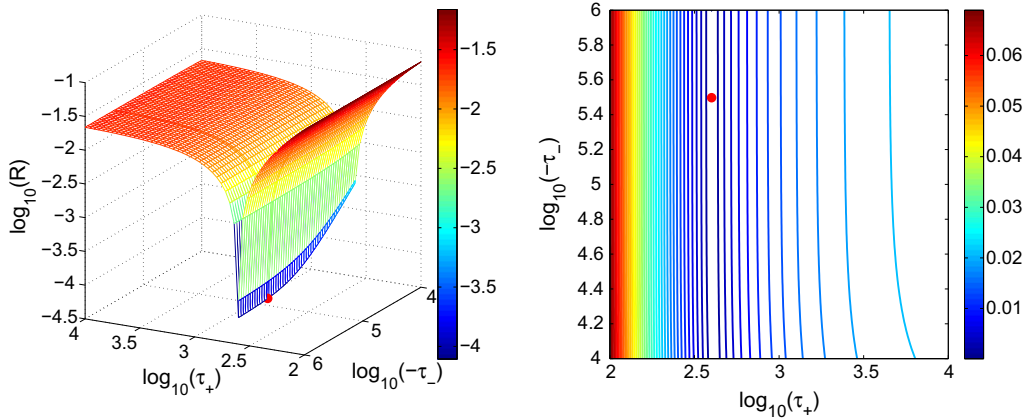


Fig. 2. Surface (left) and contour (right) plots of the L_2 error ($R(\tau_+, \tau_-)$) of the numerical solution obtained by the penalty scheme on solving Eq. (3) subject to boundary conditions Case (C). The error corresponding to the error minimized penalty parameters is marked as a red dot. $N = 16$. (For interpretation of the references to colour in this figure legend, the reader is referred to the web version of this article.)

3. Generalization of the method

In this section we present a direct Poisson solver based on the pseudospectral penalty and the matrix diagonalization methods for problems defined on a rectangular domain.

3.1. Direct solver for Poisson equations in 3D

Consider the Poisson equation

$$\nabla^2 u(x, y, z) = f(x, y, z), \quad (x, y, z) \in [-1, 1] \times [-1, 1] \times [-1, 1], \tag{14}$$

subject to the boundary conditions

$$\mathcal{B}_\pm^x u(\pm 1, y, z) = g_\pm^x(y, z), \quad \mathcal{B}_\pm^x = \alpha_\pm^x \pm \beta_\pm^x \partial_x, \tag{15a}$$

$$\mathcal{B}_\pm^y u(x, \pm 1, z) = g_\pm^y(x, z), \quad \mathcal{B}_\pm^y = \alpha_\pm^y \pm \beta_\pm^y \partial_y, \tag{15b}$$

$$\mathcal{B}_\pm^z u(x, y, \pm 1) = g_\pm^z(x, y), \quad \mathcal{B}_\pm^z = \alpha_\pm^z \pm \beta_\pm^z \partial_z, \tag{15c}$$

where ∇^2 is the Laplace operators, $\mathcal{B}_\pm^x, \mathcal{B}_\pm^y$ and \mathcal{B}_\pm^z are boundary operators acting on the boundary surfaces $x = \pm 1, y = \pm 1$ and $z = \pm 1$, respectively, α_\pm^v and β_\pm^v for $v = x, y, z$ are parameters characterizing the imposed boundary conditions at the surfaces, and ∂_v is the partial derivative with respect to the variable v .

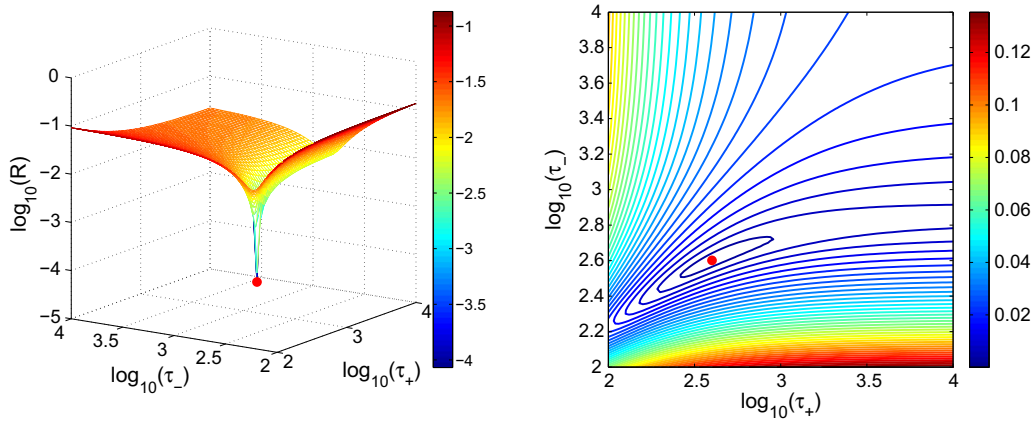


Fig. 3. Surface (left) and contour (right) plots of the L_2 error $R(\tau_+, \tau_-)$ of the numerical solution obtained by the penalty scheme on solving Eq. (3) subject to boundary conditions Case (D). The error corresponding to the error minimized penalty parameters is marked as a red dot. $N = 16$. (For interpretation of the references to colour in this figure legend, the reader is referred to the web version of this article.)

Table 3
Convergent test of the problem, Eq. (1) subject to boundary conditions Case (C), Eq. (6).

N	Present method		Strongly enforced BC	
	L_2 error	L_∞ error	L_2 error	L_∞ error
16	7.5861e-03	8.2458e-03	8.2730e-01	7.6315e-01
20	8.4171e-05	8.9049e-05	2.2776e-02	2.1001e-02
24	4.2298e-07	4.4719e-07	2.1196e-04	1.9540e-04
28	1.1169e-09	1.2001e-09	8.9051e-07	8.2080e-07
32	1.5770e-12	1.6215e-12	1.9692e-09	1.8149e-09

Table 4
Convergent test of the problem, Eq. (1) subject to boundary conditions Case (D), Eq. (7).

N	Present method		Strongly enforced BC	
	L_2 error	L_∞ error	L_2 error	L_∞ error
16	7.7124e-03	8.3458e-03	8.2730e-01	7.6315e-01
20	8.7012e-05	9.1708e-05	2.2776e-02	2.1001e-02
24	4.4364e-07	4.7063e-07	2.1189e-04	1.9534e-04
28	1.1853e-09	1.2869e-09	8.9054e-07	8.2082e-07
32	1.7921e-12	1.9433e-12	1.9697e-09	1.8153e-09

Table 5
Convergent test of the problem, Eq. (1) subject to boundary conditions Case (E), Eq. (8).

N	Present method		Strongly enforced BC	
	L_2 error	L_∞ error	L_2 error	L_∞ error
16	6.1177e-03	6.0597e-03	2.7512e-01	2.5438e-01
20	6.6056e-05	6.1317e-05	7.5796e-03	7.0003e-03
24	3.3923e-07	3.0780e-07	7.0574e-05	6.5133e-05
28	9.2113e-10	8.3299e-10	2.9660e-07	2.7361e-07
32	1.4328e-12	1.3012e-12	6.5625e-10	6.0519e-10

To solve Eq. (14), we introduce the three dimensional grid points

$$(x_i, y_j, z_k) = - \left(\cos \left(\frac{i\pi}{N_x} \right), \cos \left(\frac{j\pi}{N_y} \right), \cos \left(\frac{k\pi}{N_z} \right) \right), \quad 0 \leq i/j/k \leq N_x/N_y/N_z.$$

The associated three dimensional Lagrange interpolating functions $L_{i,j,k}(x,y,z)$ are constructed as

$$L_{i,j,k}(x,y,z) = l_i^x(x) l_j^y(y) l_k^z(z),$$

where $l_i^x(x)$, $l_j^y(y)$ and $l_k^z(z)$ are the one dimension Lagrange interpolating functions based on the grid points x_i , y_j and z_k , respectively. We construct the numerical solution v as

$$v(x, y, z) = \sum_{k=0}^{N_z} \sum_{j=0}^{N_y} \sum_{i=0}^{N_x} L_{i,j,k}(x, y, z) v_{i,j,k}$$

satisfying the penalty scheme

$$\begin{aligned} \nabla^2 v_{i,j,k} = & f_{i,j,k} + \tau_x^- \delta_{0i} (\mathcal{B}_-^x v_{0,j,k} - g_-^x(y_j, z_k)) + \tau_x^+ \delta_{N_x i} (\mathcal{B}_+^x v_{N_x,j,k} - g_+^x(y_j, z_k)) + \tau_y^- \delta_{0j} (\mathcal{B}_-^y v_{i,0,k} - g_-^y(x_i, z_k)) \\ & + \tau_y^+ \delta_{N_y j} (\mathcal{B}_+^y v_{i,N_y,k} - g_+^y(x_i, z_k)) + \tau_z^- \delta_{0k} (\mathcal{B}_-^z v_{i,j,0} - g_-^z(x_i, y_j)) + \tau_z^+ \delta_{N_z k} (\mathcal{B}_+^z v_{i,j,N_z} - g_+^z(x_i, y_j)), \end{aligned} \tag{16}$$

where $f_{i,j,k} = f(x_i, y_j, z_k)$. The scheme can be expressed as

$$\sum_{r=0}^{N_x} A_{i,r} v_{r,j,k} + \sum_{s=0}^{N_y} B_{j,s} v_{i,s,k} + \sum_{t=0}^{N_z} C_{k,t} v_{i,j,t} = F_{i,j,k}, \tag{17}$$

where

$$A_{i,r} = \frac{d^2 l_r^x(x_i)}{dx^2} - \tau_x^- \delta_{0i} \left(\alpha_x^- - \beta_x^- \frac{dl_r^x(x_i)}{dx} \right) - \tau_x^+ \delta_{N_x i} \left(\alpha_x^+ + \beta_x^+ \frac{dl_r^x(x_i)}{dx} \right), \quad 0 \leq i, r \leq N_x, \tag{18a}$$

$$B_{j,s} = \frac{d^2 l_s^y(y_j)}{dy^2} - \tau_y^- \delta_{0j} \left(\alpha_y^- - \beta_y^- \frac{dl_s^y(y_j)}{dy} \right) - \tau_y^+ \delta_{N_y j} \left(\alpha_y^+ + \beta_y^+ \frac{dl_s^y(y_j)}{dy} \right), \quad 0 \leq j, s \leq N_y, \tag{18b}$$

$$C_{k,t} = \frac{d^2 l_t^z(z_k)}{dz^2} - \tau_z^- \delta_{0k} \left(\alpha_z^- - \beta_z^- \frac{dl_t^z(z_k)}{dz} \right) - \tau_z^+ \delta_{N_z k} \left(\alpha_z^+ + \beta_z^+ \frac{dl_t^z(z_k)}{dz} \right), \quad 0 \leq k, t \leq N_z, \tag{18c}$$

$$F_{i,j,k} = f_{i,j,k} - \tau_x^- \delta_{0i} g_-^x(y_j, z_k) - \tau_x^+ \delta_{N_x i} g_+^x(y_j, z_k) - \tau_y^- \delta_{0j} g_-^y(x_i, z_k) - \tau_y^+ \delta_{N_y j} g_+^y(x_i, z_k) - \tau_z^- \delta_{0k} g_-^z(x_i, y_j) - \tau_z^+ \delta_{N_z k} g_+^z(x_i, y_j) \tag{18d}$$

Let \mathbf{A} , \mathbf{B} and \mathbf{C} be the matrices with entries as $A_{i,r}$, $B_{j,s}$ and $C_{k,t}$, respectively. Assume that the matrices \mathbf{A} , \mathbf{B} and \mathbf{C} have the following transformation

$$\mathbf{A} = \mathbf{X}^{-1} \Lambda^x \mathbf{X}, \quad \Lambda^x = \text{diag}(\lambda_0^x, \lambda_1^x, \dots, \lambda_{N_x}^x), \tag{19a}$$

$$\mathbf{B} = \mathbf{Y}^{-1} \Lambda^y \mathbf{Y}, \quad \Lambda^y = \text{diag}(\lambda_0^y, \lambda_1^y, \dots, \lambda_{N_y}^y), \tag{19b}$$

$$\mathbf{C} = \mathbf{Z}^{-1} \Lambda^z \mathbf{Z}, \quad \Lambda^z = \text{diag}(\lambda_0^z, \lambda_1^z, \dots, \lambda_{N_z}^z), \tag{19c}$$

where λ_i^x , λ_j^y and λ_k^z are the eigenvalues of the matrices \mathbf{A} , \mathbf{B} and \mathbf{C} , and \mathbf{X} , \mathbf{Y} and \mathbf{Z} are the eigenvector matrices of \mathbf{A} , \mathbf{B} and \mathbf{C} , respectively. Then, we can first compute

$$\tilde{F}_{r,s,t} = \frac{1}{\lambda_r^x + \lambda_s^y + \lambda_t^z} \sum_{i=0}^{N_x} \sum_{j=0}^{N_y} \sum_{k=0}^{N_z} X_{r,i}^{-1} Y_{s,j}^{-1} Z_{t,k}^{-1} F_{i,j,k}, \tag{20}$$

in which $X_{r,i}^{-1}$, $Y_{s,j}^{-1}$ and $Z_{t,k}^{-1}$ are matrix elements of \mathbf{X}^{-1} , \mathbf{Y}^{-1} and \mathbf{Z}^{-1} , respectively. Then, numerical solution is computed as

$$v_{i,j,k} = \sum_{r=0}^{N_x} \sum_{s=0}^{N_y} \sum_{t=0}^{N_z} X_{i,r} Y_{j,s} Z_{k,t} \tilde{F}_{r,s,t}, \tag{21}$$

with $X_{i,r}$, $Y_{j,s}$ and $Z_{k,t}$ being the matrix elements of \mathbf{X} , \mathbf{Y} and \mathbf{Z} .

For the two dimensional problems

$$\nabla^2 u(x, y) = f(x, y), \quad (x, y) \in [-1, 1] \times [-1, 1],$$

$$\mathcal{B}_\pm^x u(\pm 1, y) = g_\pm^x(y), \quad \mathcal{B}_\pm^x = \alpha_\pm^x \pm \beta_\pm^x \partial_x,$$

$$\mathcal{B}_\pm^y u(x, \pm 1) = g_\pm^y(x), \quad \mathcal{B}_\pm^y = \alpha_\pm^y \pm \beta_\pm^y \partial_y,$$

the scheme can be deduced from the above formulation as

$$F_{ij} = f_{ij} - \tau_x^- \delta_{0i} g_-^x(y_j) - \tau_x^+ \delta_{N_x i} g_+^x(y_j) - \tau_y^- \delta_{0j} g_-^y(x_i) - \tau_y^+ \delta_{N_y j} g_+^y(x_i),$$

$$\tilde{F}_{r,s} = \frac{1}{\lambda_r^x + \lambda_s^y} \sum_{i=0}^{N_x} \sum_{j=0}^{N_y} X_{r,i}^{-1} Y_{s,j}^{-1} F_{ij}, \quad v_{ij} = \sum_{r=0}^{N_x} \sum_{s=0}^{N_y} X_{i,r} Y_{j,s} \tilde{F}_{r,s}.$$

Unlike the one dimensional problem, we are unable to conduct a multidimensional analysis to determine the values of the penalty parameters. However, as we shall see later from the numerical results, adopting the penalty parameters obtained from the one dimensional analysis in the multidimensional schemes also computes error minimized results. This may be due to the fact that the 2D and 3D schemes are based on tensor product formulation which possibly preserve the error minimized property of the one-dimensional scheme. The theoretical issue may be worth to be analyzed in the future.

The matrix diagonalization method relies on the eigenvalue–eigenvector decomposition of the matrices \mathbf{A} , \mathbf{B} and \mathbf{C} (see Eqs. (19a)–(19c)). In this study we assume that these matrices can be diagonalized based on the following results obtained by others. The eigenvalue spectra of these matrices, depending on the values of the penalty parameters and the imposed boundary conditions, have been investigated theoretically and numerically in several studies. For $|\tau_+| = |\tau_-| \rightarrow \infty$ the present formulation recovers the traditional method with boundary conditions enforced strongly. Gottlieb and Lustman [7] proved that the eigenvalues of the traditional method are distinct and negative, indicating that the matrices \mathbf{A} , \mathbf{B} and \mathbf{C} can be diagonalized. For sufficiently large values of the penalty parameters, Funaro and Gottlieb [5] showed analytically that the non vanishing eigenvalues of these matrices, resulting from the penalty formulation with Neumann boundary conditions, are distinct and negative. Hesthaven and Gottlieb [11] mentioned that the eigenvalue spectra of these matrices resulting from the penalty formulation remain distinct for a wide positive value range of these penalty parameters by numerical computations. In addition to these known results, we have also verified the assumption by conducting extensive computations of the eigenvalue spectra of these matrices for a wide value range of these penalty parameters, including negative values of the parameters. Our computations indicate that the eigenvalue spectra remain distinct. Thus, we are confident that this assumption is reasonable.

3.2. Numerical validations

We have conducted a series of numerical experiments to validate the present method. The results are present next.

3.2.1. 2D problem

Consider $u = \sin(4\pi x)\sin(4\pi y)$ satisfying the 2D Poisson equation

$$\frac{\partial^2 u}{\partial x^2} + \frac{\partial^2 u}{\partial y^2} = -32\pi^2 \sin(4\pi x)\sin(4\pi y), \quad (x, y) \in [-1, 1] \times [-1, 1] \quad (22)$$

subject to the following boundary conditions:

Case (A),

$$u(\pm 1, y) \pm \frac{\partial u(\pm 1, y)}{\partial x} = \pm 4\pi \sin(4\pi y), \quad \frac{\partial u(x, \pm 1)}{\partial y} = 4\pi \sin(4\pi x). \quad (23)$$

Case (B),

$$u(\pm 1, y) = 0, \quad u(x, \pm 1) = 0. \quad (24)$$

Case (C),

$$u(-1, y) = 0, \quad \frac{\partial u(1, y)}{\partial x} = 4\pi \sin(4\pi y), \quad u(x, -1) = 0, \quad u(x, 1) + \frac{\partial u(x, 1)}{\partial y} = 4\pi \sin(4\pi x). \quad (25)$$

To investigate the error behavior as the penalty parameters vary, Eq. (22) subject to boundary conditions Case (A), is solved by the penalty scheme. Since along each coordinate direction the boundary conditions imposed at the two ends are of the same kind, we take $\tau_x^\pm = \tau_x$ and $\tau_y^\pm = \tau_y$. The error as function of τ_x and τ_y is demonstrated in Fig. 4, for $N = 20$. It is shown clearly that the error surface has a dip minimum, and the error corresponding to the error minimized penalty parameters τ_x and τ_y is at the dip. The results indicate that the error minimizing penalty parameter obtained from the 1D analysis remain valid for 2D problems.

Table 6 present the convergence studies of the error minimized scheme on solving the 2D Poisson equation subject to boundary conditions Case (A) as N increases. It is shown that the penalty scheme with error minimized penalty parameters indeed computes solutions with better accuracy before the error is driven down to the numerical noise level.

Table 7 presents the convergence study of the method on solving Eq. (22) subject to boundary conditions Case (B). This test problem has been used in many research works, and our results are compared to those obtained by other methods [9,4,21]. It is shown that the solution computed by the method is more accurate than that computed by the Chebyshev tau method [9]. Compared to the pseudospectral approximation with boundary conditions enforced strongly [4], we see that the present penalty scheme computes solutions with better accuracy, even at the numerical noise level. In addition, our results are as accurate as those obtained by the most accurate Chebyshev Galerkin method [21], for $N = 16$ and $N = 32$. For higher values of N it is observed that the present solution accuracy is limited to $\mathcal{O}(10^{-14})$ and can not be further improved by increasing N , indicating that the round-off error has affected the accuracy of the solution. On the other hand, the Chebyshev Galerkin method [21] which uses specially constructed bases, has better round-off error performance. This may be due to the boundary conditions are exactly satisfied in Galerkin method, while the boundary conditions are only approximately satisfied in current method.

Table 8 presents the convergence study of the method on solving Eq. (22) subject to boundary conditions Case (C). For this case the boundary conditions imposed at parallel sides are of different kinds. Compared to the traditional approach it is shown that the penalty scheme computes solutions with better accuracy.

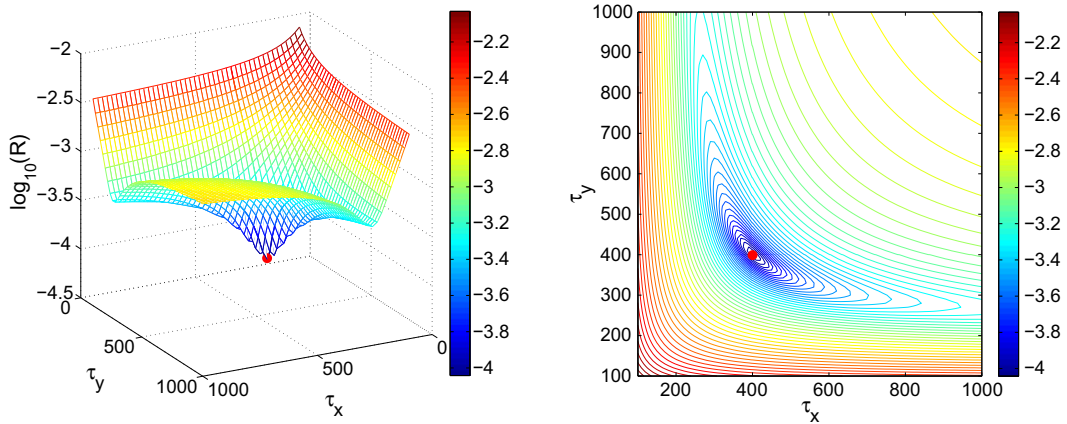


Fig. 4. Surface and contour plots of $\log_{10}(L_2 \text{error})$ as a function of the penalty parameters τ_x and τ_y for $N_x = N_y = 20$. Test problem: $u_{xx} + u_{yy} = -32\pi^2 \sin(4\pi x)\sin(4\pi y)$ subject to boundary conditions Case (A), Eq. (23).

Table 6
Convergence test of the 2D Poisson equation, Eq. (22), subject to boundary condition Case (A), Eq. (23).

N	Present method		Strongly enforced BC	
	L_2 error	L_∞ error	L_2 error	L_∞ error
16	7.7325e-03	5.2042e-03	1.0911e-01	9.3090e-02
20	9.1325e-05	6.8995e-05	3.0619e-03	2.5662e-03
24	4.9615e-07	3.8162e-07	2.8567e-05	2.3930e-05
28	2.2247e-12	1.9539e-12	2.6613e-10	2.2226e-10
32	7.3045e-14	9.4147e-14	1.9322e-14	2.3648e-14
48	4.0532e-14	5.5681e-14	5.9653e-14	7.2664e-14
64	8.7292e-14	6.6391e-14	1.0678e-13	1.2695e-13

Table 7
Convergence test of 2D Poisson equation, Eq. (22), subject to boundary conditions Case (B), Eq. (24). CT: Chebyshev tau method [9]; CC: Chebyshev collocation method [4]; CG: Chebyshev Galerkin [21].

N	Present method		CT	CC	CG
	L_2 error	L_∞ error	L_∞ error	L_∞ error	L_∞ error
16	6.89e-03	5.25e-03	3.33e-02	5.25e-03	5.22e-03
20	8.54e-05	6.26e-05		7.52e-05	
24	4.75e-07	3.76e-07	6.89e-06	4.05e-07	
32	2.17e-12	1.78e-12	4.77e-11	2.87e-12	2.17e-12
40	1.24e-14	2.05e-14		1.47e-12	
48	9.40e-15	1.03e-14	1.90e-12	3.63e-12	
64	3.15e-14	5.05e-14	8.67e-13	3.90e-12	6.11e-15

3.2.2. 3D problem

We give our final test example. Consider $u = \sin(4\pi x) \sin(4\pi y) \sin(4\pi z)$ satisfying the 3D Poisson equation

$$\frac{\partial^2 u}{\partial x^2} + \frac{\partial^2 u}{\partial y^2} + \frac{\partial^2 u}{\partial z^2} = -48\pi^2 \sin(4\pi x) \sin(4\pi y) \sin(4\pi z), \quad (x, y) \in [-1, 1] \times [-1, 1] \times [-1, 1] \tag{26}$$

subject to the following boundary conditions:

$$u(\pm 1, y, z) = 0, \quad \frac{\partial u(1, y, z)}{\partial x} = 4\pi \sin(4\pi y) \sin(4\pi z), \tag{27a}$$

$$\frac{\partial u(x, -1, z)}{\partial y} = 4\pi \sin(4\pi x) \sin(4\pi z), \quad u(x, 1, z) + \frac{\partial u(x, 1, z)}{\partial y} = 4\pi \sin(4\pi x) \sin(4\pi z), \tag{27b}$$

$$u(x, y, -1) - \frac{\partial u(x, y, -1)}{\partial z} = -4\pi \sin(4\pi x) \sin(4\pi y), \quad \frac{\partial u(x, y, 1)}{\partial z} = 4\pi \sin(4\pi x) \sin(4\pi y). \tag{27c}$$

The problem is solved by the penalty scheme and the pseudospectral formulation with boundary condition enforced strongly. The convergence study is presented in Table 9. It is shown that the penalty scheme with the error minimized τ indeed computes more accurate approximations for $N < 32$. However, as $N \geq 32$ the system of equations becomes large we observe that the error can not be driven down due to the round off error.

Table 8

Convergent test of 2D Poisson equation, Eq. (22) subject to boundary conditions Case (C), Eq. (25).

N	Present method		Strongly enforced BC	
	L_2 error	L_∞ error	L_2 error	L_∞ error
16	7.30e-03	5.28e-03	6.75e-02	1.00e-01
20	8.84e-05	6.75e-05	1.87e-03	2.75e-03
24	4.87e-07	3.80e-07	1.74e-05	2.57e-05
28	2.21e-12	1.93e-12	1.68e-10	2.43e-10
32	1.59e-14	1.94e-14	1.94e-11	2.25e-11
48	2.08e-14	2.74e-14	6.12e-11	8.92e-11
64	3.75e-14	4.24e-14	1.43e-11	3.31e-11

Table 9

Convergence test of the 3D problem, Eq. (26) subject to the boundary conditions Eq. (27).

N	Present method		Strongly enforced BC	
	L_2 error	L_∞ error	L_2 error	L_∞ error
16	9.0627e-03	5.4835e-03	4.5057e-02	5.6987e-02
20	1.1572e-04	8.7926e-05	1.3111e-03	1.6651e-03
24	6.5795e-07	5.0986e-07	1.2725e-05	1.5583e-05
28	3.0727e-12	2.6552e-12	1.2452e-10	1.4530e-10
32	2.0128e-14	2.8533e-14	1.1011e-14	1.3784e-14
48	2.5304e-14	3.2713e-14	1.5377e-14	1.5321e-14
64	8.4110e-14	1.1653e-13	3.0008e-14	3.7415e-14

3.3. Computational issues

As to computing efficiency, the asymptotic operation count for current method in 3D case based on Eqs. (20) and (21) is $2N_x N_y N_z (N_x + N_y + N_z)$, and its counterpart for 2D case is $2N_x N_y (N_x + N_y)$ [10]. Obviously, it is far superior to method expressing Laplace operator in tensor product. For an FFT-based method the asymptotic operation count is basically $2N_x N_y N_z (\log(N_x) + \log(N_y) + \log(N_z))$ for 3D case, and $2N_x N_y (\log(N_x) + \log(N_y))$ for 2D case. Indeed, our method which relies on extensive matrix-matrix multiplications is inferior to FFT-based methods in theory. However, this inferiority also depends on hardware. For moderate N_x , N_y , and N_z , it is not necessarily inferior in computers nowadays [3]. Of course, for large grid resolution, FFT-based methods remain the the best choice.

Not only the present penalty formulation has an advantage over the traditional pseudospectral method [4] in accuracy, it is also very easy to implement. In the traditional approach one needs to use the boundary conditions to algebraically eliminate the collocated field values at the boundary points in the discretized partial differential equations. For Dirichlet boundary conditions, the tradition approach can still be implemented easily. However, if Neumann or Robin boundary condition is involved, the eliminating procedure increases the complexity in coding. As we have seen the expression of the scheme in this section, the boundary conditions are directly appended to the discretized partial differential equations. This straightforward approach, thus, makes the penalty scheme very easy in coding.

We end this section by a brief discussion on applying the present formulation for discretizing the Laplace operator in heat equations. We want to emphasis that the proposed penalty formulation for the Laplace operator is for elliptic problems, not for parabolic ones. In fact, applying the present pseudospectral penalty Laplace operator for heat equations involving Dirichlet boundary conditions, will lead to unstable computations, because the matrix resulting from the present pseudospectral penalty discretization is not semi-negative definite. When Dirichlet boundary condition is involved it is found from numerical computations that all the eigenvalues of the discretized Laplace operator are distinct. However, there are two positive eigenvalues approaching positive infinity as N increases, and this is the origin of the instability. We have devised method to overcome this issue and will present it elsewhere due to the scope of this study.

4. Concluding remarks

We have presented a pseudospectral penalty direct solver for Poisson equations subject to general boundary conditions defined on rectangular domain. In the present formulation the values of the penalty parameter are chosen analytically such that the error is minimized. From numerical experiments the present method with error minimized parameters, indeed, computes solutions with better accuracy compared to those obtained by the traditional approach which strongly enforces boundary conditions. Since the present and the traditional pseudospectral methods are only different by the imposition of boundary conditions, the present formulation can be adopted easily into the traditional solver to improve the accuracy of Poisson solvers.

Compared to the modal expansion spectral methods, the pseudospectral method based on Lagrange interpolation basis offers more flexibility on solving partial differential equations with variable coefficients. With the use of the penalty methodology of imposing boundary conditions as shown in the present study, it is also possible to improve the accuracy of other pseudospectral direct Poisson solvers in polar and cylindrical coordinates with boundary conditions enforced strongly.

As mentioned in [5] the solution of a partial differential equation satisfies the equation arbitrary close to the boundary. Taking this argument into account, the penalty formulation which includes the discretized equations at the boundaries instead of discarding them, thus, yield numerical solutions with better accuracy, also as observed in the present results. This implicates that the penalty methodology can be a very promising approach to construct pseudospectral schemes with better accuracy for fourth order elliptic partial differential equations. For this type of equations four boundary conditions are specified. As a consequence, the traditional pseudospectral formulation with strongly enforced boundary conditions discards four discretized equations to make into a well determined system. With the use of the error minimized penalty method, these discarded equations can be included in the formulation to improve the accuracy of solutions. We hope to report this development in the near future.

Acknowledgements

This work is partially supported by National Science Council of Taiwan under grant NSC-99-2115-M-009-012-MY3 (for Chun-Hao Teng), NSC-100-2115-M-035-001 (for Tzyy-Leng Horng), and NSC-100-2632-E-035-001-MY3 (for Tzyy-Leng Horng). The author Chun-Hao Teng is supported by the National Science Council of Taiwan under Research Fellow Program NSC-99-2811-M-009-047.

References

- [1] H. Chen, Y. Su, B.D. Shizgal, A direct spectral collocation Poisson solver in polar and cylinder coordinates, *J. Comput. Phys.* 160 (2000) 453–469.
- [2] H. Dang-Vu, C. Delcarte, An accurate solution of the Poisson equation by the Chebyshev collocation method, *J. Comput. Phys.* 104 (1993) 211–220.
- [3] W.S. Don, A. Solomonoff, Accuracy and speed in computing the Chebyshev collocation derivatives, *SIAM J. Sci. Comput.* 16 (1995) 1253–1268.
- [4] U. Ehrenstein, R. Peyret, A Chebyshev collocation method for the Navier–Stokes equations with application to double-diffusive convection, *Int. J. Numer. Methods fluids* 9 (1989) 427–452.
- [5] D. Funaro, D. Gottlieb, A new method of imposing boundary conditions in pseudospectral approximations of hyperbolic equations, *Math. Comput.* 51 (1988) 599–613.
- [6] D. Funaro, D. Gottlieb, Convergence results for pseudospectral approximations of hyperbolic systems by a penalty-type boundary treatment, *Math. Comput.* 57 (1991) 585–596.
- [7] D. Gottlieb, L. Lustman, The spectrum of the Chebyshev collocation operator for the heat equation, *SIAM J. Numer. Anal.* 20 (1983) 909–921.
- [8] D. Gottlieb, S. Orszag, *Numerical Analysis of Spectral Methods: Theory and Applications*, SIAM, Philadelphia, 1977.
- [9] D.B. Haidvogel, T. Zang, The accurate solution of Poisson's equation by expansion in Chebyshev polynomials, *J. Comput. Phys.* 30 (1979) 167–180.
- [10] P. Haldenwang, G. Labrosse, S. Abboudi, Chebyshev 3-D spectral and 2-D pseudospectral solvers for the Helmholtz equation, *J. Comput. Phys.* 55 (1984) 115–128.
- [11] J.S. Hesthaven, D. Gottlieb, A stable penalty method for the compressible Navier–Stokes equations: I. Open boundary conditions, *SIAM J. Sci. Comput.* 17 (1996) 579–612.
- [12] J.S. Hesthaven, A stable penalty method for the compressible Navier–Stokes equations: III. Multidimensional domain decomposition schemes, *SIAM J. Sci. Comput.* 20 (1999) 62–93.
- [13] J.S. Hesthaven, Spectral penalty methods, *Appl. Numer. Math.* 33 (2000) 23–41.
- [14] J.S. Hesthaven, T. Warburton, Nodal high-order methods on unstructured grids: I. Time-domain solution of Maxwell's equations, *J. Comput. Phys.* 181 (2002) 186–221.
- [15] J.S. Hesthaven, S. Gottlieb, D. Gottlieb, *Spectral Methods for Time-Dependent Problems*, Cambridge University Press, Cambridge UK, 2007.
- [16] Y.-L. Huang, J.-G. Liu, W.-C. Wang, An FFT based fast Poisson solver on spherical shells, *Commun. Comput. Phys.* 9 (2011) 649–667.
- [17] H.C. Ku, R.S. Hirsh, T. Taylor, A pseudospectral method for solution of the three-dimensional incompressible Navier–Stokes equations, *J. Comput. Phys.* 70 (1987) 462–493.
- [18] C. Lanczos, *Applied Analysis*, Prentice-Hall, Englewood Cliffs, N.J., 1956.
- [19] R.E. Lynch, J.R. Rice, D.H. Thomas, Direct solution of partial difference equations by tensor product methods, *Numer. Math.* 6 (1964) 185–199.
- [20] M.C. Navarro, H. Herrero, S. Hoyas, Chebyshev collocation for optimal control in a thermoconvective flow, *Commun. Comput. Phys.* 5 (2009) 649–666.
- [21] J. Shen, Efficient spectral-Galerkin method II. Direct solvers of second and fourth order equations by using Chebyshev polynomials, *SIAM J. Sci. Comput.* 16 (1995) 74–87.
- [22] J. Shen, L.-L. Wang, Some recent advances on spectral methods for unbounded domains, *Commun. Comput. Phys.* 5 (2009) 195–241.